Journal of Chemistry

Innovative Strategies and Emerging Technologies for Food Safety

Lead Guest Editor: Kyung-Min Park
Guest Editors: Sang-Hyun Park and Toshinori Shimanouchi

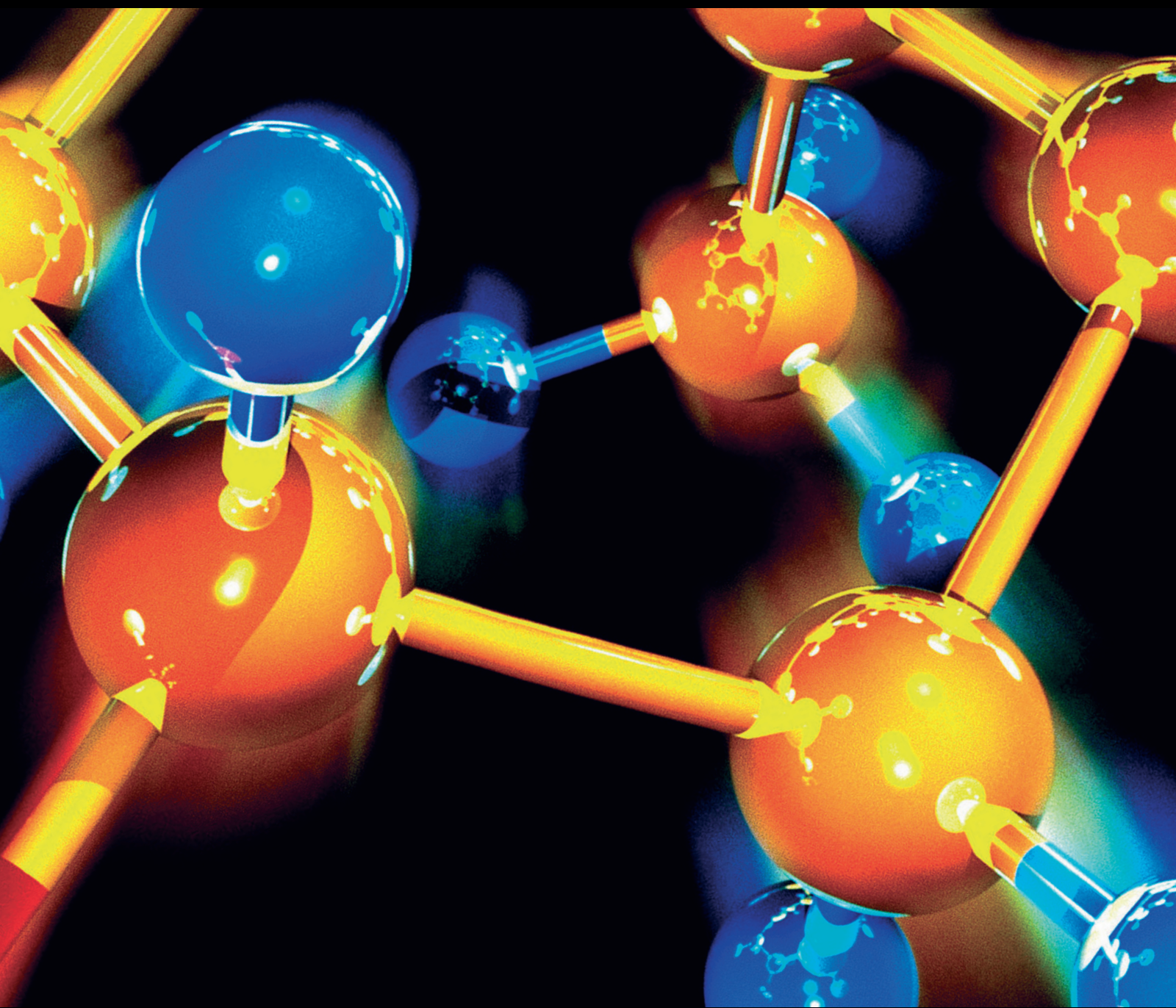

Innovative Strategies and Emerging Technologies for Food Safety

Journal of Chemistry

Innovative Strategies and Emerging Technologies for Food Safety

Lead Guest Editor: Kyung-Min Park
Guest Editors: Sang-Hyun Park and Toshinori Shimanouchi

Contents

Hindawi
Journal of Chemistry
Volume 2019, Article ID 4276426, 2 pages
https://doi.org/10.1155/2019/4276426

Editorial

Innovative Strategies and Emerging Technologies for Food Safety

Kyung-Min Park,[1] **Sang-Hyun Park**,[2] **and Toshinori Shimanouchi**[3]

[1]*Department of Food Science and Biotechnology, Wonkwang University, Iksan 54538, Republic of Korea*
[2]*Department of Food Science and Technology, Kongju National University, Yesan, Chungnam 32439, Republic of Korea*
[3]*Graduate School of Environment and Life Science, Okayama University, 3-1-1 Tsushimanaka, Okayama 700-8530, Okayama, Japan*

Correspondence should be addressed to Kyung-Min Park; kmpark79@wku.ac.kr

Received 8 April 2019; Accepted 8 April 2019; Published 15 May 2019

The need for enhancing microbial safety and quality of foods without compromising the nutritional, functional, and sensory characteristics has created an increasing interest across the globe in innovative technologies for food preservation [1]. Emerging food processing technologies, such as physical, chemical, and biological methods, have been advanced by the food industry and academia during the last few decades. This is in an attempt to meet the need of producing safe foods of high quality. These emerging technologies could significantly contribute to the production of microbiologically safe foods with high quality [2]. Moreover, the production will be of shorter processing time, reduced operational cost, and environmental friendship compared to the conventional food processing technologies, which will eventually benefit the food industry. However, each emerging technology has its own limitation. Therefore, future research should be conducted in order to apply these technologies at a commercial level. With this background, many researchers have worked toward the development and optimization of several emerging food processing technologies. The special issue consists of six research papers that were selected from various submissions. While these papers may not fully cover the topics mentioned above, they represent the rich and many-faceted knowledge.

Shimanouchi et al. conducted the hydrolysis of disaccharides by using a microcapillary system under hydrothermal conditions (up to 190°C at 10 MPa and pH 4–11). The hydrolysis reaction showed a sigmoidal progression with time, especially under alkaline conditions. An analysis using a kinetic model yielded a reaction induction period. The specific pH value (pH^{amb}) at the induction time, which is the pH value corresponding to the progression of disaccharide hydrolysis, was peculiar to each disaccharide. Finally, the calculation of the electron density around the oxygen atom of the glycosidic bond between the saccharides was found to roughly predict the pH^{amb} value required for the progression of the hydrolysis.

Some importers of marine products have practiced the fraud of artificially injecting water into *Octopus minor* for the purpose of increasing their weights prior to the freezing process. These rampant practices have recently become a serious social issue, and they threaten public health. Lee et al. developed a nondestructive method for verifying adulterated *Octopus minor* through measuring dielectric properties by using the coaxial probe method. The dielectric loss factor (ε'') values of the adulterated octopuses were much lower than normal octopuses. The ε'' values from the normal frozen octopus were significantly different from the adulterated and imported frozen octopuses. Additionally, the ε'' values from the adulterated frozen octopus group, whose weight gain rate was less than 20%, were significantly different from other adulterated octopus groups with a higher weight gain rate than 20%. The ε'' values from the adulterated frozen octopus groups with a range of weight gain rate between 20% and 30% were quite similar to the imported frozen octopuses. Therefore, it was found that the measurement of the ε'' values from an *Octopus minor* has a great possibility to distinguish between

normal frozen octopuses and artificially water-injected frozen octopuses.

Mineral oil hydrocarbon (MOH) contamination in food has become a major concern in the past decade. This is after it was brought to light that the substances might potentially be harmful to human health. Ethylene vinyl alcohol copolymer (EVOH) is a key material of interest as a functional barrier against substances migrating from recycled paperboard. This is due to its outstanding barrier properties. Maes et al. reported that all films containing 3 or 5 μm EVOH were found to be good barriers, showing no breakthrough values over 1% of the initial concentration found in the paperboard. Moreover, they could easily compete with monolayer polyethylene terephthalate (PET, 12 μm). The multilayer with 3 μm polyamide 6/6.6 copolymer (PA 6/6.6) showed higher breakthrough values for both the 4-methylbenzophenone (MBP) and di-*n*-propyl phthalate (DPP) than the other materials, however, below the 1% threshold value. However, anthracene (ANT) showed substantial breakthrough values of about 2%, indicating that PA 6/6.6 might not offer enough protection against low-weight mineral oil aromatic hydrocarbon (MOAH) components.

Even though liposomes have been used as nutrient delivery carriers in the cosmetic, food, and pharmaceutical industries, they still suffer from the critical issue caused by the use of halogenated solvents, such as chloroform, which may be harmful to humans. Yang et al. screened non-halogenated solvents as candidate substitutes for the chloroform based on their physicochemical properties. They also prepared combined mixtures using various ratios of each candidate to obtain physicochemical properties similar to the chloroform. Based on the results of random combination trials with numerous candidates, the ethyl acetate : *n*-hexane = 4 : 1 (v/v) was selected to be the optimum ratio because it could form stable inverted micelles and a transparent liposome solution without phase separation. The ethyl acetate and *n*-hexane mixture are a potential substitute for chloroform, which may resolve the concerns regarding the toxicity of residual halogenated solvents in lipid nanovesicles.

Choi et al. expressed α-glucanotransferase from *Bacteroides thetaiotaomicron* (BtαGTase) in *Escherichia coli* and characterized. The BtαGTase catalyzed the transglycosylation reactions that produced only glycosyl or maltosyl transfer products, which are preferable for the generation of transglycosylated products with high yields. The 1-deoxynojirimycin (DNJ) glycosylation product G1-DNJ was generated using the BtαGTase, and the inhibitory effect of G1-DNJ was analyzed. A kinetic study of the inhibition revealed that the G1-DNJ inhibited α-glucosidase to a greater extent than DNJ did. However, it did not show any inhibitory effects toward α-amylase, suggesting that G1-DNJ is a potential candidate for the prevention of diabetes.

Joung et al. studied in vitro biodegradation of Bombyx mori silk fibroin (SF) by using food-grade proteolytic enzymes to replace acid hydrolysis. Based on the residual protein quantity and yield of amino acids (AAs) after enzymatic hydrolysis, they evaluated the proteolytic enzyme process of the SF. FoodPro and Alcalase that are classified as alkaline proteases were selected as two of the best candidate enzymes for the hydrolysis of SF. A 2-stage enzymatic treatment by using a combination of FoodPro and Flavourzyme in a sequence for a reaction time of 6 hours was developed to enhance the efficiency of the proteolytic process. The regenerated SF and its enzymatic hydrolysates were characterized by performing a UV-visible spectra, gel electrophoresis, and size-exclusion chromatography analyses. In the 2-stage treatment using FoodPro initially and Flavourzyme thereafter, the aggregates and high molecular weight proteins of the SF were dissociated and degraded into the low-molecular-weight proteins/peptides (10–15 kDa and 27 kDa). SF hydrolysates, as functional food, might enzymatically be produced by using the commercial food-grade proteolytic enzymes.

By compiling these papers, we hope to enrich our readers and researchers with respect to the most recent progresses in the field of innovative strategies and emerging technologies for food safety.

Conflicts of Interest

The editors declare that they have no conflicts of interest regarding the publication of this special issue.

Acknowledgments

The guest editors would like to thank all the authors for their contribution to this special issue and appreciate all reviewers for their time and valuable comments to improve the quality of these papers.

Kyung-Min Park
Sang-Hyun Park
Toshinori Shimanouchi

References

[1] M. Niakousari, H. H. Gahruie, M. Razmjooei, S. Roohinejad, and R. Greiner, "Effects of innovative processing technologies on microbial targets based on food categories: comparing traditional and emerging technologies for food preservation," in *Innovative Technologies for Food Preservation*, pp. 133–185, 2018.

[2] J. Colette, K. Tatiana, M. Edyta, L. Craig, and R. Valquiria, "Mapping trends in novel and emerging food processing technologies around the world," *Innovative Food Science and Emerging Technologies*, vol. 31, pp. 14–27, 2015.

Hindawi
Journal of Chemistry
Volume 2019, Article ID 9502856, 14 pages
https://doi.org/10.1155/2019/9502856

Review Article

Recent Development of Optimization of Lyophilization Process

Hidenori Kawasaki,[1,2] Toshinori Shimanouchi,[1] and Yukitaka Kimura[1]

[1]*Graduate School of Environmental and Life Science, Okayama University, 3-1-1, Tsuhima-naka, Kitaku, Okayama, Japan*
[2]*Formulation R&D Center, CMC R&D Division, Shionogi & Co., Ltd., 1-3, Kuise, Amagasaki, Hyogo, Japan*

Correspondence should be addressed to Yukitaka Kimura; yktkkimu@cc.okayama-u.ac.jp

Received 22 September 2018; Revised 12 January 2019; Accepted 26 March 2019; Published 5 May 2019

Academic Editor: Emiliano Fratini

The objective of this review is to survey the development of the optimization of lyophilization. The optimization study of the lyophilizer has been roughly developing by the order of (i) trial-and-error approach, (ii) process modeling using mathematical models, (iii) scalability, and (iv) quality-by-design. From the conventional lyophilization studies based on the trial-and-error, the key parameters to optimize the operation of lyophilization were found out, i.e., critical material attributes (CMAs), critical process parameters (CPPs), and critical quality attributes (CQAs). The mathematical models using the key parameters mentioned above have been constructed from the viewpoints of the heat and mass transfer natures. In many cases, it is revealed that the control of the primary drying stage determines the outcome of the lyophilization of products, as compared with the freezing stage and the secondary drying stage. Thus, the understanding of the lyophilization process has proceeded. For the further improvement of the time and economical cost, the design space is a promising method to give the possible operation range for optimizing the lyophilization operation. This method is to search the optimized condition by reducing the number of key parameters of CMAs, CPPs, and CQAs. Alternatively, the transfer of lyophilization recipe among the lab-, pilot-, and production-scale lyophilizers (scale-up) has been examined. Notably, the scale-up of lyophilization requires the preservation of lyophilization dynamics between the two scales, i.e., the operation of lab- or pilot-scale lyophilizer under HEPA-filtrated airflow condition. The design space determined by focusing on the primary drying stage is large and involves the undesired variations in the quality of final products due to the heterogeneous size distribution of ice crystals. Accordingly, the control of the formation of the ice crystal with large size gave impact on the product quality and the productivity although the large water content in the final product should be improved. Therefore, the lyophilization should take into account the quality by design (QbD). The monitoring method of the quality of the product in lyophilization process is termed the "process analytical technology (PAT)." Recent PAT tools can reveal the lyophilization dynamics to some extent. A combination of PAT tools with a model/scale-up theory is expected to result in the QbD, i.e., a quality/risk management and an *in situ* optimization of lyophilization operation.

1. Introduction

A shelf time of drug products and foods has been demanded to extend a period of time. It is also of importance to maintain their storage characteristics. The most key factor to deteriorate the product quality is water included in drug products and foods. Therefore, an appropriate drying method should be used to remove water from the drug products and foods. Well-known drying technologies are the lyophilization [1, 2], spray drying [3], and reduced-pressure drying [4]. In the manufacturing of pharmaceutical drug products such as unstable chemicals and sterile products, the lyophilization (or freeze drying) has been widely used as an effective means [1, 2, 5]. Meanwhile, lyophilization that is not optimized could take days or even weeks to terminate, which is a time- and energy-intensive process [6–10].

A failure of lyophilization gives a serious cost impact. This is because vials of several thousand scales are lyophilized at a time in the commercial scale production of the pharmaceutical drug. The same was true for the lyophilization of foods. In the earlier studies, a scale-up of the laboratory-scale lyophilization and a transfer of lyophilization recipe into other types of instruments has been studied in a manner of the trial-and-error method [11, 12].

Some researchers have suggested the practical advice for the design of lyophilization processes for pharmaceuticals [13] and foods [14–16]. Nevertheless, the design based on trial-and-error experiments often causes an instability in product quality. This results in an increase of manufacturing costs. Therefore, the existing scale-up theory is far from being sufficient. And so, a control method for the production-scale lyophilization needs to be amended. Such a problem has been claimed specifically in the area of pharmaceutical and food engineering.

1.1. Pharmaceuticals. In 2002, the Food and Drug Administration (FDA) announced a significant new initiative, Pharmaceutical Current Good Manufacturing Practices (CGMPs), for the 21st Century. In additional, guidance on process analytical technology (PAT) to meet the 21st-century challenges was represented by the FDA in 2004. In 2009, based on the agreement in the International Council for Harmonization, Technical Requirements for Pharmaceuticals for Human Use (ICH) Q8 (R2) Pharmaceutical Development was updated and the principle of quality by design (QbD) was described [17]. QbD means a systematic approach to development that begins with predefined objectives and emphasizes product and process understanding and process control, based on sound science and quality risk management.

The critical elements of QbD are the *Design Space* and *Process Analytical Technology* (PAT) [18]. According to "ICH Q8 Pharmaceutical Development Guidance" [17], a design space is the multidimensional combination of input variables and process parameters that have been demonstrated to provide assurance of quality. In order to proceed with the pharmaceutical development using a QbD approach, three key philosophies of *Critical Quality Attributes* (CQAs), *Critical Process Parameters* (CPPs), and *Critical Material Attributes* (CMAs) have been guided in the pharmaceutical industry. CQAs are physical, chemical, biological, or microbiological property or characteristic that should be within an appropriate limit, range, or distribution to ensure the desired product quality. CPPs are process parameters whose variability has an impact on a CQA and therefore should be monitored or controlled to insure the process produces the desired quality. CMAs are attributes of input materials whose variability has an impact on a CQA and therefore should be monitored or controlled to insure the process produces the desired quality. CQAs, CPPs, and CMAs should be clarified to develop based on a QbD approach. These attributes that include variables accepted so far are listed in Table 1. In accordance with the principles of ICH Q9, a risk assessment to identify and rank process parameters that may impact CQAs based on scientific knowledge and experiments will be conducted and effective control strategies will be developed to minimize the risks to acceptable levels. On the other hand, the PAT is an integral part of QbD, because the paradigm relies on the use of real-time process monitoring and control as a part of an overall control strategy [18]. To design robust control strategies, the design space and PAT are useful. In other words, the optimization of the lyophilization process should be provided by means of CQAs, CPPs, and CMAs, along the design space and PAT. For this purpose, the relationship between the three parameters and the two methods should be described.

1.2. Food Engineering. The lyophilization is of capital importance in the area of food engineering. This technique is often used in the case of the production of dried foods of noodle, pasta, fruits, vegetables, shrimps, meats, and fishes. The main reason is that foods mentioned above are perishable and difficult to preserve as fresh products. These dried products can be easily stored, transported at relatively low cost, and have reduced packing costs, and their low water content delays microbial spoilage. Thus, the variety of lyophilization techniques have been built up, i.e., the air-, freeze-, microwave- and sun-drying methods [14, 15]. The quality of the final product is of importance in every technique, which is the same as QbD in drugs.

For extending the shelf life of final products, the encapsulation technique has been recently and widely studied [19]. The bioactive compounds are encapsulated by the wall materials by the lyophilization [14, 19–21]. Typical bioactive compounds are vitamin E, anthocyanins, fish oil, catechin, and α-tocopherol [19]. The encapsulation permits to improve the stability, extend the shelf-life, minimize the environmental stress, and increase the retention percentage. Also, the influence of the wall materials to the core materials have been widely examined [19]. Meanwhile, the encapsulation recipe obtained by the lab-scale lyophilizer is uneasy to be transferred into the production scale lyophilizer. Therefore, the encapsulation process is practically fine-tuned in the production scale. A difficulty in the optimization of lyophilization process is thus involved in the food engineering.

As overviewed in the field of the pharmaceutical and food engineering, the robust strategy for optimizing the lyophilization process is amended. In this review, we survey the recent strategy to optimize the lyophilization process. First, the lyophilization is overviewed in the viewpoints of physicochemical and operation of lyophilizers, in order to discuss by which parameters the operation can be optimized. The optimization of the lyophilization is discussed on a basis of the trial-and-error approach and the mathematical modeling approach. The scale-up theory based on the model is also compared. Finally, we discuss the future perspectives to break through the present lyophilization.

2. Overview on Lyophilization

The lyophilization process of the food engineering is in general the same as that in pharmaceutical field. Accordingly, the lyophilization process of the pharmaceutical field will be explained in this section. This process normally consists of three stages: (1) freezing stage, (2) primary drying stage, and (3) secondary drying stage, as schematically depicted in Figure 1(a).

Table 1: Potential critical material attributes, critical process parameters, and critical quality attributes.

Critical material attributes (CMAs)	Critical process parameters (CPPs)	Critical quality attributes (CQAs)
(i) Glass transition temperature	(i) Freezing temperature	(i) Related substances
(ii) Eutectic temperature	(ii) Freezing rate	(ii) Appearance
(iii) Cake collapse temperature	(iii) Annealing temperature/time	(iii) Water content
(iv) Product temperature	(iv) Primary drying temperature/pressure/time	(iv) Reconstitution time
(v) Water vapor transfer resistance of the dried layer (R_p)	(v) Secondary drying temperature/pressure/time	

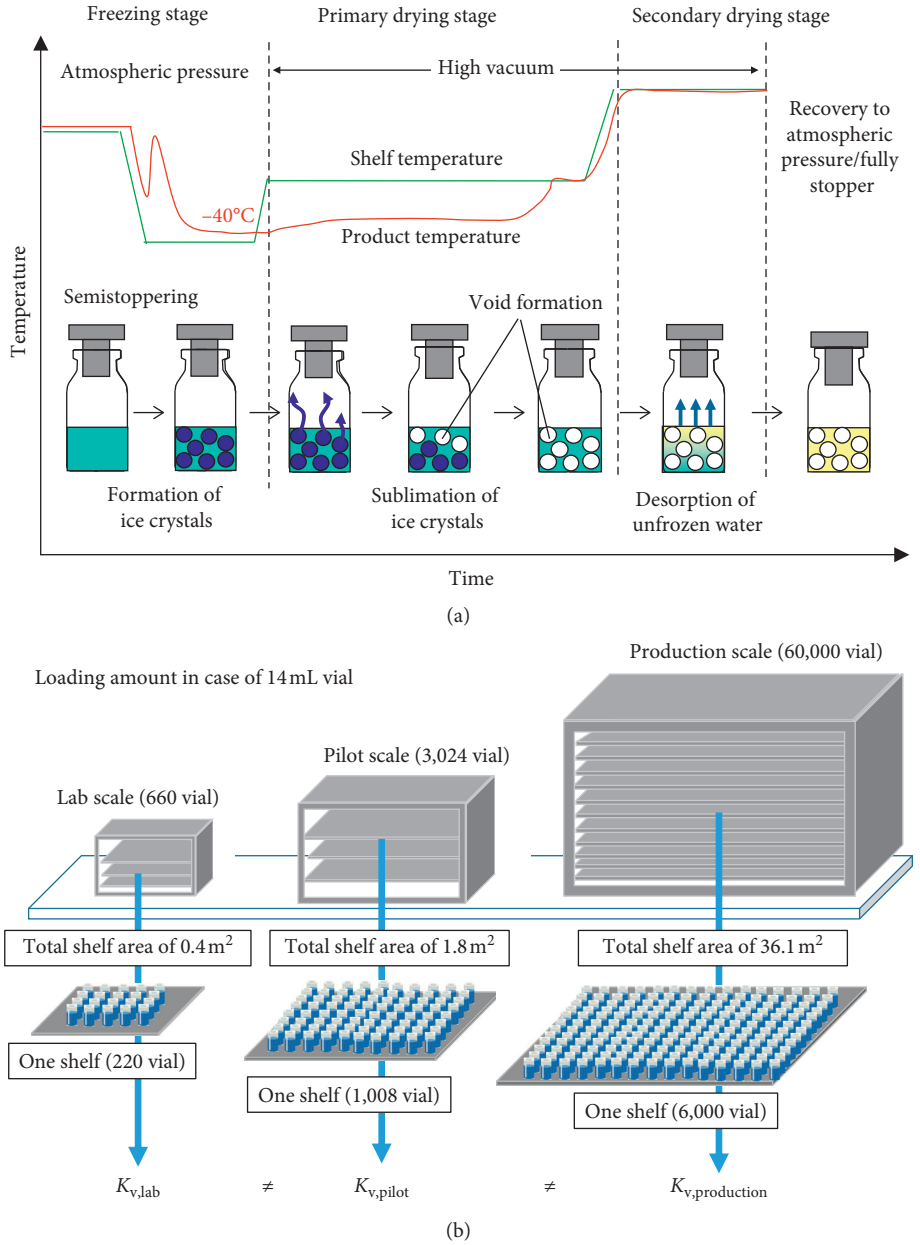

Figure 1: (a) Schematic illustration of lyophilization process. Green and red curves represent the shelf temperature and product temperature, respectively. (b) Comparison of lab, pilot, and production lyophilizers.

The freezing stage is the first stage of freeze drying. Water is a target of the freezing stage in the pharmaceutical and food engineering fields. Accordingly, we focus on water in this review. The freezing operation alters water into ice to separate from other solute components. In this process, the incontinuous temperature change is often observed as shown in Figure 1, which is termed "supercooling." The supercooling often occurs depending on the freezing rate.

The freezing is normally finished within a few hours [22, 23].

The primary drying stage is also called as a sublimation drying stage. In this stage, the chamber pressure is reduced below the equilibrium vapor pressure of ice. The shelf temperature is stepwise elevated, followed by a heat transfer from the shelf surface into the product. This heat transfer induces the sublimation of ice in vials. Thereafter, the sublimated vapor is transferred to the condenser and then turns into ice once more. The heat lost from the product as a latent heat of sublimation will be supplied again from the shelf [24]. As shown in Figure 1(a), the stage requiring the longest time among three stages in the lyophilization process is the primary drying stage, i.e., the primary drying stage needs the heavy economical cost. Therefore, the optimization and shortening of the time for the primary drying stage have been widely studied [25–30].

The secondary drying stage is the step where the product temperature elevates higher temperature than the primary drying stage (Figure 1(a)). There is water that did not turn into ice during the freezing phase and was captured inside the solute components as nonfreezing water. It is this step where a diffusion and desorption of remaining water occur in the product. The objective of secondary drying is to reduce the final residual water content to an acceptable level. Although this stage is usually completed within a few hours, it is an indispensable step in the lyophilization because the remaining water deteriorates the quality of products.

Next, three types of lyophilizers are introduced. Figure 1(b) is a schematic illustration of the lyophilizers of the lab-, pilot-, and production scales. A lab-scale lyophilizer can accommodate up to 660 vials by three shelves. This scale has been widely applied to obtain CPPs and optimize the lyophilization process. Later, the pilot scale is applied to bridge between the pilot- and production-scale lyophilizers. This pilot-scale lyophilizer can accommodate 3,024 vials by three shelves. Lastly, the operational optimization of parameters depicted in Figure 1(a) scales up to the production-scale lyophilizer. The production-scale lyophilizer can accommodate up to 60,000 vials by ten shelves. A final goal is to elucidate and optimize the operational conditions for the production-scale lyophilizer. The sort of investigation for the purpose is summarized in Table 2 and Figure 2. The optimization of operational conditions is surveyed from the following section.

3. Development from Trial-and-Error Approach to Scientific Approach

In general, the lyophilizer has the different heat transfer nature depending on the types of lyophilizers and their scale. Accordingly, to determine the optimal operating condition required the trial-and-error approach in the earlier studies. As stated in the last section, the primary drying stage takes the longest time in any scale lyophilizer. Therefore, the shortening of the primary drying stage is always an issue in terms of economic cost of a production scale. Inevitably, the accomplishment of lyophilization process is likely to be not a considerable level in the trial-and-error approach (Figure 2).

In the beginning, the freeze-drying process was, in a manner of trial-and-error, examined under the various conditions to find out the critical parameters. An improper freeze drying of the product occurs in the case where the product temperature largely rises during the drying stage, which is termed a "collapse" [30]. By continuously reducing the temperature of a bulk solution under the atmospheric pressure, the solution indicates a supercooled state below the freezing temperature (Figure 1(a)), followed by the elevation of the temperature up to around the equilibrium freezing point. This is because of the heat of crystallization caused by the ice nucleation. Thereafter, the continuous removal of heat results in the growth of ice crystals. Moreover, in the case where water is captured in solute components, the solution will be transferred to the ice with exclusion of the nonfreezing water [68]. This is because water is separated from solute components at the eutectic temperature (T_e). Then, the solute components are considerably concentrated. For examples, it is well known that mannitol, glycine, sodium chloride, and phosphate buffer are crystallized during the freezing process at a certain concentration [45]. In the case of drugs or excipients used as injection products bearing a high affinity to water, they rarely form eutectic crystals during the freezing process. The concentrated effect of the solute below the glass-transition temperature (T_g') forms the amorphous solids with the low molecular mobility, which is termed "glass transition." As the empirical determination of T_g' value, the low-temperature differential scanning calorimetry (DSC) is a promising method. The large elevation of the product temperature at the primary drying stage is subject to induce a collapse of the product [35]. The collapse temperature (T_c) can be determined by the freeze-drying microscopy. T_c is the temperature above which the lyophilized product loses its macroscopic structure and cake collapses during the primary drying process. It is well known that T_c is higher than T_g' by approximately 2°C [69]. The proper primary drying at the temperature lower than T_c allows us to obtain an acceptable lyophilized product. Thus, T_g', T_e, and T_c are CMA (see Table 2).

Alternatively, the transfer resistance of dried layers to water vapor flow can improve the drying process. The primary drying stage is controlled by the heat and mass transfer, as illustrated schematically in Figure 1(a). First, we will clarify the heat transfer in the lyophilizer. The heat medium yields the heat to the shelf surface, followed by the heat transfers to the bottom of the vial through three routes: (i) a heat transfer mediated by the gas (mainly vapor) that is present at the space between the shelf surface and the vial; (ii) a heat transfer at the contact area of bottom surface of the vial with the shelf; and (iii) the third route is the radiant heat from the walls of the lyophilizer. As stated in Section 6, the factor (iii) cannot be negligible [55]. Generally, the heat from the bottom of the vial is supplied to the sublimation interface via the frost layer. This heat is consumed as the latent heat of sublimation. Consequently, ice turns to vapor by these heat transfers, followed by the formation of the dried layer to play a role for the resistor against the sublimation. The formation of the dried layer suppresses the sublimation rate. Therefore, the drying resistance due to the dried layer

Table 2: Summary of the optimization of lyophilization.

	Target variables	Notes	Ref.
Trial-and-error without mathematical model	CQAs, CPPs, CMAs	Optimization of freezing process	[13, 31, 32, 33]
		Optimization of primary drying process	[12]
		Optimization of secondary drying process	[34]
Use of mathematical model	CMAs (T_b, R_p, and so on) and CPPs (T_s, P_c, the drying time, and so on)	A partial differential equation (PDE)	[31, 34–44]
		A model predictive control (MPC)	[29, 42, 45, 46]
		A computational fluid dynamics (CFD)	[15, 47, 48]
		K_v-based modeling	[49]
Designs space	P_c-dm/dt plane (Figure 4)	Control of primary drying process	[13, 17, 18, 50–52]
		Control of freezing process	[53]
Scale-up	K_v, P_c	Vial-position dependency of K_v	[12, 54]
		A use of empty vials at the edge of the shelf	[17]
		Equivalent resistance model under the dust-free condition using HEPA-filtered airflow (without empty vials)	[55]
Process analytical technology (PAT)	K_v, R_p, T_b, and P_c, dm/dt	In-line optimization	[56–67]

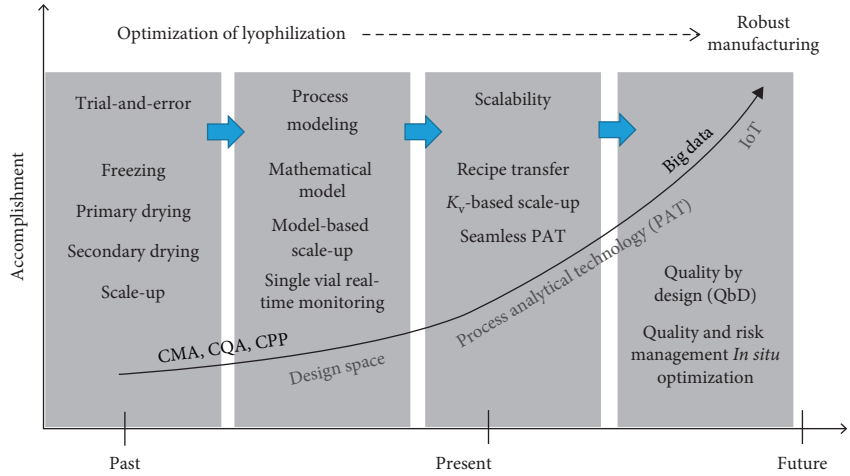

Figure 2: Possible technological transition and sublimation of lyophilization strategy for QbD in the pharmaceutical field. CQA: critical quality attribute; CPP: critical process parameter; CMA: critical material attribute; IoT: Internet of things.

has been quantified as the water vapor transfer resistance of the dried layer R_p [55]. A control of R_p enables the control of the heat input to the product, and the primary drying temperature will be optimized. Based on the R_p, the endpoint of primary drying as the CPP can be estimated. Thus, throughout the trial-and-error approaches, important variables have been found out.

According to the review by Tang and Pikal, the design of freeze-drying processes is quite difficult without further attempts at optimization [13]. The design based on the trial-and-error gives the information on CQAs, CPPs, and CMAs that are required in the optimization of the lyophilization recipe.

4. Process Modeling

Throughout enormous investigations with an approach of trial-and-error, the important CQAs, CPPs, and CMAs have been found out (Tables 1 and 2). In order to minimize the trial-and-error experiments, the mathematical model for the prediction of the optimized T_b value based on CQAs, CPPs, and CMAs has been thereafter developed [31, 34–44], as shown in Table 2. Owing to this, the accomplishment of lyophilization process is improved to some extent (Figure 2).

Modeling for the primary drying stage has been conducted based on the heat and mass transfer model, rather than a modeling with respect to the freezing [31] and secondary drying stages [34]. The initial modeling of the primary drying stage [35, 36, 37] took into account all the contributions to mass transfer resistance, e.g., the dried layer, the stopper, and the chamber. The model based on the partial differential equation (PDE) [38–41] and model predictive control (MPC) [42, 45, 46] has been developed and modified. Previous works regarding PDE and MPC were the numerical study. Notably, Hottot and his coworkers have developed and modified the model to fit the experimental data [70, 71]. Fissore and Barresi have described the multidimensional models and their main

drawback: their equations involve a lot of parameters, whose value cannot be easily obtained by means of experiments with a small uncertainty and calculation cost becomes high [27]. In the latest research, a computational fluid dynamics (CFD) has been attempting to deeply understand the mass and heat transfer in the drying chamber and condenser of the lyophilizer [47, 48]. Using CFD to a pilot-scale lyophilizer with four shelves, the heterogeneous velocity field, pressure distribution, and temperature distribution could be observed. The flow of water vapor could be also visualized: the vapor sublimated from vials is forced to flow towards the edge of the shelf and go to the duct on the wall to be collected in the condenser. Therefore, a numerical study can come to impart not only the qualitative confirmation of experimental solutions but also the validation of prediction by means of PDE and MPC.

In contrast, some of the recent modeling has become simpler than that covered by the literatures [27]. To our best knowledge, the heat and mass transfer model presented by Pikal et al. [49] is the earliest simplified model to focus on the role of the vial. Their simplified model that is based on the mass and heat transfer phenomena in the vial on the shelf is schematically illustrated in Figure 3(a). The mass loss over time (dm/dt) after the lyophilization is experimentally obtained to determine the amount of water used for the sublimation of ice. Ultimately, the vial heat transfer coefficient (K_v) is calculated from the shelf surface temperature (T_s), the product temperature (T_b), latent heat of ice (ΔH_s), cross-sectional area of vial calculated from its outer diameter (A_v), and dm/dt, according to the following equation:.

$$K_v = \frac{\Delta H_s (dm/dt)}{A_v (T_s - T_b)}. \quad (1)$$

As shown in Figure 3(a), the heat transfer into the vial consists of three hear transfers: (i) the contact heat transfer; (ii) gas heat transfer; and (iii) radiant heat transfer. Their heat transfer coefficients were defined as K_c, K_g, and K_r, respectively. According to the previous reports [5, 22], K_c and K_r do not depend on the chamber pressure (P_c) and the K_g value depends on P_c as is described as a function of $K_g = bP_c/(1 + cP_c)$ (b and c are the positive constants). In the case where the three heat transfers mentioned above are driven by the same temperature difference, K_v will obey the relationship of $K_v = K_c + K_g + K_r$. Accordingly, the following equation can be elucidated:

$$K_v = a + \frac{bP_c}{1 + cP_c}. \quad (2)$$

This relationship between K_v and P_c has been often used in the operational design of lyophilization [23, 54, 72].

As shown in Figure 1, T_s, T_b, and P_c are monitored during the lyophilization. The point at which T_b increases sharply toward the setting T_s value was determined as the drying endpoint for analysis. From T_s, T_b, and pressure profile of the equilibrium vapor pressure of ice (P_{ice}) on the sublimation interface and the vacuum pressure (defined as P_c) in the lyophilizer, the R_p value of dried layers with a cross-sectional area (A_p) was calculated according to the following equation:

$$R_p = \frac{A_p (P_{ice} - P_c)}{(dm/dt)}. \quad (3)$$

Equation (3) also yields the drying time. In the optimization of the primary drying stage, this equation is of great importance. The drying time calculated by equation (3) strongly depends on the architecture of lyophilization instrument, dimension of the shelf, arrangement of vials on the shelf, and environmental conditions.

Thus, the process modeling based on the mathematical model has been developed by taking into account (i) CMAs (T_b, R_p, and so on) and (ii) CPPs (T_s, P_c, the drying time, and so on).

5. Design Space

To construct the efficient operation recipe requires the adequate variables. It was plausible that one of the CPPs is the primary drying stage from the viewpoint of economical cost or operational time.

In the earlier studies, it has been clarified that the lyophilization process in the lab-, pilot-, production-scale lyophilizer depends on the position of vials on the shelf. Fissore and Barresi categorized three types of vials in terms of the overall heat transfer nature (Figure 3(a)) [27]. For example, vials of the group 1 are placed in the central part of the shelf. They are not affected by radiation from chamber wall. Vials of groups 2 and 3 are placed in the second and the first rows on each side of the shelf. Then, they are affected in different ways by radiation from the chamber walls. The sublimation behavior depended on the position of vials as shown in Figure 3(b) [55]. Thus, the position dependency of overall heat transfer nature of vials made it complex to elucidate and transfer the recipe from one to another instrument. Therefore, the same recipe obtained in the lab-scale equipment cannot generally be used without modifications to freeze-dry the product in a pilot- or production-scale lyophilizer (Figure 1(b)).

In the report from Chang and Fischer, they have already presented the graph similar to Figure 4, although not the point of the article [50]. Lyophilization process depends on the plural variables. Therefore, the optimization of lyophilization process as a whole can be considered as the multidimensional analysis. To indicate the typical optimized operational conditions, let us imagine the plane of P_c-dm/dt as shown in Figure 4. A lyophilizer has a desired operational condition where P_c cannot be controlled in a highly vacuumed condition or at an accelerated sublimation rate (i.e., a choked flow limit). Once both the K_v and R_p values are determined, both the sublimation interface temperature and the drying time (sublimation rate) during the primary drying stage can be predicted from equations (1)–(3) [13, 17, 18]. The upper and lower limit of product temperature was set to draw the solid line with a negative slope at the constant R_p. Also, the dashed curves of dm/dt as a function of P_c can be drawn at the constant T_s value, by combining equations (1) and (2). Varying T_s from −20 to

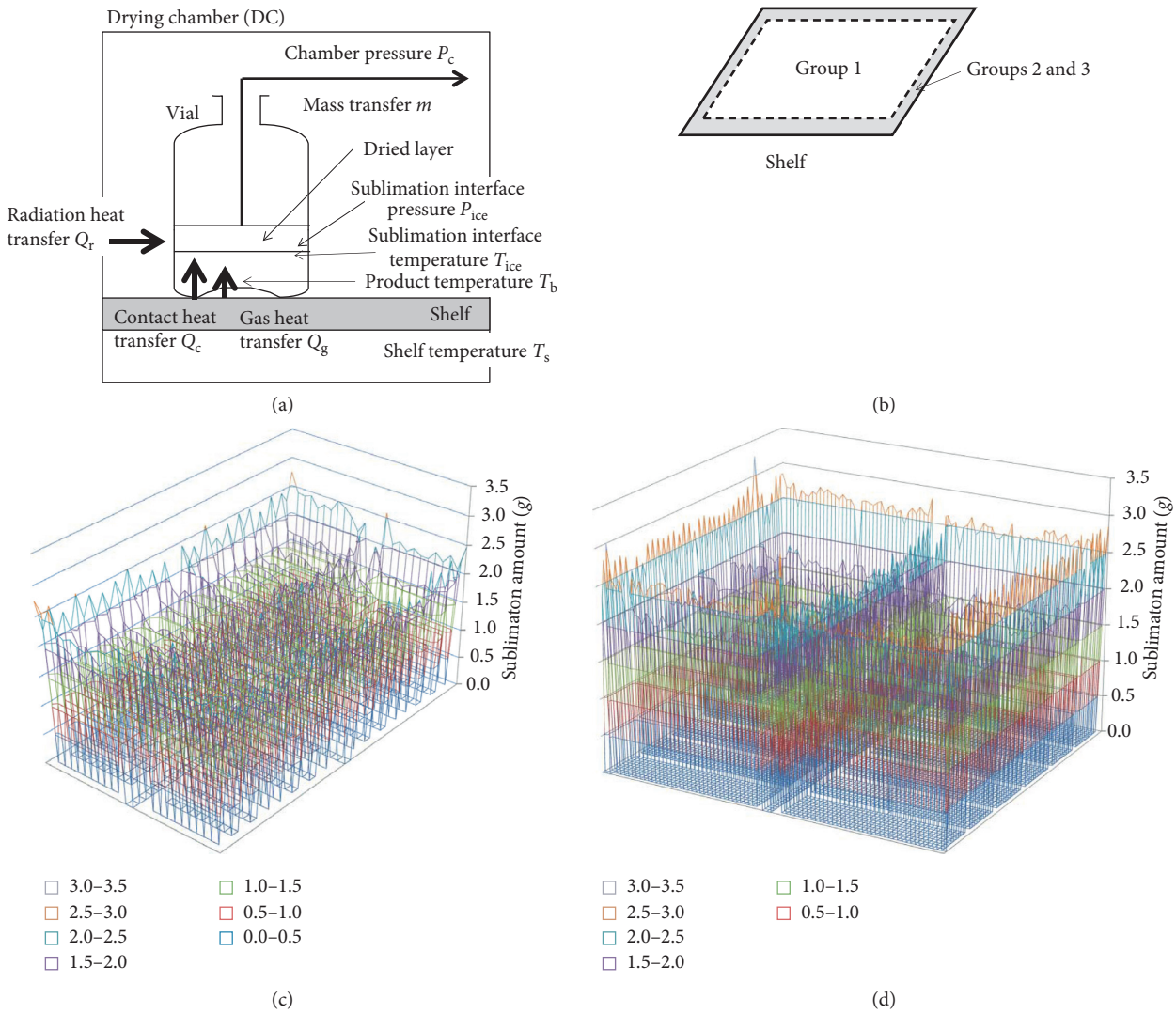

Figure 3: (a) Heat and mass transfer model for lyophilization. (b) Categorization of vials on the shelf. Group 1: vials are placed in the central part of the shelf; Groups 2 and 3: vials are placed in the second and the first rows on each side of the shelf, respectively. This categorization is based on the literature [27]. Distribution of sublimed amount of ice from the vials on the shelf. (c) 1,008 vials, (d) 6,000 vials. Data were redrawn based on [55].

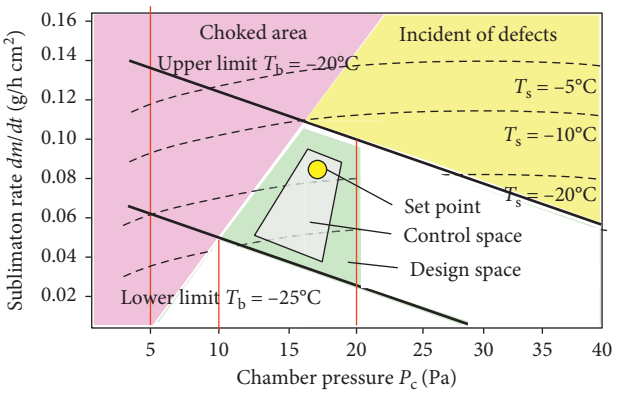

Figure 4: Example of design space. Typical determination method of design space is described in Section 5.

–5°C, the dashed curve shifts to the positive direction of dm/dt axis. In order to avoid the reduction of dm/dt, the P_c should be maintained to the lower pressure below 20 Pa. When the line $P_c = 20$ is drowning, the trapezoid region is formed, which is termed *Design space*. In line with this, the region where the product quality is not damaged and at the same time, where stable manufacturing can be performed is expected to be established [51, 52]. However, the stable operation has been performed in a practical level to tolerate the quality variations that occur in the freezing stage. Accordingly, a larger design space has been used to afford the excess safety factors. The set of wide range of both sublimation interface temperature and the drying time (sublimation rate) often comes to be a cause of the variations in the size of ice crystals. Thus, a design space is an optimized

operation method based on the equipment capability, K_v, and R_p (Table 2), which can improve the accomplishment of lyophilization process (Figure 2). At present, it looks like the design space obtained in the lab-scale lyophilizer, without any change, has not been applied to the pilot- or production-scale lyophilizers yet.

6. Scale-Up Theory

As stated in the last section, the lyophilization recipe such as the design space was limited to the target lyophilizer and could not be transferred to other equipments. As the understanding of the lyophilization process has progressed, the mathematical models based on parameters that dominate the lyophilization process have been developed [24–29]. In some studies, the higher temperature of products and reduction of resistance of the frost layer to vapor flow results in the improvement of the primary drying efficiency [27–29]. Accordingly, the key parameters are selected to construct the scale-up theory by focusing on the primary drying stage.

In the practical equipment, the excess heat input often causes the deviation from the operation after its optimization of the lab-scale equipment. The radiation from the shelf and from chamber walls is a main reason for the excess heat transfer to the product as stated in Section 5 (Figure 3(a)) [27]. The K_v value definitely depends on the position of vials on the shelf [27, 28, 55], which possibly becomes the obstacle to establish the scale-up theory for the production lyophilizer. In actual, the sublimated amount of ice at the position in the shelf was influenced by the radiation heat transfer from the wall of the machine (1,008 vials) (Figure 3(c)) [55]. The radiation effect of the wall in the case of 6,000 vials was significant as compared with the case of 1,008 vials. The K_v values at the edge were higher than those in the center positions in the shelf [17, 55]. Notably, the K_v values were dependent on the P_c. In the scale-up, the selection of the treatment of K_v at the edge and center positions is a key factor because the production lyophilization at large scale possesses the high portion of vials at the edge position to the ones in the central position than the lab-scale lyophilization. Previously [54], the scalable application of equation (2) was demonstrated in all scales of lyophilizers, in other words, a kind of the scale-up of K_v. Since the position dependency of K_v is still adopted, Fissore and Barresi have proposed to place the empty vial at the edge of the shelf [17]. Due to this idea, this recipe could improve the defect of products, although the reduction of productivity corresponding to the number of empty vials is there (Table 2).

In contrary, the scale-up theory without using empty vials has also been demanded from the viewpoint of the cost impact. Alternatively, the latest scale-up theory, termed *the equivalent resistance model* by Kawasaki et al. [55], is introduced in this paragraph. Generally, the dynamics in the lyophilization remains in all scales of lyophilizers to succeed in the scale-up, i.e., the R_p values of lab- and production-scale are equivalent [27]. Meanwhile, the operating condition where the R_P values at the lab and production scale are equivalent has been still unclear. Kawasaki et al. focused on the result that the production-scale lyophilization is performed under HEPA-filtered airflow condition. The R_p value determined by the pilot lyophilizer (1,008 vials) under HEPA-filtrated airflow condition should be able to be extended to the production-scale lyophilizer. Based on this idea, the lyophilization of 60,000-vial scale based on the R_p obtained at the pilot scale has achieved the yield of 99% or more without the use of empty vial placed as groups 2 and 3 (Figure 5) [55]. That is why a use of the dust-free condition using a HEPA-filtrated airflow is an indispensable condition for the preservation of R_p value between lab and production scale. Thus, the equivalent resistance model bridges the gap between the laboratory and production scale.

Therefore, the K_v and R_p values are key parameters to construct the scale-up theory (Figure 2). Specifically, it is likely that the equivalent resistance model permits to use the same design space among the lab-, pilot-, and production-scale lyophilizers, which would enable us to perform an efficient and robust process design using the design space (Table 2).

7. Control of Freezing Process

The freezing stage determines the degree of variations in the productivity as well as the product quality. Then, this stage is one of the most critical stages in the lyophilization process, as shown in Figure 1. One of the CPPs is the freezing stage. Since water does not voluntarily freeze and maintains its supercooled state, the freezing temperature cannot be directly controlled. We first focus on the effect of the freezing temperature. The higher freezing temperature (lower degree of supercooling) results in the formation of the larger size of the ice crystals, as shown in Figure 6. The larger the size of the ice crystals is, the higher the primary drying efficiency achieved. In earlier studies [73], it has been reported that the vials loading the product temperature sensors possibly indicate a bit of high freezing temperature, as compared with those without sensors. It is natural that their sublimation rate will be accelerated enough to alter the drying endpoint. Apart from this, an elevation of the freezing temperature by 1°C can shorten the primary drying time by 3% [74]. On the other hand, the size of the ice crystals determines their specific surface area. The size of the specific surface area determines the diffusion and desorption rate in the secondary drying stage [13, 74]. A high freezing temperature results in the formation of large size of the ice, which reduces the specific surface area. A study reported that this caused the secondary drying efficiency to decrease, increasing the moisture residue in the finished product [22]. Accordingly, it is expected that the control of the freezing temperature during the freezing stage might contribute to design a robust drying process.

An annealing is usually used to control the freezing temperature during the freezing stage [13]. The annealing is a simple holding of the product under the temperature condition above the final freezing temperature for a defined period to crystallize the components. This technique allows the crystallization with improved crystallinity [13]. Annealing above T_g' causes growth of ice crystals, inducing

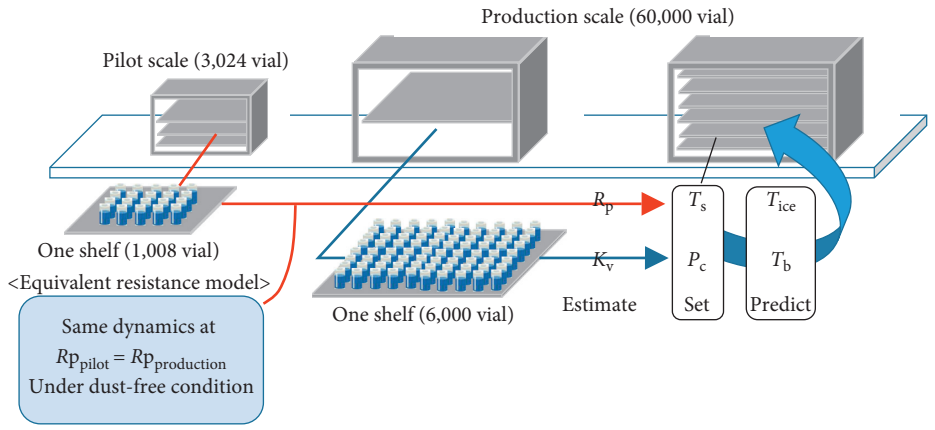

Figure 5: Scale-up theory based on the equivalent resistance model [55]. In this illustration, the equipment of the pilot scale can accommodate the three shelves. The equipment of the production scale accommodates ten shelves.

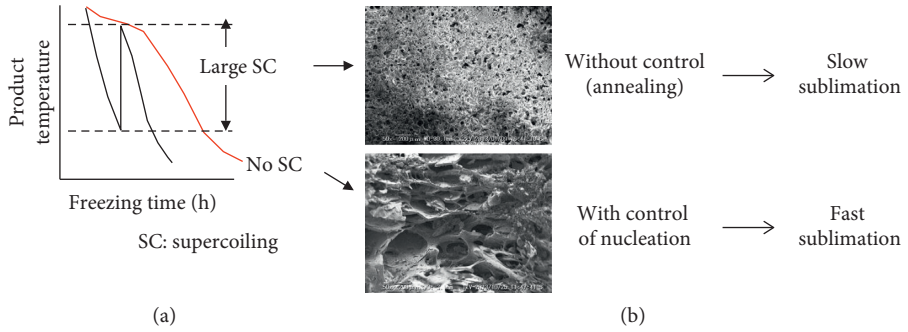

Figure 6: Schematic illustrations on controlled nucleation of ice [53]. (a) Time course of product temperature at a different freezing rate. (b) Scanning electron microscopy of lyophilized samples with and without control of nucleation of ice.

the reduction of R_p value of the product to shorten the primary drying time [32, 33].

Recently, the advantages and disadvantages concerning the ice nucleation techniques have been reported [75, 76]. The pressurization and depressurization technique was a powerful approach to control the ice nucleation behavior. For examples, the pressure inside the lyophilizer is elevated to 0.28~0.29 MPa by using nitrogen or argon gas and quickly decreased to 0.11 MPa (within 3 s). Due to this, the ice nuclei can be formed on the surface of the liquid in the vials [77]. Possible main driving forces for the ice nucleation are considered to be (i) the vibrational disturbance caused by the sudden depressurization, (ii) the cooling of liquid surface of cold gas contacting, or (iii) the local evaporation of liquid surface during the sudden depressurization [78].

Kawasaki et al. have demonstrated the ice crystal size has an impact on the product quality and the productivity [53]. In order to inhibit the supercooling of the solution and to control the size of ices formed in the drug product during the freezing stage, the (de)pressurization technique was combined with the control of freezing rate. This approach enabled us to reduce the R_p value during the primary drying stage. Accordingly, this approach was termed the ice nucleation control. Its beneficial point is shortening the primary drying time. The reduced R_p made it possible to set the robust design space for the primary drying stage. For example, the control space could be set instead of the design space as shown in Figure 4, and a compactification of the trapezoid region could be achieved [53], which can avoid the trial-and-error for searching optimized operational conditions. Selecting the *set point* in the trapezoid region in Figure 4 could achieve the uniform products with higher productivity (no collapsed cake in 726 vials) [53]. However, the method by Kawasaki et al. has the drawback that the increase in residual water content in lyophilized cake may affect the solid stability and burden the primary and secondary drying stages (imagine the large ice crystal in a vial in Figures 1 and 6). Thus, the determination of the maximum allowable water content in the product that is one of the CQAs would be required.

8. Process Analytical Technology

As shown in Figure 2, the selection of critical parameters to well operate the lyophilization gives the motivation to develop an *in situ* optimization technology. The monitoring data of temperature and pressure in the equipment could give much information so that not only the practitioner but also the academia could get the plausible interpretation regarding the deeper understanding of lyophilization principle. Thus, a technology to aim the abovementioned goal is termed process analytical technology (PAT). Relating PAT tools for the monitoring of the primary drying stage are summarized in Table 3. The PAT tools have been developed

Table 3: Process analytical technology (PAT) methods in the lyophilization.

Target	PAT method	Measurement parameter	Ref.
Single vial	Thermocouple (TC)	T_b	M^*
	Resistance thermal detectors (RTD)	T_b	[60]
	Temperature remote interrogation system (TEMPRIS)	T_b	[60]
Batch	Pirani vs capacitance manometer	P_c	[61]
	Mass spectrometer	Partial pressure of gas	[63]
	Tunable diode laser absorption spectroscopy (TDLAS)	Water vapor concentration	[63, 64]
	Manometric temperature measurement (MTM)	T_b, T_{ice}	[51, 55, 65]
	Valveless monitoring system (VMS)	T_b	[66]
	Temperature measurement by sublimation rate (TMbySR)	T_b	[67]

*Many researchers have used this method to measure the product temperature. Therefore, specific literature cannot be exemplified.

for the monitoring of a single vial and batch operation. There are some scientific reports that evaluated the (dis)advantages of these techniques [56–59].

A wire thermocouple (TC), resistance thermal detectors (RTDs), and temperature remote interrogation system (TEMPRIS) are representatives of PAT tools for single vial. TC is a popular technology to monitor the temperature at the tip of the detector. However, the wire thermocouples are difficult to be adjusted at the center bottom position in the vials (group 3 in Figure 3(b)), and the T_b-profile mapping in the pilot or production lyophilizer is often not available. In addition, the biased measurement of temperature relative to vials without sensors is problematic. The same was true for RTD [60]. In order to solve these problems, TEMPRIS as a wireless temperature sensor can be remarked as an effective means. TEMPRIS is always available to be adjusted at the center bottom in the vials, and therefore, narrow variations in the T_b-profile intrabatch and interbatch are expected, and also the endpoint of primary drying is expected to be monitored correctly. In addition, the possibility to use the same sensors in the laboratory, pilot, and production lyophilizer helps us to perform scale-up experiments easily and rapidly. A TEMPRIS system for application in freeze drying is well evaluated in the previous report [60]. In the development phase of lyophilization cycle, a single vial monitoring as a PAT tool is useful since the T_b-profile mapping that includes the difference in the temperature profile of the vials placed at the center and edge position in the lyophilizer should be understood to optimize the lyophilization cycle. As discussed above, TEMPRIS is a powerful PAT method to monitor the single vial.

Batch monitoring as a PAT method is effective to monitor the designed lyophilization cycle, deepen the cycle, and perform continuous cycle improvement. Pirani gauge is usually used in the lyophilizer. This principle is to measure the thermal conductivity of the gas in the drying chamber, and nitrogen gas is used as a calibration gas [61]. It is not nitrogen gas but water vapors that are produced during the primary drying stage. For the reason, the Pirani gauge often reads approximately 60% higher than a capacitance manometer, due to approximately 1.6 times thermal conductivity of nitrogen to water vapor [62]. In addition, Pirani is then dependent on the gas composition in the chamber [61]. From the above nature, the Pirani pressure could indicate the primary drying endpoint with a sharper pressure decrease toward the capacitance manometer pressure. The mass spectrometer is a candidate PAT tool to determine the endpoint of primary drying and secondary drying. Some potential applications to pharmaceutical lyophilization are reported [63]. Tunable diode laser absorption spectroscopy (TDLAS) that can directly measure the water vapor concentration in the duct connecting the chamber and the condenser allows in-line monitoring of the dm/dt value [64]. Therefore, TDLAS is also an effective tool to estimate the K_v and R_p values in equations (1) and (3). Meanwhile, TDLAS is still now an expensive technique which is not a standard accessory with lyophilizer. Manometric temperature measure (MTM), that is a well-known technology to monitor the primary drying stage [51, 55, 65], is a technique to measure the T_b value during primary drying by isolating the valve between the chamber and the condenser within approximately 30 s to analyze the pressure rise. Notably, MTM can yield both T_{ice} and R_p. The problem in MTM is that most production-scale lyophilizers have the difficulty in isolation of the valve between the chamber and the condenser within 30 s. Besides, T_b changes cannot be monitored during the later stage of primary drying and the period of transition from primary drying to secondary drying, due to no or little pressure rise originated from the completion of the sublimation of ice.

In contrast to the difficulty in the valve operation within 30 s as claimed in the MTM system, the valveless monitoring method (VMS) has been developed [66]. The VMS is the monitoring system without a valve operation for a lab-scale lyophilizer. The dm/dt should be estimated from the variation of P_c because the sublimation of ice is followed by the release of water vapor to the interior of the equipment. From equations (1)–(3), the parameters, e.g., K_v, R_p, and T_b, are obtainable from the dm/dt. Therefore, VMS makes it possible to monitor the parameters in a noninvasive manner. Furthermore, Kawasaki and his coworkers have reported the method to determine the endpoint of the primary drying stage, based on the T_b obtainable from the dm/dt, which termed the "temperature measurement by sublimation rate (TMbySR)" [67]. The TMbySR as well as VMS is the method to monitor the T_b without a valve operation. Limited to the

lab-scale lyophilizer, TMbySR could be applicable independent of vial numbers [67].

Thus, the representative PAT tools were introduced in this section. The monitoring of specific parameters has clarified the dynamics of lyophilization to some extent. For more sophisticated monitoring, the PAT tool should be combined with the mathematical model describing the dynamics of lyophilization. In such a sense, the model-based PAT tool would be helpful for a quality management in pharmaceuticals freeze-drying, e.g., the application of these PAT tools for in-line process optimization is promising by combining with the MPC (see Section 4). Besides, the highly QbD is expected to be achieved thorough the offline calculation of the design space of the process [59].

9. Possible Innovation Required to Breakthrough

Several aspects to advance the technology in the pharmaceutical lyophilization are considered: new elemental technology, although conducted at small scale or attempted in the field other than the pharmaceutical field. For examples, a microwave-assisted freeze-drying (MFD) has been proposed in the food engineering field [79]. Freeze-drying coupled with a microwave heat source can speed up the drying rate and improve the product quality [79]. Few experiments are required to be extended from the lab-to production-scale lyophilizer; the knowledge or experiments are separated between different scales. With the goal to effectively scale-up the promising method at a lab scale, the seamless scale-up procedure would be required.

The position-dependent model based on the thermodynamics in K_v has been improved previously [54]. As long as one of the operation conditions to achieve the same dynamics of R_p between pilot- and production-scale lyophilizer, the methodology that the K_v value obtained at lab scale is transferred to the production scale should be investigated to clarify the requisite condition for using the same K_v value after scale-up procedure. The further development of scale-up theory is expected to achieve the seamless use of K_v from the lab scale to the production scale.

Reduction of the cost impact at the primary drying stage can be in principle designed based on equations (1)–(3). As evidently seen in these equations, the sublimation of ice is the important phenomena and its rate dm/dt is the most essential CPP in the primary drying stage. If not only K_v and R_p but also T_b can be calculated from dm/dt at the production scale, the operation system would be more robust. This motivation is identical to both the VMS and TMbySR in PAT tool. At present, an attempt using VMS and TMbySR has been limited to the lab scale [66, 67]. The possibility of scalable application of both methods would be required for the seamless use of K_v and R_p from the lab scale; e.g., the influence of vial number on shelves among lab, pilot, and production scales (Figure 1(b)). As stated before, the ice nucleation control based on the freezing temperature makes it possible to control the dm/dt. Therefore, the application of the above technology would afford a seamless and rapid decision-making over the freezing and drying stages. This is one of the promising operation systems for the lyophilization because the quality of products is no longer tested into them, i.e., quality-by-design.

During these years, a risk analysis for a pilot-scale freeze dryer has been reported for the construction of the basis for the risk-based decision-making in plant and process design of a freeze-dryer [80]. In the future, the PAT tool might contribute to the risk management of each scale freeze dryer. Furthermore, the PAT tool would obtain the enormous big data from the equipment at each scale [81]. Important principle might be hidden behind the big data. For effective analysis, the use of the Internet of things (IoT) together with big data from PAT tool and the models including CFD would bring the rapid decision-making well fused with the practitioner's experiences [81–84]. The author expects that the operational research based on IoT and big data will be developed to improve the accomplishment of the lyophilization, as shown in Figure 2.

Conflicts of Interest

The authors declare that they have no conflicts of interest.

References

[1] S. A. Mahdavi, S. M. Jafari, M. Ghorbani, and E. Assadpoor, "Spray-drying microencapsulation of anthocyanins by natural biopolymers: a review," *Drying Technology*, vol. 32, no. 5, pp. 509–518, 2014.

[2] GR. Nireesha, L. Divya, C. Sowmya, N. Venkateshan, M. Niranjan Babu, and V. Lavakumar, "Lyophilization/freeze drying-an review," *International Journal of Novel Trends in Pharmaceutical Sciences*, vol. 3, pp. 87–98, 2013.

[3] S. H. Peighambardoust, A. Golshan Tafti, and J. Hesari, "Application of spray drying for preservation of lactic acid starter cultures: a review," *Trends in Food Science and Technology*, vol. 22, no. 5, pp. 215–224, 2011.

[4] S. Freitas, H. P. Merkle, and B. Gander, "Ultrasonic atomisation into reduced pressure atmosphere-envisaging aseptic spray-drying for microencapsulation," *Journal of Controlled Release*, vol. 95, no. 2, pp. 185–195, 2004.

[5] P. Matejtschuk, K. Malik, and C. Duru, "Lyophilization-freeze drying of biologicals: process development to ensure biostability," *American Pharmaceutical Review*, vol. 12, pp. 54–58, 2009.

[6] M. J. Pikal, "Freeze-drying of proteins. Part I: process design," *BioPharm*, vol. 3, pp. 18–28, 1990.

[7] Y. Liu, Y. Zhao, and X. Feng, "Exergy analysis for a freeze-drying process," *Applied Thermal Engineering*, vol. 28, no. 7, pp. 675–690, 2008.

[8] S. L. Nail and L. A. Gatin, "Freeze-drying: principles and practice," in *Pharmaceutical Dosage Forms: Parenteral Medications*, K. E. Avis, H. A. Lieberman, and L. Lechman, Eds., vol. 2, pp. 163–233, Marcel Dekker, New York, NY, USA, 1993.

[9] F. Franks, "Freeze drying: from empiricism to predictability," *Cryo-Letters*, vol. 11, pp. 93–110, 1990.

[10] A. I. Liapis and R. Bruttini, "Exergy analysis of freeze drying of pharmaceuticals in vials on trays," *International Journal of Heat and Mass Transfer*, vol. 51, no. 15-16, pp. 3854–3868, 2008.

[11] S. C. Tsinontides, P. Rajniak, D. Pham, W. A. Hunke, J. Placek, and S. D. Reynolds, "Freeze drying-principles and practice for successful scale-up to manufacturing," *International Journal of Pharmaceutics*, vol. 280, no. 1-2, pp. 1–16, 2004.

[12] W. Y. Kuu, L. M. Hardwick, and M. J. Akers, "Correlation of laboratory and production freeze drying cycles," *International Journal of Pharmaceutics*, vol. 302, no. 1-2, pp. 56–67, 2005.

[13] X. Tang and M. J. Pikal, "Design of freeze-drying processes for pharmaceuticals: practical advice," *Pharmaceutical Research*, vol. 21, no. 2, pp. 191–200, 2004.

[14] S. Kamiloglu, G. Toydemir, D. Boyacioglu, J. Beekwilder, R. D. Hall, and E. Capanoglu, "A review on the effect of drying on antioxidant potential of fruits and vegetables," *Critical Reviews in Food Science and Nutrition*, vol. 56, no. 1, pp. S110–S129, 2016.

[15] D. Dehnad, S. M. Jafari, and M. Afrasiabi, "Influence of drying on functional properties of food biopolymers: from traditional to novel dehydration techniques," *Trends in Food Science and Technology*, vol. 57, pp. 116–131, 2016.

[16] N. Malekjani and S. M. Jafari, "Simulation of food drying processes by Computational Fluid Dynamics (CFD); recent advances and approaches," *Trends in Food Science and Technology*, vol. 78, pp. 206–223, 2018.

[17] International Conference on Harmonization of Technical Requirements for Registration of Pharmaceuticals for Human Use, ICH Harmonized Tripartite Guidance, Pharmaceutical Developent Q8 (R2), August 2009.

[18] S. L. Nail and J. A. Searles, "Elements of quality by design in development and scale-up of freeze-dried parenterals," *BioPharm International*, vol. 21, pp. 44–52, 2008.

[19] P. N. Ezhilarasi, P. Karthik, N. Chhanwal, and C. Anandharamakrishnan, "Nanoencapsulation techniques for food bioactive components: a review," *Food and Bioprocess Technology*, vol. 6, no. 3, pp. 628–647, 2013.

[20] S.-M. Jafari, K. Mahdavi-Khazaei, and A. Hemmati-Kakhki, "Microencapsulation of saffron petal anthocyanins with cress seed gum compared with Arabic gum through freeze drying," *Carbohydrate Polymers*, vol. 140, pp. 20–25, 2016.

[21] K. Mahdavi-Khazaei, S. M. Jafari, M. Ghorbani, and A. Hemmati-Kakhki, "Application of maltodextrin and gum Arabic in microencapsulation of saffron petal's anthocyanins and evaluating their storage stability and color," *Carbohydrate Polymers*, vol. 105, pp. 57–62, 2014.

[22] F. Franks, "Freeze-drying of bioproducts: putting principles into practice," *European Journal of Pharmaceutics and Biopharmaceutics*, vol. 45, no. 3, pp. 221–229, 1998.

[23] J. Li, T. Viverette, M. Virgin, M. Anderson, and P. Dalal, "A study of the impact of freezing on the lyophilization of a concentrated formulation with a high fill-depth," *Pharmaceutical Development and Technology*, vol. 10, no. 2, pp. 261–272, 2005.

[24] M. J. Pikal, S. Rambhatla, and R. Ramot, "The impact of the freezing stage in lyophilization: effects of the ice nucleation temperature on process design and product quality," *American Pharmaceutical Review*, vol. 5, pp. 48–53, 2002.

[25] J. M. Goldman, H. T. More, O. Yee et al., "Optimization of primary drying in lyophilization during early-phase drug development using a definitive screening design with formulation and process factors," *Journal of Pharmaceutical Sciences*, vol. 107, no. 10, pp. 2592–2600, 2018.

[26] N. Daraoui, P. Dufour, H. Hammouri, and A. Hottot, "Model predictive control during the primary drying stage of lyophilisation," *Control Engineering Practice*, vol. 18, no. 5, pp. 483–494, 2010.

[27] D. Fissore and A. A. Barresi, "Scale-up and process transfer of freeze-drying recipes," *Drying Technology*, vol. 29, no. 14, pp. 1673–1684, 2011.

[28] R. Pisano, D. Fissore, A. A. Barresi, and M. Rastelli, "Quality by design: scale-up of freeze-drying cycles in pharmaceutical industry," *AAPS PharmSciTech*, vol. 14, no. 3, pp. 1137–1149, 2013.

[29] T. Kodama, H. Sawada, H. Hosomi et al., "Optimization of primary drying condition for pharmaceutical lyophilization using a novel simulation program with a predictive model for dry layer resistance," *Chemical and Pharmaceutical Bulletin*, vol. 62, no. 2, pp. 153–159, 2014.

[30] M. J. Pikal, "Use of laboratory data in freeze drying process design: heat and mass transfer coefficients and the computer simulation of freeze drying," *Journal of Parenteral Science and Technology*, vol. 39, pp. 115–139, 1985.

[31] A. Hottot, R. Peczalski, S. Vessot, and J. Andrieu, "Freeze-drying of pharmaceutical proteins in vials: modeling of freezing and sublimation steps," *Drying Technology*, vol. 24, no. 5, pp. 561–570, 2006.

[32] J. A. Searles, J. F. Carpenter, and T. W. Randolph, "Annealing to optimize the primary drying rate, reduce freezing-induced drying rate heterogeneity, and determine T_g' in pharmaceutical lyophilization," *Journal of Pharmaceutical Sciences*, vol. 90, no. 7, pp. 872–887, 2001.

[33] M. J. Pikal, S. Shah, D. Senior, and J. E. Lang, "Physical chemistry of freeze-drying: measurement of sublimation rates for frozen aqueous solutions by a microbalance technique," *Journal of Pharmaceutical Sciences*, vol. 72, no. 6, pp. 635–650, 1983.

[34] A. I. Liapis and R. Bruttini, "Freeze-drying of pharmaceutical crystalline and amorphous solutes in vials: dynamic multi-dimensional models of the primary and secondary drying stages and qualitative features of the moving interface," *Drying Technology*, vol. 13, no. 1-2, pp. 43–72, 1995.

[35] M. J. Pikal, "Use of laboratory data in freeze drying process design: heat and mass transfer coefficients and the computer simulation of freeze drying," *Journal of Parenteral Science and Technology*, vol. 39, pp. 115–139, 1985.

[36] S. Rambhatla and M. J. Pikal, "Heat and mass transfer issues in freeze-drying process development," in *Lyophilization of Biopharmaceuticals*, H. R. Constantino, Ed., AAPS Press, Arlington, VA, USA, 2004.

[37] P. Chouvenc, S. Vessot, J. Andrieu, and P. Vacus, "Optimization of the freeze-drying cycle: a new model for pressure rise analysis," *Drying Technology*, vol. 22, no. 7, pp. 1577–1601, 2004.

[38] H. Sadikoglu, A. I. Liapis, and O. K. Crosser, "Optimal control of the primary and secondary drying stages of bulk solution freeze drying in trays," *Drying Technology*, vol. 16, no. 3-5, pp. 399–431, 1998.

[39] H. Sadikoglu, M. Ozdemir, and M. Seker, "Optimal control of the primary drying stage of freeze drying of solutions in vials using variational calculus," *Drying Technology*, vol. 21, no. 7, pp. 1307–1331, 2003.

[40] J. I. Lombraña and J. M. Díaz, "Heat programming to improve efficiency in a batch freeze-drier," *Chemical Engineering Journal*, vol. 35, no. 3, pp. B23–B30, 1987.

[41] J. Lombraña and J. Díaz, "Coupled vacuum and heating power control for freeze-drying time reduction of solutions in phials," *Vacuum*, vol. 37, no. 5-6, pp. 473–476, 1987.

[42] M. Mahmood and P. Mhaskar, "Enhanced stability regions for model predictive control of nonlinear process systems," *AIChE Journal*, vol. 54, no. 6, pp. 1487–1498, 2008.

[43] V. R. Koganti, E. Y. Shalaev, M. R. Berry et al., "Investigation of design space for freeze-drying: use of modeling for primary drying segment of a freeze-drying cycle," *AAPS PharmSciTech*, vol. 12, no. 3, pp. 854–861, 2011.

[44] W. Y. Kuu and S. L. Nail, "Rapid freeze-drying cycle optimization using computer programs developed based on heat and mass transfer models and facilitated by tunable diode laser absorption spectroscopy (TDLAS)," *Journal of Pharmaceutical Sciences*, vol. 98, no. 9, pp. 3469–3482, 2009.

[45] S. L. Nail, S. Jiaang, S. Chongprasert, and S. A. Knopp, "Fundamentals of freeze-drying," in *Development and Manufacture of Protein Pharmaceuticals*, S. L. Nail and M. J. Akers, Eds., Kluwer Academic/Plenum Publisher, New York, NY, USA, 2002.

[46] V. M. Zavala and L. T. Biegler, "Optimization-based strategies for the operation of low-density polyethylene tubular reactors: nonlinear model predictive control," *Computers & Chemical Engineering*, vol. 33, no. 10, pp. 1735–1746, 2009.

[47] A. A. Barresi, V. Rasetto, and D. L. Marchisio, "Use of computational fluid dynamics for improving freeze-dryers design and process understanding. Part 1: modelling the lyophilisation chamber," *European Journal of Pharmaceutics and Biopharmaceutics*, vol. 129, pp. 30–44, 2018.

[48] D. L. Marchisio, M. Galan, and A. A. Barresi, "Use of computational fluid dynamics for improving freeze-dryers design and process understanding. Part 2: condenser duct and valve modelling," *European Journal of Pharmaceutics and Biopharmaceutics*, vol. 129, pp. 45–57, 2018.

[49] M. J. Pikal, M. L. Roy, and S. Shah, "Mass and heat transfer in vial freeze-drying of pharmaceuticals: role of the vial," *Journal of Pharmaceutical Sciences*, vol. 73, no. 9, pp. 1224–1237, 1984.

[50] B. S. Chang and N. L. Fischer, "Development of an efficient single-step freeze-drying cycle for protein formulations," *Pharmaceutical Research*, vol. 12, no. 6, pp. 831–837, 1995.

[51] S. A. Velardi, V. Rasetto, and A. A. Barresi, "Dynamic parameters estimation method: advanced manometric temperature measurement approach for freeze-drying monitoring of pharmaceutical solutions," *Industrial and Engineering Chemistry Research*, vol. 47, no. 21, pp. 8445–8457, 2017.

[52] S. M. Patel and M. J. Pikal, "Lyophilization process design space," *Journal of Pharmaceutical Sciences*, vol. 102, no. 11, pp. 3883–3887, 2013.

[53] H. Kawasaki, T. Shimanouchi, K. Takahashi, and Y. Kimura, "Effect of controlled nucleation of ice crystals on the primary drying stage during lyophilization," *Chemical and Pharmaceutical Bulletin*, vol. 66, no. 12, pp. 1122–1130, 2018.

[54] M. J. Pikal, R. Bogner, V. Mudhivarthi, P. Sharma, and P. Sane, "Freeze-drying process development and scale-up: scale-up of edge vial versus center vial heat transfer coefficients, kV," *Journal of Pharmaceutical Sciences*, vol. 105, no. 11, pp. 3333–3343, 2016.

[55] H. Kawasaki, T. Shimanouchi, M. Yamamoto, K. Takahashi, and Y. Kimura, "Scale-up procedure for primary drying process in lyophilizer by using the vial heat transfer and the drying resistance," *Chemical and Pharmaceutical Bulletin*, vol. 66, no. 11, pp. 1048–1056, 2018.

[56] S. M. Patel and M. Pikal, "Process analytical technologies (PAT) in freeze-drying of parenteral products," *Pharmaceutical Development and Technology*, vol. 14, no. 6, pp. 567–587, 2009.

[57] N. Malik, O. Gouseti, and S. Bakalis, "Effect of freezing with temperature fluctuations on microstructure and dissolution behavior of freeze-dried high solid systems," *Energy Procedia*, vol. 123, pp. 2–9, 2017.

[58] S. Bosca, A. A. Barresi, and D. Fissore, "On the robustness of the soft sensors used to monitor a vial freeze-drying process," *Drying Technology*, vol. 35, no. 9, pp. 1085–1097, 2017.

[59] D. Fissore, "Model-based PAT for quality management in pharmaceuticals freeze-drying: state of the art," *Frontiers in Bioengineering and Biotechnology*, vol. 5, 2017.

[60] S. Schneid and H. Gieseler, "Evaluation of a new wireless temperature remote interrogation system (TEMPRIS) to measure product temperature during freeze drying," *AAPS PharmSciTech*, vol. 9, no. 3, pp. 729–739, 2008.

[61] S. L. Nail and W. Johnson, "Methodology for in-process determination of residual water in freeze-dried products," *Developments in Biological Standardization*, vol. 74, pp. 137–150, 1992.

[62] S. M. Patel, T. Doen, and M. J. Pikal, "Determination of end point of primary drying in freeze-drying process control," *AAPS PharmSciTech*, vol. 11, no. 1, pp. 73–84, 2010.

[63] J. P. Connelly and J. V. Welch, "Monitor lyophilization with mass spectrometer gas analysis," *PDA Journal of Pharmaceutical Science and Technology*, vol. 47, pp. 70–75, 1993.

[64] H. Gieseler, W. J. Kessler, M. Finson et al., "Evaluation of tunable diode laser absorption spectroscopy for in-process water vapor mass flux measurements during freeze drying," *Journal of Pharmaceutical Sciences*, vol. 96, no. 7, pp. 1776–1793, 2007.

[65] X. Tang, S. L. Nail, and M. J. Pikal, "Freeze-drying process design by manometric temperature measurement: design of a smart freeze-dryer," *Pharmaceutical Research*, vol. 22, no. 4, pp. 685–700, 2005.

[66] R. Pisano, D. Fissore, and A. A. Barresi, "Noninvasive monitoring of a freeze-drying process for tert-butanol/water cosolvent-based formulations," *Industrial and Engineering Chemistry Research*, vol. 55, no. 19, pp. 5670–5680, 2016.

[67] H. Kawasaki, T. Shimanouchi, H. Sawada, H. Hosomi, Y. Hamabe, and Y. Kimura, "Temperature measurement by sublimation rate as a process analytical technology tool in lyophilization," *Journal of Pharmaceutical Sciences*, 2019, In press.

[68] T. W. Patapoff and D. E. Overcashier, "The importance of freezing on lyophilization cycle development," *Biopharm*, vol. 15, pp. 16–21, 2002.

[69] M. J. Pikal and S. Shah, "The collapse temperature in freeze drying: dependence on measurement methodology and rate of water removal from the glassy phase," *International Journal of Pharmaceutics*, vol. 62, no. 2-3, pp. 165–186, 1990.

[70] A. Hottot, J. Andrieu, S. Vessot, E. Shalaev, L. A. Gatlin, and S. Ricketts, "Experimental study and modeling of freeze-drying in syringe configuration. Part I: freezing step," *Drying Technology*, vol. 27, no. 1, pp. 40–48, 2009.

[71] A. Hottot, J. Andrieu, V. Hoang, E. Y. Shalaev, L. A. Gatlin, and S. Ricketts, "Experimental study and modeling of freeze-drying in syringe configuration. Part II: mass and heat transfer parameters and sublimation end-points," *Drying Technology*, vol. 27, no. 1, pp. 49–58, 2009.

[72] S. Dushman and J. M. Lafferty, *Scientific Foundations of Vacuum Technique*, Wiley, New York, NY, USA, 1962.

[73] M. L. Roy and M. J. Pikal, "Process control in freeze-drying: determination of the end point of sublimation drying by an electronic moisture sensor," *PDA Journal of Pharmaceutical Science and Technology*, vol. 43, no. 2, pp. 60–66, 1989.

[74] J. A. Searles, J. F. Carpenter, and T. W. Randolph, "The ice nucleation temperature determines the primary drying rate of lyophilization for samples frozen on a temperature-controlled

shelf," *Journal of Pharmaceutical Sciences*, vol. 90, no. 7, pp. 860–871, 2001.

[75] R. Geidobler and G. Winter, "Controlled ice nucleation in the field of freeze-drying: fundamentals and technology review," *European Journal of Pharmaceutics and Biopharmaceutics*, vol. 85, no. 2, pp. 214–222, 2013.

[76] J. C. Kasper and W. Friess, "The freezing step in lyophilization: physico-chemical fundamentals, freezing methods and consequences on process performance and quality attributes of biopharmaceuticals," *European Journal of Pharmaceutics and Biopharmaceutics*, vol. 78, no. 2, pp. 248–263, 2011.

[77] A. K. Konstantinidis, W. Kuu, L. Otten, S. L. Nail, and R. R. Sever, "Controlled nucleation in freeze-drying: effects on pore size in the dried product layer, mass transfer resistance, and primary drying rate," *Journal of Pharmaceutical Sciences*, vol. 100, no. 8, pp. 3453–3470, 2011.

[78] T. H. Gasteyer, R. R. Sever, B. Hunek, N. Grinter, and M. L. Verdone, "Lyophilization system and method," Patent US20070186437, 2007.

[79] K. Fan, M. Zhang, and A. S. Mujumdar, "Recent developments in high efficient freeze-drying of fruits and vegetables assisted by microwave: a review," *Critical Reviews in Food Science and Nutrition*, 2018, In press.

[80] S. Bosca, D. Fissore, and M. Demichela, "Reliability assessment in a freeze-drying process," *Industrial and Engineering Chemistry Research*, vol. 56, no. 23, pp. 6685–6694, 2017.

[81] A. G. Dossetter, G. Ecker, H. Laverty, and J. Overington, "'Big data' in pharmaceutical science: challenges and opportunities," *Future Medicinal Chemistry*, vol. 6, no. 8, pp. 857–864, 2014.

[82] L. Richter and G. F. Ecker, "Medicinal chemistry in the era of big data," *Drug Discovery Today: Technologies*, vol. 14, pp. 37–41, 2015.

[83] S. J. Lusher, R. McGuire, R. C. van Schaik, C. D. Nicholson, and J. de Vlieg, "Data-driven medicinal chemistry in the era of big data," *Drug Discovery Today*, vol. 19, no. 7, pp. 859–868, 2014.

[84] S. J. Lusher and T. Ritschel, "Finding the right approach to big data-driven medicinal chemistry," *Future Medicinal Chemistry*, vol. 7, no. 10, pp. 1213–1216, 2015.

Hindawi
Journal of Chemistry
Volume 2019, Article ID 2903252, 10 pages
https://doi.org/10.1155/2019/2903252

Research Article

Structural and Physicochemical Characteristics of Granular Malic Acid-Treated Sweet Potato Starch Containing Heat-Stable Resistant Starch

Chinwoo Kwon,[1] Ha Ram Kim,[1] Tae Wha Moon,[1,2] Seung Hyun Lee,[3] and Chang Joo Lee[4]

[1]*Department of Agricultural Biotechnology, Seoul National University, Seoul, Republic of Korea*
[2]*Center for Food and Bioconvergence and Research Institute of Agriculture and Life Sciences, Seoul National University, Seoul 08826, Republic of Korea*
[3]*Department of Biosystems Machinery Engineering, Chungnam National University, Daejeon 34134, Republic of Korea*
[4]*Department of Food Science and Biotechnology, Wonkwang University, Iksan, Jeonbuk 54538, Republic of Korea*

Correspondence should be addressed to Chang Joo Lee; cjlee@wku.ac.kr

Received 20 September 2018; Revised 7 December 2018; Accepted 24 December 2018; Published 23 January 2019

Guest Editor: Toshinori Shimanouchi

This study investigated the structural and physicochemical characteristics of malic acid-treated sweet potato starch. Sweet potato starch mixed with various concentrations of malic acid solution underwent either thermal or nonthermal treatment. Observation of samples under a light microscope ensured the maintenance of granular shape and the Maltese cross. FT-IR spectra displayed a distinct carbonyl peak at 1722 cm^{-1}, and analysis of the degree of substitution (DS) indicated an increase in the extent of ester bonds with increasing concentrations of malic acid. The DS of 2.0M-130 (0.214) was the highest and that of 0.5M-130 was the lowest (0.088) among the reacted starches. In vitro digestion test revealed an increased amount of resistant starch when a high concentration of malic acid was used. In addition, thermally treated samples maintained a higher content of resistant starch (RS) after 30 min of cooking at 100°C. After cooking, 2.0M-130 had an RS fraction of 53.4% which was reduced to 49.9% after cooking, revealing greater heat stability compared with nonthermally treated samples. The structure of malic acid-treated starch was investigated using a differential scanning calorimeter (DSC), an X-ray diffractometer, a rapid visco analyzer (RVA), and analysis of apparent amylose content. The results showed that thermal and malic acid treatment of starch caused not only partial hydrolysis but also rearrangement of the crystalline area and helix structure of starch by esterification. Analysis of malic acid-treated starch, using a rapid visco analyzer showed no pasting properties, due to lack of its swelling caused by the malic acid cross link.

1. Introduction

Starch is used in many kinds of food and serves as a major source of energy for humans. For nutritional purposes, starch can be classified into three categories based on the rate of its enzymatic digestion: rapidly digestible starch (RDS), slowly digestible starch (SDS), and resistant starch (RS) [1]. RS is also defined as the sum of starch and degraded starch products that resist digestion in the small intestine of healthy people [2]. The RS content of starch is affected by the amylose/amylopectin ratio, physical form, degree of gelatinization, storage, and thermal treatment [3, 4]. Depending on the cause of resistance, RS can be further divided into five categories [5, 6]: RS1, physically inaccessible starch due to entrapment; RS2, raw starch granules with crystallinity; RS3, retrograded starch; RS4, chemically modified starch; and RS5, amylose-lipid complexes. Chemical modification has been known to not only raise in vitro digestion resistance of starches, reducing postprandial glucose and insulin concentration, but also maintain sensory attributes of the final foods [7]. Degradation of RS in the large intestine has physiological

benefits, including the stimulation of intestinal bacterial activity by prebiotic effect leading to the microbial fermentation and production of short-chain fatty acids, which eventually decrease the pH in colon [6]. Upadhyaya, et al. [8] had reported that consumption of RS4 led to an abundance of *Bifidobacterium adolescentis*, *Parabacteroides distasonis*, and *Christensenella minuta* in the gut. In addition, RS also has health beneficial effects such as prevention of colon cancer, hypoglycemic effects, hypocholesterolemic effects, and inhibition of fat accumulation [9, 10].

Polyfunctional carboxylic acids such as malic, tartaric, citric, and glutaric acid have been used in the synthesis and rheological characterization of hydrogels [11]. Xie and Liu [12] used citric acid and high temperature to increase the RS content of corn starch. Compared to inorganic acids, citric acid is nutritionally harmless, and increasing the degree of substitution (DS) of starch by ester bond with the citrate decreased the rate of digestion by pancreatin [9, 13]. Kim et al. [14] reported that glutaric acid treatment at 115°C affected the structural and digestion properties of adley starch but lost the Maltese cross pattern in its granule. Studies on citric acid-rice starch by Shin et al. [15] showed that acid treatment hydrolyzed the branching points of amylopectin, leading to an increased apparent amylose content. According to Kim and Shin [9], a structural difference, such as in the number of carboxyl groups, can affect the physicochemical properties of starch. However, the cross-linking capability of malic acid, in reference to starch, has not yet been reported. Malic acid is a C4 carboxylic acid with two carboxyl groups, comprising 69%–92% of all organic acids in grape berries and leaves [16]. It is also naturally produced by many organisms without showing any nutritional harm. The U.S. Food and Drug Administration classifies malic acid as "generally recognized as safe (GRAS)," and Food Chemicals Codex (FCC) specifications list DL-malic acid as a food-grade organic acid [17]. In industries, Malic acid has been used as food additive in the United States and European Union.

Sweet potato, *Ipomoea batatas*, is a creeping dicotyledonous plant belonging to the Convolvulaceae family. Sweet potato has been a traditional source of starch in Asian countries and is one of the world's most important food crops used as an ingredient in various products such as noodles, breads, and cakes [18]. The potential supply of sweet potato starch is exhaustive and cost-efficient. In addition, its components such as dietary fiber, carotenoids, vitamins, and minerals are health beneficial [19]. Therefore, industrial interest is highly focused on the use of native and modified sweet potato starch. Consequently, extensive research regarding the chemical/physical/enzymatic modifications of sweet potato starch should be performed to deepen the understanding of its functional properties.

The purposes of this study were to produce sweet potato starch with low digestion property and heat stability by malic acid treatment as well as to assess its physicochemical properties, maintaining granule shape.

2. Materials and Methods

2.1. Materials. Sweet potato starch was purchased from Seoahn Co. (Buan, Jeollabuk-do, Korea) and DL-malic acid (M1210) was from Sigma Aldrich (St. Louis, MO, USA). The enzymes used in starch digestion were porcine pancreatin (P7545, activity 8 × USP/g, Sigma) and amyloglucosidase (AMG 300L, activity 300 AGU/mL, Novozymes, Bagsvaerd, Denmark).

2.2. Preparation of Malic Acid-Treated Starch. DL-malic acid was dissolved in water to prepare solutions of various concentrations (0.5, 1.0, 1.5, and 2.0 M) with pH adjusted to 3.5 by 10 M NaOH. Sweet potato starch (20 g) and 20 mL of different concentrations of malic acid solution were mixed and kept in a stainless-steel bowl for 16 h at room temperature. The bowls were then placed in an air-drying oven at 50°C for 24 h. The dried mixture was ground and placed either in an air-drying oven at 130°C or at room temperature for 12 h. It was washed thoroughly with distilled water to remove unreacted malic acid, dried in an air drying oven at 50°C, and ground. Samples were named according to their processing condition in the concentration-temperature format. A starch sample, which underwent the same procedure with distilled water (DW-130) and with 2.0 M malic acid solution at 25°C for 16 h (2M-25), was used as the control.

2.3. Optical Microscopy. Malic acid-treated starches were observed under a light microscope (CSB-HP3, Sam Won Scientific, Seoul, Korea) with and without a polarizing plate. Glycerol was used to disperse the sample on a glass slide with minimal air bubbles. A digital camera (Nikon, Tokyo, Japan) was used to take the photographs.

2.4. Fourier Transform-Infrared Spectroscopy (FT-IR). FT-IR spectra (VERTEX80v; Bruker, Billerica, MA, USA) were used to obtain the IR spectra. The spectra were measured ranging from 4000 to 600 cm^{-1}, in the transmission mode, at a resolution of 4 cm^{-1} and normalized using the 1315 cm^{-1} peak of starch CH_2 vibrations. The samples were diluted with KBr (1 : 100, v/v) before acquisition.

2.5. Degree of Substitution (DS). Degree of substitution was determined to estimate the average number of hydroxyl groups substituted with malic acid per anhydroglucose unit in starch. The measurement was performed following the method of by Xu et al. [20], with some modifications. Malic acid-treated starch (0.5 g) was placed in a 250 mL glass beaker with 50 mL of distilled water. The pH was measured after stirring the mix for 1 h at 30°C. To each beaker, 25 mL of 0.5 *N* NaOH was added to release the substituted groups from the malic acid-treated starch, and the solution was stirred for 24 h at 50°C. The excess NaOH was titrated back to original pH with 0.05 *N* HCl. DS was calculated as follows:

$$\mathrm{DS} = \frac{162 \times \left(N_{\mathrm{NaOH}} \times V_{\mathrm{NaOH}} - N_{\mathrm{HCl}} \times V_{\mathrm{HCl}}\right)}{1{,}000 \times W - 116.09 \times \left(N_{\mathrm{NaOH}} \times V_{\mathrm{NaOH}} - N_{\mathrm{HCl}} \times V_{\mathrm{HCl}}\right)}, \quad (1)$$

where DS is the degree of substitution, W is the sample weight (g), N_{NaOH} is the normality of NaOH, V_{NaOH} is the volume of NaOH, N_{HCl} is the normality of HCl, 161 is glucose molecular weight, 116.09 is malic acid molecular weight used to back titrate, and V_{HCl} is the volume of HCl used for back titration.

2.6. In Vitro Digestibility. In vitro digestibility was measured following the method of Englyst et al. [1] with slight modifications by Shin et al. [15]. To prepare enzyme solutions, porcine pancreatin (2 g) was added to 24 mL distilled water in a 50 mL glass beaker and stirred for 10 min. The solution was then centrifuged at 1500 × g, for 10 min at 4°C, to obtain a cloudy supernatant. The supernatant (20 mL) was mixed with 0.4 mL of amyloglucosidase and 3.6 mL of distilled water. To a 2 mL microtube with 30 mg of starch sample, 0.75 mL of sodium acetate buffer (0.1 M, pH 5.2) and a glass bead were added and either cooked for 30 min or not cooked at all. After cooling the tube to 37°C, 0.75 mL of the enzyme solution was added and incubated in a shaking incubator (240 rpm). The tubes were taken out after 10 and 240 min, boiled for 10 min in a heating block to stop the reaction, and cooled to room temperature. The tubes were centrifuged at 5000 × g, for 10 min at 4°C. The amount of glucose in the supernatant was measured by the GOD-POD kit (Embiel Co., Gunpo, Korea). The amount of glucose after 10 min of enzyme reaction at 37°C indicated RDS and that obtained after incubation for 10–240 min was SDS. RS was the starch not hydrolyzed after 240 min of incubation.

2.7. X-Ray Diffraction. X-ray diffraction analysis was performed using an X-ray diffractometer (D8 ADVANCE with DAVINCI, Bruker, Karlsruhe, Germany) operating at 40 kV and 40 mA producing CuK_{α} radiation of 1.5418 Å wavelength, scanning through the 2θ range of 3–30°, and having a step time of 0.5 sec. The relative crystallinity was calculated using the software developed by the instrument manufacturer (EVA, 2.0).

2.8. Thermal Properties. Thermal properties were determined using a differential scanning calorimeter (Pyris Diamond DSC, Perkin-Elmer, Waltham, MA, USA). Distilled water (40 μL) was added to 10 mg of the sample in a stainless-steel DSC pan and sealed. The pan was kept at room temperature for more than 4 h for equilibration and uniform mixing. The sample pan was heated gradually from 30°C to 130°C at 5°C/min with an empty pan as the reference. To avoid condensation during the scan, dry nitrogen was flushed in the space surrounding the sample chamber. Onset (T_o), peak (T_p), and conclusion (T_c) temperatures, as well as gelatinization enthalpies (ΔH), were measured using the Pyris software.

2.9. Apparent Amylose Content. Apparent amylose content was measured according to the colorimetric method outlined by the AACC International Approved Method 61–03 [21]. The samples (20 mg) were precisely weighed in 15 mL tubes and dispersed with 200 μL of absolute ethanol. The tubes were boiled for 10 min after adding 1.8 mL of 50% NaOH. The cooled solution (1 mL) was placed in each tube with 9 mL of distilled water. Diluted sample solutions were put into a 15 mL tube containing 9 mL of distilled water and 100 μL of 1 N acetic acid. Lugol solution (200 μL; 0.2% I_2 + 2.0% KI, Sigma) was added and kept in dark for 20 min. Absorbance of the colored sample solution was measured at 620 nm.

2.10. Pasting Properties. A Rapid Visco Analyzer (RVA-3D, Newport Scientific, Warriewood, Australia) was used to investigate the pasting properties of sweet potato starch and malic acid-treated starch. For each analysis, 2.5 g of starch was added to an RVA canister with 25 mL of distilled water. The measurement followed the AACC standard method 2, which includes a 23 min heating and cooling profile.

2.11. Statistical Analyses. All experiments were triplicated, and the mean values and standard deviations are reported. Duncan's multiple range test was used to analyze the variance and the mean separations ($p < 0.05$). The statistical analyses were conducted using SPSS for Windows 22.0 software (IBM, Armonk, NY, USA).

3. Results and Discussion

3.1. Photomicrographs. The granular shape of the various malic acid-treated starch samples was investigated using a light microscope (Figure 1). The shape of starches including the malic acid-treated samples had round, semioval, oval spherical, and round polygonal shapes, which was consistent with preivious studies [19, 22]. The malic acid-treated starch granules were not ruptured even at malic acid concentrations as high as 2.0 M. According to Hirashima et al. [23], granules of starch were all broken at pH below 3.0, when more glucose chains were observed, compared to those in higher pH-treated samples. However, in the range of pH 4.0–6.0, the granule shape was retained while at pH above 3.5, less glucose chains leached out, and less fracture of starch granules occurred [23]. Beyond pH 3.5, the granular shape of the malic acid-treated starches was not ruptured, despite the high concentration of malic acid. The Maltese cross was observed using a polarizing plate, confirming the inner ordered semicrystalline structure and radially ordered alignment of amylose and amylopectin [14, 24]. All samples showed the Maltese cross, implying that the regular ordered inner structure of starch was mostly retained even after the thermal treatment in the presence of malic acid. Therefore, it

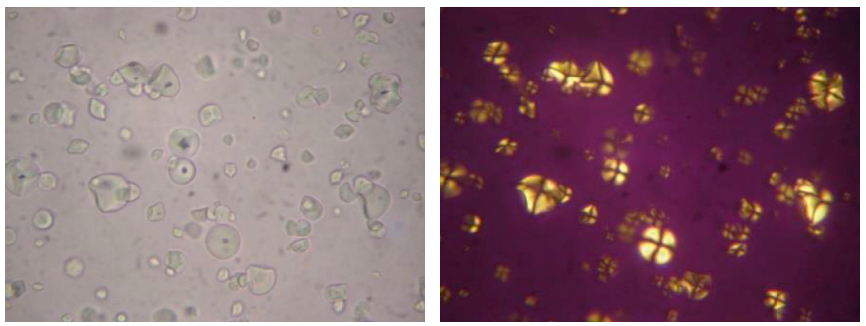

(a)

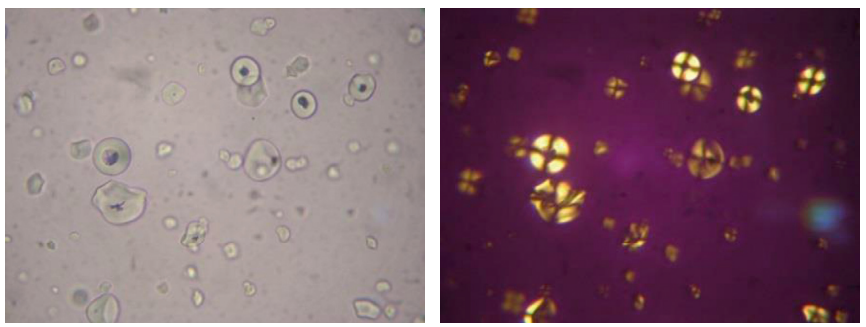

(b)

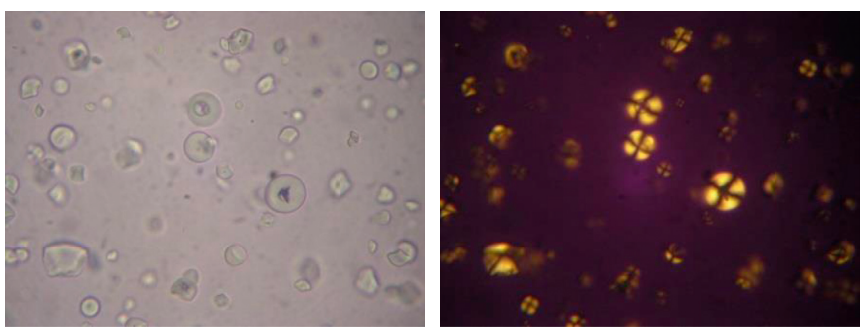

(c)

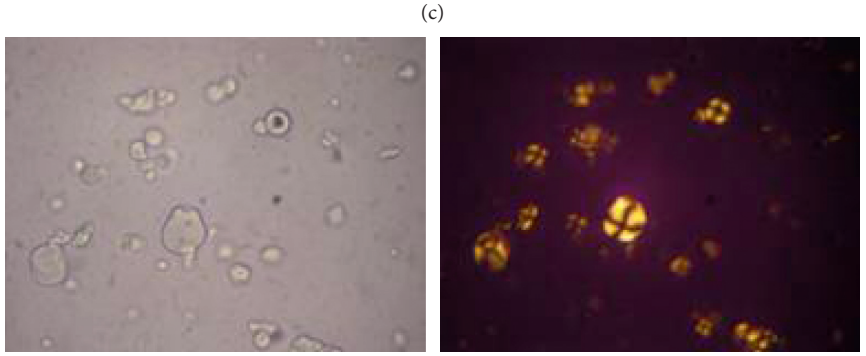

(d)

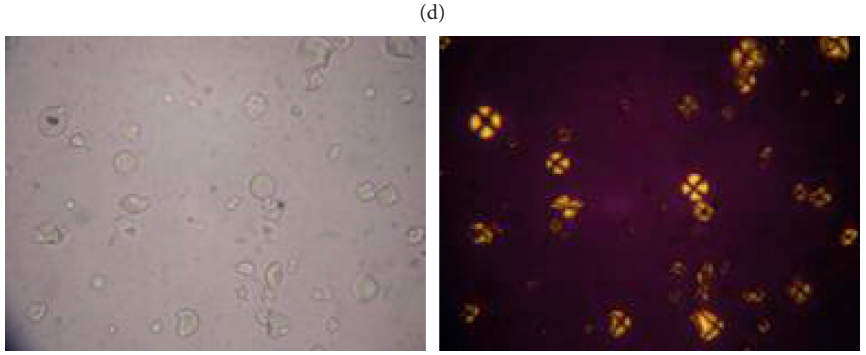

(e)

Figure 1: Continued.

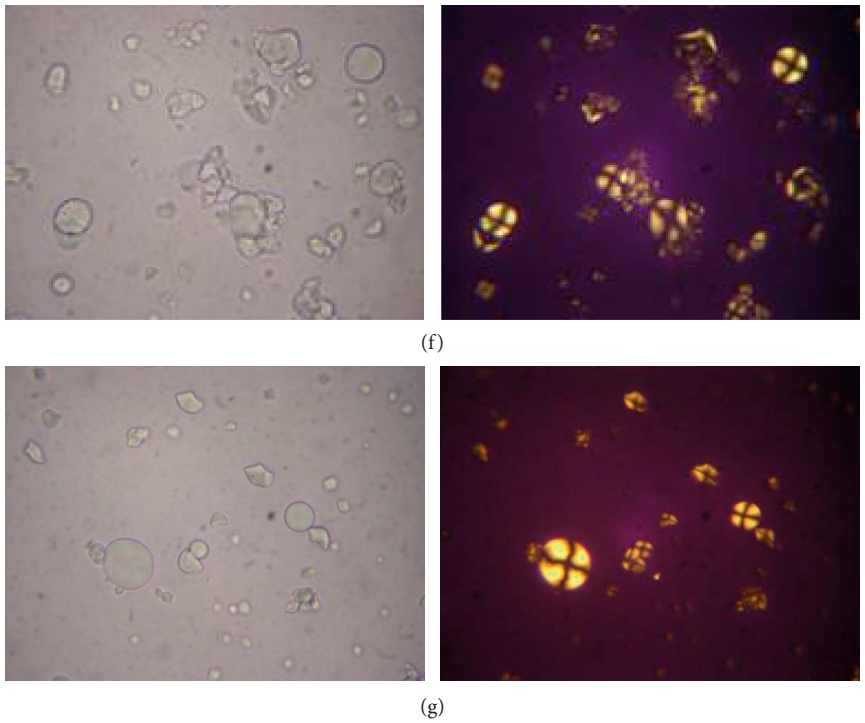

Figure 1: Light micrographs of raw and malic acid-treated sweet potato starches (magnification 400×): (a) raw, (b) 2.0M-25, (c) DW-130, (d) 0.5M-130, (e) 1.0M-130, (f) 1.5M-130, and (g) 2.0M-130; 1-under visible light and 2-under polarized light.

could be assumed that the changes observed were caused not by the change of granular shape but by the effect of malic acid on the inner structure of starch.

3.2. FT-IR. FT-IR spectroscopy can determine the structural characteristics, in terms of the functional groups in malic acid-treated starches. The peak in the range of 3000 to 3500 cm^{-1} indicates the presence of hydroxyl groups in starch, and the one at 2930 cm^{-1} indicates C-H bond stretching [25]. The peak between 980 and 1200 cm^{-1} can be attributed to C-O stretching vibration [26]. The peak near 1730 cm^{-1} is a carbonyl peak [14, 27], and the starches that reacted with malic acid at 130°C commonly had a remarkable carbonyl peak at 1722 cm^{-1} regardless of malic acid concentration (Figure 2). However, the starches kept at room temperature for 12 h, or at 130°C without malic acid, had no carbonyl peak. These results could be explained by the destruction of some parts of inter- and intramolecular hydrogen bonds by heat, thereby leading to the formation of an ester bond between starch and malic acid. The peak intensity of thermally treated samples with a higher concentration of malic acid was higher compared with those with low concentration of malic acid as shown in Figure 2. This intensity appeared to be highly correlated to both degrees of substitution and RS content of malic acid-treated starch. As the peak intensity of samples increased, the content of RS also gradually increased ($p < 0.05$). The RS content of DW-130 and 2.0M-130 were 27.0% and 53.4%, respectively. This result was consistent with the report on glutarate-treated starch by Kim et al. [14].

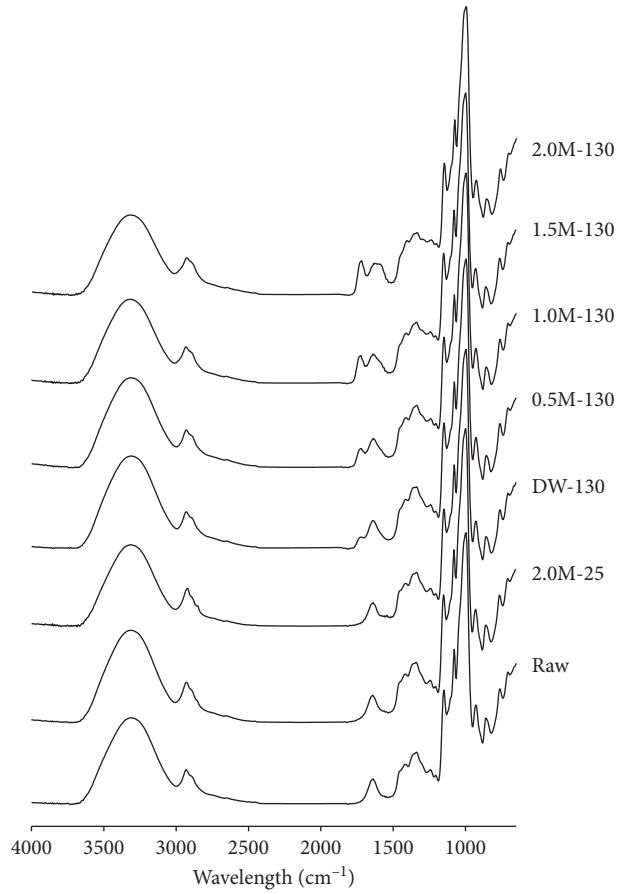

Figure 2: FT-IR spectra of raw and malic acid-treated sweet potato starches.

Table 1: Degree of substitution and in vitro digestibility of raw and malic acid-treated sweet potato starches.

Sample	DS	Noncooked starch			Cooked starch		
		RDS (%)	SDS (%)	RS (%)	RDS (%)	SDS (%)	RS (%)
Raw	n/d	14.5 ± 1.20^{a}	52.9 ± 4.20^{d}	32.6 ± 3.07^{bc}	59.6 ± 5.90^{c}	19.8 ± 2.45^{d}	20.6 ± 3.52^{a}
2.0M-25	n/d	15.5 ± 0.25^{a}	55.2 ± 2.41^{d}	29.3 ± 2.24^{ab}	67.9 ± 3.38^{de}	13.7 ± 4.04^{c}	18.4 ± 0.80^{a}
DW-130	n/d	21.1 ± 0.73^{b}	51.8 ± 1.76^{d}	27.0 ± 1.79^{a}	71.8 ± 3.71^{e}	8.67 ± 3.65^{b}	19.5 ± 1.16^{a}
0.5M-130	0.088 ± 0.0068^{a}	36.4 ± 1.53^{c}	28.7 ± 1.19^{c}	34.9 ± 1.51^{c}	69.9 ± 1.79^{e}	3.57 ± 2.65^{ab}	26.6 ± 4.27^{b}
1.0M-130	0.127 ± 0.0094^{b}	48.5 ± 2.73^{e}	12.8 ± 0.87^{b}	38.7 ± 1.86^{d}	64.0 ± 0.31^{cd}	1.83 ± 0.69^{a}	34.2 ± 0.96^{c}
1.5M-130	0.184 ± 0.0058^{c}	46.9 ± 1.16^{e}	6.63 ± 1.86^{a}	46.5 ± 2.83^{e}	52.8 ± 1.55^{b}	3.87 ± 2.61^{ab}	43.3 ± 1.93^{d}
2.0M-130	0.214 ± 0.0029^{d}	41.9 ± 0.74^{d}	4.72 ± 0.70^{a}	53.4 ± 0.69^{f}	45.2 ± 0.84^{a}	4.86 ± 2.39^{ab}	49.9 ± 2.57^{e}

DS, degree of substitution; RDS, rapidly digestible starch; SDS, slowly digestible starch; RS, resistant starch; n/d, not detected. The values with different superscripts in each column are significantly different ($p < 0.05$) by Duncan's multiple range test.

3.3. Degree of Substitution (DS). The DS of thermally treated samples is shown in Table 1. The value increased with the concentration of malic acid. While 2.0M-130 had the highest DS value of 0.214, 0.5M-130 had the lowest DS (0.088) among the malic acid-treated starches. This substitution level was much higher than that in citric acid-substituted starches (0.027), reacted at 128.4°C for 13.8 h [15]. DS is generally related to the number of carboxyl groups in organic acids and the steric hindrance between them, which can interrupt the ester bond formation. For example, acetic acid, which has only one carboxylic group and smaller molecular size compared to other organic acids, has the ability to reach a high substitution level [20]. Malic acid, which has two carboxyl groups, can theoretically form two ester bonds, whereas citric acid can make three ester bonds.

3.4. In Vitro Digestion of Samples. Table 1 presents the proportion of RDS, SDS, and RS fractions. The concentration gradient of malic acid without thermal treatment showed no significant difference in RS content (data not shown). Regarding the digestibility of DW-130, raw, and 2.0M-25, there were no significant differences between RS and SDS content, but a difference was observed in RDS, which could have been due to the high heat treatment. On the other hand, thermal treatment along with malic acid increased the content of RS. Thermally and malic acid-treated starch showed an increased RS content from 27.0% (DW-130) to 53.4% (2.0M-130). The DS of substituted starches and RS fractions were highly correlated ($r = 0.967$, $p < 0.01$). In addition, malic acid and heat treatment decreased SDS from 51.8% (DW-130) to 4.72% (2.0M-130) depending on the concentration of the malic acid solution. However, the content of RDS was the highest in 1.0M-130 (48.5%) and decreased with increasing concentrations of malic acid. This result suggested that some parts of the amylose and amylopectin structure were destroyed under acidic heating conditions so the RDS fraction increased until 1.0M-130 but the other part forming ester bonds with malic acid became the RS fraction. According to Huber & BeMiller [28], the more the cross-linked starch, the more the entry of α-amylase molecules through the starch porous channel inhibited, and hence, more resistance to digestion. Therefore, as the DS of malic acid-treated starch increased, intrusion of α-amylase was inhibited by the ester bond between malic acid and starch chain. However, if the cross link fully blocked α-amylase intrusion, there should be no increase of RDS. The interference of cross links in the complexation of α-amylase and starch might be another reason for the increased RS [9, 29]. Despite the diffusion of α-amylase after granule intrusion, the cross-linked part of starch chain resists digestion.

Since the starch used in food industry usually undergoes a cooking step, high heat treatment could possibly destroy the ester bond, thereby decreasing RS. Digestion fractions of cooked samples were also investigated. Apart from the nonreacted starches that showed considerable decrease in RS content, 2.0M-130 had 49.9% of RS fraction, which reduced from 53.4%. Other malic acid-treated starches also had decreased RS content but they were still highly correlated with the DS ($r = 0.983$, $p < 0.01$). The proportion of the RS fraction of DW-130 samples decreased from 27.0% to 19.5% upon cooking. The cooking procedure changed the RS proportions drastically from that of the nonthermally treated samples, whereas the thermally malic acid-treated samples had high content of heat-stable RS in high amount, which indicates the presence of a rigid ester bond.

3.5. X-Ray Diffraction. The X-ray diffraction patterns are shown in Figure 3. The internal order of a starch granule is demonstrated by X-ray diffraction patterns of *A*, *B*, and *C* types [30]. Native sweet potato starch showed the *C*-type pattern with diffraction intensities at 5.6°, 11.5°, 15.3°, 17.4°, 23.2°, and 26.3° at the angle 2θ. *C*-type starches have been subclassified into C_a, C_b, and C_c on the basis of their resemblance to either A-type, B-type, or that between A-type and B-type, respectively [31], and the sweet potato starch used in this study belonged to the C_b-type. Malic acid-treated starches maintained the same X-ray diffractograms, but with differences in crystallinity and peak intensity. As the concentration of malic acid solution increased, the peak intensity and crystallinity decreased (DW-130; 27.9%, 2M-130; 17.6%), indicating the influence of heat-moisture treatment and the possibility of acid hydrolysis. The decreased crystallinity of DW-130 was seemed to be caused by the heat-moisture treatment. Lee et al. [32] reported that hydrothermal treatment decreased the major peaks' intensities and their crystallinity. The crystallinity of malic acid-treated samples was lower than that of raw starch

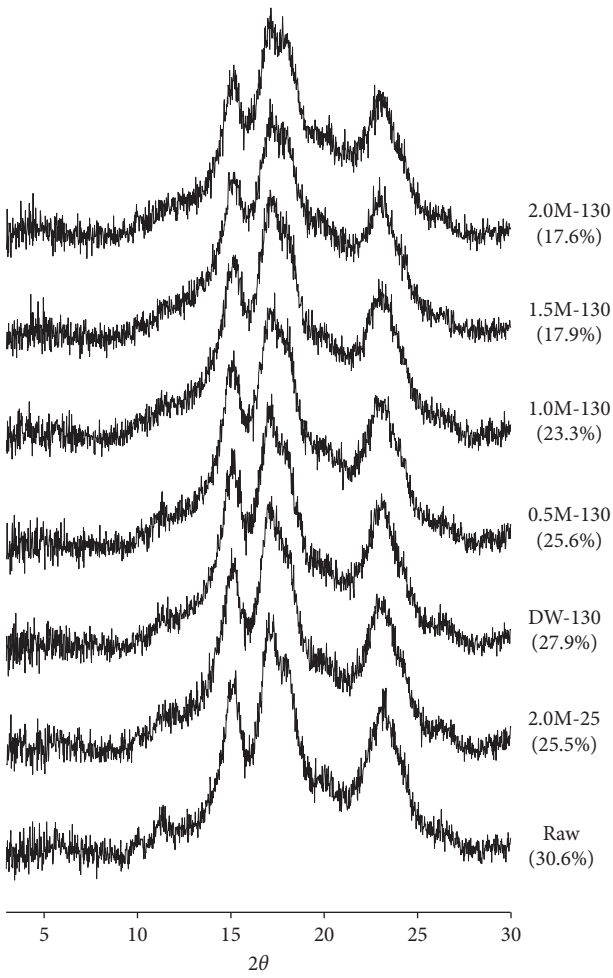

Figure 3: X-ray diffraction patterns and relative crystallinity of raw and malic acid-treated sweet potato starches. Numbers in parentheses indicate the percentage of crystallinity.

due to acid hydrolysis and heat treatment during preparation. This result was consistent with the report on glutarate-treated starch by Kim et al. [14] and citrate-treated starch by Xie et al. [33]. Hydrogen bonds are known to sustain a double helical structure, but when substituted by ester bonds, changes in double helical structure induce rearrangement of the crystalline and semicrystalline structure, hence lowering relative crystallinity.

3.6. Gelatinization Parameters. The gelatinization parameters of various malic acid-treated starches are shown in Table 2. Raw and 2.0M-25 samples had no significant difference in the T_o, T_p, T_c, ΔH, and even $T_c - T_o$. However, DW-130 had lower T_o (57.7), T_p (66.6), T_c (71.3), and $T_c - T_o$ (14.9), and higher ΔH (13.6), which could have resulted from the heat-moisture treatment. Increasing the concentration of malic acid decreased T_o, T_p, T_c, and ΔH, but increased $T_c - T_o$. Consequently, 2.0M-130 had lower T_o (44.0), T_p (50.8), T_c (62.0), and ΔH (2.89) and higher $T_c - T_o$ (18.1) compared with other samples. DSC measures the primary hydrogen bonds that stabilize the double helices within the granules [34] and the quality and quantity of crystalline area by measuring the change in heat energy [30]. The decreased T_o, T_p, T_c, ΔH, and increased $T_c - T_o$, in this study, suggested that the internal crystalline structure and helical structure of the malic acid-treated starch could have been disrupted and become a heterogeneous structure with rearrangement compared to the unmodified starches. If most of the crystalline area was destroyed, no peak would be expected in the X-ray diffractogram; however, the X-ray diffraction patterns of malic acid-treated starch were almost the same as those of raw starch and nonthermally treated starches. Therefore, malic acid, which penetrated into starch granules, may have not only partially hydrolyzed the starch chain into shorter chains, but also rearranged the crystalline structure of the granules by substituting the hydrogen bonds with ester bonds. With increased short chain, melting temperature decreased, which could be highly related to the decrease of SDS and increase of RDS. Decrease of ΔH corresponds to a reduced amount of hydrogen bonds and is related to increased DS and a higher fraction of heat-stable RS.

3.7. Apparent Amylose Content. The apparent amylose contents of various malic acid-treated starches are presented in Table 3. Compared to the raw and nonthermal group, samples with high DS values showed decreased apparent amylose content. Apparent amylose contents of 2.0M-25 and DW-130 showed no significant difference with raw starch ($p > 0.05$). However, the increasing concentration of malic acid with heating decreased the apparent amylose content of the samples and that of 2.0M-130 was the lowest (20.7%). The citric acid-treated starch had increased amount of apparent amylose content with the same treatment because of the hydrolysis, which mainly occurred at the branching point [15], but the opposite trend was observed in this study. Mussulman and Wagoner [35] and Robin et al. [36] suggested that acid hydrolysis mainly occurred during the conditioning step. However, structural analyses showed that most of the starch chain breakdown occurred during the heating step under the influence of both acid and heat. Consequently, the decline of apparent amylose content was due to the rearrangement of the starch helix by the ester bond upon malic acid treatment, and there could be increased amount of short chains due to hydrolysis, which are too short to form the iodine complex.

3.8. Pasting Properties. The pasting properties of raw and malic acid-treated starches are shown in Figure 4. The use of thermal treatment with malic acid can lead to lower peak viscosity because of less swollen granules. Cross-linked starches reacted under low pH conditions are reported to have reduced swelling power [37]. Starch samples, which were only conditioned in malic acid solution (2.0M-25), showed a similar RVA curve with raw starch. Raw starch and 2.0M-25 had peak viscosity at 88.3°C and also had similar setback viscosity. As DW-130 indicated changes in structure which seemed to be the effect of slight the heat-moisture treatment, lower peak viscosity, and setback viscosity were detected by RVA, which could also be due to the effect of heat-moisture treatment. Malic acid-treated starches had

Table 2: Gelatinization parameters of raw, control, and malic acid-treated starches.

Sample	T_o (°C)	T_p (°C)	T_c (°C)	$T_c - T_o$ (°C)	ΔH (J/g)
Raw	60.5 ± 0.28^{e}	68.2 ± 0.07^{f}	72.4 ± 1.59^{d}	11.9 ± 1.83^{a}	16.1 ± 0.89^{d}
2.0M-25	60.7 ± 0.21^{e}	68.2 ± 0.16^{f}	72.6 ± 0.37^{d}	11.8 ± 0.31^{a}	16.6 ± 0.46^{d}
DW-130	57.7 ± 0.13^{d}	66.6 ± 0.31^{e}	71.3 ± 0.64^{d}	13.6 ± 0.77^{ab}	14.9 ± 0.66^{d}
0.5M-130	52.4 ± 0.19^{c}	63.9 ± 0.25^{d}	68.4 ± 0.26^{c}	16.0 ± 0.33^{bc}	12.1 ± 1.63^{c}
1.0M-130	46.0 ± 0.10^{b}	60.1 ± 0.48^{c}	65.3 ± 0.36^{b}	19.4 ± 0.26^{c}	10.5 ± 1.54^{c}
1.5M-130	45.4 ± 0.73^{ab}	53.0 ± 0.47^{b}	63.5 ± 0.19^{ab}	18.2 ± 0.73^{c}	7.50 ± 1.07^{b}
2.0M-130	44.0 ± 2.04^{a}	50.8 ± 1.02^{a}	62.0 ± 2.46^{a}	18.1 ± 4.34^{c}	2.90 ± 0.72^{a}

T_o, onset temperature; T_p, peak temperature; T_c, conclusion temperature; $T_c - T_o$, temperature range of crystal melting; ΔH, enthalpy change. The values with different superscripts in each column are significantly different ($p < 0.05$) by Duncan's multiple range test.

Table 3: Apparent amylose content of raw and malic acid-treated sweet potato starches.

Sample	Apparent amylose content (%)
Raw	26.9 ± 0.75^{d}
2.0M-25	26.4 ± 0.59^{cd}
DW-130	26.4 ± 0.13^{cd}
0.5M-130	25.4 ± 0.63^{c}
1.0M-130	23.0 ± 0.68^{b}
1.5M-130	23.6 ± 0.65^{b}
2.0M-130	20.7 ± 0.42^{a}

The values with different superscripts in each column are significantly different ($p < 0.05$) by Duncan's multiple range test.

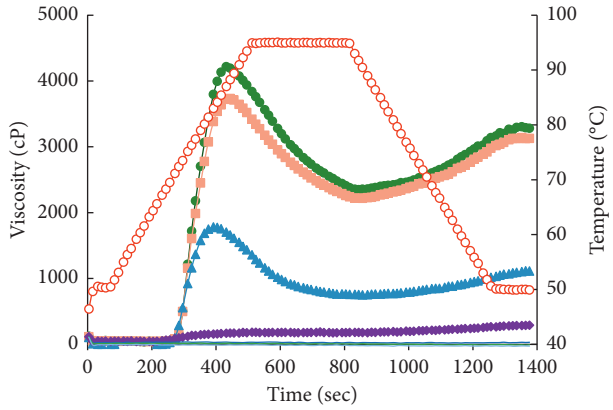

Figure 4: Rapid visco analyzer: raw and malic acid-treated sweet potato starches: ●, raw starch; ■, 2.0M-25; ▲, DW-130; ♦, 0.5M-130; —, 1.0M-130, 1.5M-130, 2.0M-130; ○, temperature.

lower and linear RVA profiles (1.0M-130, 1.5M-130, and 2.0M-130). This result was similar to the dramatically decreased pasting viscosity and linear RVA curve of citric acid-treated starch due to its nonswelling property [12]. The higher the concentration of malic acid solution used, the lesser the viscosity observed. Shukri and Shi [38] had reported that high level of cross-linking inhibits the swelling of starch granules because of less hydrogen bonding between the helical structures in starch. Similar to the previous studies on citrate and acetate starches that reported increased stability of cooked starch as compared to native starch [37], malic acid-treated starch with high DS also showed heat-stability not only toward gelatinization but also toward retrogradation due to the malic acid cross link.

4. Conclusions

Heat treatment with a high concentration of malic acid solution on sweet potato starch caused considerable changes in the internal structure of starch maintaining its granular shape. Moreover, DS values and FT-IR spectra showed ester bond formation between malic acid and the starch. The RS fraction of sweet potato starch drastically increased with the ester bond formation, and these RS fractions had remarkable heat-stable characteristics. Structural analyses by light microscopy, XRD, DSC, RVA, and AAC obviously demonstrated a low degree of hydrolysis in starch chains (even at pH 3.5 of malic acid solution) upon thermal treatment with malic acid and rearrangment of the crystalline area and alterations of the double helix by the substitution of the hydrogen bond by an ester bond. Rapid visco analyzer (RVA) showed no pasting property of malic acid-treated starches due to its nonswell properties caused by the malic acid cross-link. This information about the structural characteristics and heat-stable properties of RS in digestion can be used to develop a low-digestible food ingredient and lead to further application of the study.

Data Availability

The data used to support the findings of this study are available from the corresponding author upon request.

Disclosure

This article is based on the thesis submitted by Chinwoo Kwon as part of the requirements for his master's degree at Seoul National University [39].

Conflicts of Interest

The authors declare that they have no conflicts of interest regarding the publication of this article.

Acknowledgments

This work was supported by the National Research Foundation of Korea (NRF) grant funded by the Korean government (MSIP) (no. NRF-2016R1C1B2015506).

References

[1] H. N. Englyst, S. M. Kingman, and J. H. Cummings, "Classification and measurement of nutritionally important starch fractions," *European Journal of Clinical Nutrition*, vol. 46, no. 2, pp. S33–S50, 1992.

[2] I. Goñi, L. García-Diz, E. Mañas, and F. Saura-Calixto, "Analysis of resistant starch: a method for foods and food products," *Food Chemistry*, vol. 56, no. 4, pp. 445–449, 1996.

[3] D. Sievert and Y. Pomeranz, "Enzyme-resistant Starch 1. Characterization and evaluation by enzymatic, thermoanalytical, and microscopic methods," *Cereal Chemistry*, vol. 66, pp. 342–347, 1989.

[4] J. Tovar, *Bioavailability of starch in processed legumes*, Ph.D. thesis, Department of Applied Nutrition and Food Chemistry, University of Lund Sweden, Lund, Sweden, 1992.

[5] S. G. Haralampu, "Resistant starch-a review of the physical properties and biological impact of RS3," *Carbohydrate Polymers*, vol. 41, no. 3, pp. 285–292, 2000.

[6] A. P. Nugent, "Health properties of resistant starch," *Nutrition Bulletin*, vol. 30, no. 1, pp. 27–54, 2005.

[7] M. Stewart and J. Zimmer, "A high fiber cookie made with resistant starch type 4 reduces post-prandial glucose and insulin responses in healthy adults," *Nutrients*, vol. 9, no. 3, p. 237, 2017.

[8] B. Upadhyaya, L. McCormack, A. R. Fardin-Kia et al., "Impact of dietary resistant starch type 4 on human gut microbiota and immunometabolic functions," *Scientific Reports*, vol. 6, no. 1, p. 28797, 2016.

[9] W. Kim and M. Shin, "Effects of organic acids and starch water ratios on the properties of retrograded maize starches," *Food Science and Biotechnology*, vol. 20, no. 4, pp. 1013–1019, 2011.

[10] M. G. Sajilata, R. S. Singhal, and P. R. Kulkarni, "Resistant starch-A review," *Comprehensive Reviews in Food Science and Food Safety*, vol. 5, no. 1, pp. 1–17, 2006.

[11] C. Seidel, W.-M. Kulicke, C. Heß, B. Hartmann, M. D. Lechner, and W. Lazik, "Influence of the cross-linking agent on the gel structure of starch derivatives," *Starch-Stärke*, vol. 53, no. 7, pp. 305–310, 2001.

[12] X. Xie and Q. Liu, "Development and physicochemical characterization of new resistant citrate starch from different corn starches," *Starch-Stärke*, vol. 56, no. 8, pp. 364–370, 2004.

[13] H. Klaushofer, E. Berghofer, and W. Steyrer, "Stärkecitrate - produktion und anwendungs-technische Eigenschaften," *Starch-Stärke*, vol. 30, no. 2, pp. 47–51, 1978.

[14] M. J. Kim, S. J. Choi, S. I. Shin et al., "Resistant glutarate starch from adlay: preparation and properties," *Carbohydrate Polymers*, vol. 74, no. 4, pp. 787–796, 2008.

[15] S. I. Shin, C. J. Lee, D.-I. Kim et al., "Formation, characterization, and glucose response in mice to rice starch with low digestibility produced by citric acid treatment," *Journal of Cereal Science*, vol. 45, no. 1, pp. 24–33, 2007.

[16] A. N. Lakso and W. M. Kliewer, "The Influence of temperature on malic acid metabolism in grape berries: I. enzyme responses," *Plant Physiology*, vol. 56, no. 3, pp. 370–372, 1975.

[17] I. Goldberg, J. S. Rokem, and O. Pines, "Organic acids: old metabolites, new themes," *Journal of Chemical Technology & Biotechnology*, vol. 81, no. 10, pp. 1601–1611, 2006.

[18] S. I. Shin, H. J. Kim, H. J. Ha, S. H. Lee, and T. W. Moon, "Effect of hydrothermal treatment on formation and structural characteristics of slowly digestible non-pasted granular sweet potato starch," *Starch - Stärke*, vol. 57, no. 9, pp. 421–430, 2005.

[19] F. Zhu and S. Wang, "Physicochemical properties, molecular structure, and uses of sweetpotato starch," *Trends in Food Science & Technology*, vol. 36, no. 2, pp. 68–78, 2014.

[20] Y. Xu, V. Miladinov, and M. A. Hanna, "Synthesis and characterization of starch acetates with high substitution," *Cereal Chemistry Journal*, vol. 81, no. 6, pp. 735–740, 2004.

[21] American Association of Cereal Chemists, *Approved Methods of the AACC International, Methods 61-03*, AACC International, St. Paul, MN, USA, 10th edition, 2000.

[22] S. J. Tian, J. E. Rickard, and J. M. V. Blanshard, "Physicochemical properties of sweet potato starch," *Journal of the Science of Food and Agriculture*, vol. 57, no. 4, pp. 459–491, 1991.

[23] M. Hirashima, R. Takahashi, and K. Nishinari, "Effects of citric acid on the viscoelasticity of cornstarch pastes," *Journal of Agricultural and Food Chemistry*, vol. 52, no. 10, pp. 2929–2933, 2004.

[24] W. Blaszczak, J. Fornal, S. Valverde, and L. Garrido, "Pressure-induced changes in the structure of corn starches with different amylose content," *Carbohydrate Polymers*, vol. 61, no. 2, pp. 132–140, 2005.

[25] A. Bajpai and J. Shrivastava, "*In vitro* enzymatic degradation kinetics of polymeric blends of crosslinked starch and carboxymethyl cellulose," *Polymer International*, vol. 54, no. 11, pp. 1524–1536, 2005.

[26] A. Zarski, S. Ptak, P. Siemion, and J. Kapusniak, "Esterification of potato starch by a biocatalysed reaction in an ionic liquid," *Carbohydrate Polymers*, vol. 137, pp. 657–663, 2016.

[27] C. N. Saikia, F. Ali, T. Goswami, and A. C. Ghosh, "Esterification of high α-cellulose extracted from *Hibiscus cannabinus* L.," *Industrial Crops and Products*, vol. 4, no. 4, pp. 233–239, 1995.

[28] K. C. Huber and J. N. BeMiller, "Channels of maize and sorghum starch granules," *Carbohydrate Polymers*, vol. 41, no. 3, pp. 269–276, 2000.

[29] K. S. Woo and P. A. Seib, "Cross-linked resistant starch: preparation and properties," *Cereal Chemistry Journal*, vol. 79, no. 6, pp. 819–825, 2002.

[30] D. Cooke and M. J. Gidley, "Loss of crystalline and molecular order during starch gelatinisation: origin of the enthalpic transition," *Carbohydrate Research*, vol. 227, pp. 103–112, 1992.

[31] S. Hizukuri, M. Fujii, and Z. Nikuni, "The effect of inorganic ions on the crystallization of amylodextrin," *Biochimica et Biophysica Acta*, vol. 40, pp. 346–348, 1960.

[32] C. J. Lee, S. I. Shin, Y. Kim, H. J. Choi, and T. W. Moon, "Structural characteristics and glucose response in mice of potato starch modified by hydrothermal treatments," *Carbohydrate Polymers*, vol. 83, no. 4, pp. 1879–1886, 2011.

[33] X. Xie, Q. Liu, and S. W. Cui, "Studies on the granular structure of resistant starches (type 4) from normal, high amylose and waxy corn starch citrates," *Food Research International*, vol. 39, no. 3, pp. 332–341, 2006.

[34] C. G. Biliaderis, "Thermal analysis of food carbohydrates," in *Thermal Analysis of Foods*, V. R. Harwalkar and C. Y. Ma, Eds., pp. 168–220, Elsevier Science Publishers Ltd., London, UK, 1990.

[35] W. Mussulman and J. Wagoner, "Electron microscopy of unmodified and acid-modified corn starches," *Cereal Chemistry*, vol. 45, pp. 162–171, 1968.

[36] J. P. Robin, C. Mercier, R. Charbonniere, and A. Guilbot, "Lintnerized starches. Gel-filtration and enzymatic studies of

insoluble residues from prolonged acid treatment of potato starch," *Cereal Chemistry*, vol. 51, pp. 389–406, 1974.

[37] S. O. Agboola, J. O. Akingbala, and G. B. Oguntimein, "Physicochemical and functional properties of low DS cassava starch acetates and citrates," *Starch-Stärke*, vol. 43, no. 2, pp. 62–66, 1991.

[38] R. Shukri and Y.-C. Shi, "Structure and pasting properties of alkaline-treated phosphorylated cross-linked waxy maize starches," *Food Chemistry*, vol. 214, pp. 90–95, 2017.

[39] C. Kwon, "Structural and physicochemical characteristics of granular malic acid-treated heat-stable sweet potato starch," M.D. thesis, Department of Agricultural Biotechnology, Seoul National University, Seoul, South Korea, 2018.

Hindawi
Journal of Chemistry
Volume 2019, Article ID 3985915, 9 pages
https://doi.org/10.1155/2019/3985915

Research Article

Kinetic pH Titration to Predict the Acid and Hydrothermal Conditions for the Hydrolysis of Disaccharides: Use of a Microcapillary System

Toshinori Shimanouchi,[1] **Ryota Mano**,[1] **Yu Yoshioka**,[1] **Ayaka Fukuda**,[1] **Kyung-Min Park**,[2] **and Yukitaka Kimura**[1]

[1]*Graduate School of Environment and Life Science, Okayama University, 3-1-1 Tsushimanaka, Okayama 700-8530, Okayama, Japan*
[2]*Wonkwang University, Iskan, Republic of Korea*

Correspondence should be addressed to Yukitaka Kimura; yktkkimu@cc.okayama-u.ac.jp

Received 21 September 2018; Accepted 27 November 2018; Published 2 January 2019

Academic Editor: Josefina Pons

The hydrolysis of disaccharides was conducted using a microcapillary system under hydrothermal conditions (up to 190°C at 10 MPa and pH 4–11). The hydrolysis reaction showed a sigmoidal progression with time, especially under alkaline conditions. Analysis using a kinetic model yielded the reaction induction period. The specific pH value (pH^{amb}) at the induction time, which is the pH value corresponding to the progression of disaccharide hydrolysis, was peculiar to each disaccharide. Finally, the calculation of the electron density around the oxygen atom of the glycosidic bond between saccharides was found to roughly predict the pH^{amb} value required for the progression of hydrolysis.

1. Introduction

Sugar production is an indispensable technology in food and chemical engineering. Many researchers have reported that cellulose and oligo- and disaccharides are hydrolyzed to monosaccharides [1–7]. Because cellulose is present in plant biomass [1], it is a useful resource for the preparation of sugars and other value-added materials. The hydrolysis of cellulose is, in principle, based on the cleavage of the glycosidic bond between monosaccharides and requires acidic conditions [8]. In recent years, a variety of methods including the use of metal catalysts, enzymatic treatment in ionic liquids [9–11], and hydrothermal treatment [1–3, 6, 7] have been reported to improve hydrolysis. However, the deterioration of metal catalysts and their poor reusability limit their use. In addition, enzymes and ionic liquids are expensive. Thus, the hydrolysis of sugar is not always an environmentally benign process and can be economically risky.

Water that maintains its liquid state under pressurized conditions in the temperature range of 100–374°C is called subcritical water. Subcritical water has two unique features: (i) a low relative dielectric constant [12–14] and (ii) a high ion product [15]. Because there is evidence of a high hydroxide ion concentration in supercritical water [16], the concentrations of hydrogen and hydroxyl ions in subcritical water should be also higher than those in water at room temperature. Therefore, subcritical water has been investigated for its application as acid and base catalysts [17–19]. However, there is no direct evidence of the physicochemical properties of subcritical water mentioned above, and the further application of subcritical water requires the clarification of its physicochemical property.

Recently, it has been reported that subcritical water can catalyze the hydrolysis [2–4, 6, 7, 20–24] and isomerization [25] of saccharides, as well as the hydrolysis of vegetable oil [26]. These findings demonstrate the use of subcritical water for the treatment of biomass. Further clarification of the

physicochemical properties of subcritical water would result in the effective treatment of solid biomass, such as used wood. The decomposition mechanism of sucrose has been clarified to some extent, and the decomposition of sucrose is affected by the acidity of the reaction medium [21]. It is expected that the variation in the hydrolysis behavior of disaccharides under hydrothermal conditions at different pHs is related to the physicochemical property of subcritical water.

The hydrothermal process can be carried out in a microcapillary system. Microcapillary systems permit the rapid shifting of the liquid temperature between room temperature and hydrothermal temperature [20–22, 27–29]. Therefore, the monitoring of the reaction under the hydrothermal conditions can be achieved. In particular, a shift in the pH to the acidic region occurs with increasing hydrolysis. If the pH that induces the hydrolysis of materials can be predicted from the physicochemical properties, the use of excess acid could be avoided.

In this study, we selected disaccharides as the target materials because the minimum unit process in cellulose hydrolysis is considered to be the hydrolysis of disaccharides. Then, we examined the hydrolysis behavior of disaccharides at various pHs and temperatures. From the kinetic analysis of hydrolysis under the hydrothermal conditions involving hydrochloric acid, the apparent decomposition rate constant was estimated to determine the specific pH value for hydrolysis. As a related parameter, the hydration structure of disaccharides was examined using dielectric measurements. Moreover, the relationship between the pH value and the hydration structure of disaccharides is discussed.

2. Materials and Methods

2.1. Materials. Sucrose, palatinose monohydrate, meribiose, cellobiose, turanose, trehalose, maltose, and lactose were used as disaccharides, and their general formula is $C_{12}H_{22}O_{11}$ (M_w = 342.296 g/mol). The disaccharides and other chemicals were purchased from Wako Pure Chemical Industries, Ltd. (Osaka, Japan), except trehalose, which was obtained from Hayashibara Co. Ltd. (Okayama, Japan). Other chemicals were of analytical grade.

2.2. Thermogravimetric Analysis. The thermogravimetric analysis was carried using a TG-60A (Shimadzu, Kyoto, Japan). A platinum crucible loaded with 2 to 3 mg of sucrose was first heated to 300°C from the room temperature at a heating rate of 20°C/min. N_2 gas was used as carrier gas at a flow rate of 100 mL/min.

2.3. Preparation of the Disaccharide Solutions. The disaccharides were dissolved in distilled water to adjust the final concentration to 0.5–5 wt%. To adjust the pH of the disaccharide solution, either HCl or NaOH was used. The disaccharide solution without pH adjustment had a pH of 6. The disaccharide solution was degassed for 10 min and purged with nitrogen gas to avoid the variation in pH caused by dissolving carbon dioxide in the disaccharide solution.

2.4. Apparatus of the Flow-type Reactor. A continuous flow-type reactor (Figure 1) was used to monitor the decomposition of the disaccharides following a previous report [21]. The reactor was made of stainless steel (SUS 316, GL Science, Tokyo, Japan) tubing (1.6 mm o.d. × 0.8 mm i.d.) and was immersed in an oil bath (160–190°C). The temperature of the oil bath was monitored using a thermal detector TXN-400 (AS ONE, Osaka, Japan). To terminate the reaction rapidly, the reaction mixture leaving the reactor was passed through a water bath. The pressure in the system was regulated at 10 MPa by a valve (P-880, Upchurch Scientific). The effluent was collected in a sampling vessel to analyze the sucrose concentration by high-performance liquid chromatography (HPLC).

To investigate the pH decrease during the hydrolysis, the pH of the reactor effluent of all samples was measured using a pH meter.

2.5. HPLC Analysis. The concentration of the remaining sucrose in the effluent was determined by a liquid chromatograph (LC-20AD, Shimadzu, Kyoto, Japan) equipped with a refractometer RI-8010 (TOSO, Osaka, Japan). A COSMOSIL Sugar-D packed column (4.6 mm i.d. × 250 mm) was used for the analysis of the sucrose and its hydrolysates. The 20 μL sample was injected into the column and incubated at 38°C by the column oven. The eluent was an acetonitrile/water mixture (80/20 v/v), and its flow rate was 1.6 mL/min. The determination was repeated at least three times and then averaged.

2.6. Dielectric Measurement. Dielectric dispersion analysis permits the monitoring of the dipole moment such as that of water. A network analyzer (Agilent, N5230 C; 500 MHz to 50 GHz) was used to monitor the bulk water and the water bound to disaccharides. The sample solution at a constant mixing ratio of water to disaccharide was used and maintained for 30 min at a constant temperature before starting the measurement. Thereafter, the relative permittivity (ε') and dielectric loss (ε'') of the liposome suspension were measured as a function of frequency at each temperature following previous reports [30–32]. The frequency dependence of ε' and ε'' (500 MHz to 50 GHz) was analyzed using Debye's equations:

$$\varepsilon' - \varepsilon_h' = \sum_{i=1}^{2} \frac{\Delta\varepsilon_i}{1 + \left(f/f_{ci}\right)^2}, \tag{1}$$

$$\varepsilon'' - \frac{G_{dc}}{2\pi f C_0} = \sum_{i=1}^{2} \frac{\Delta\varepsilon_i \left(f/f_{ci}\right)}{1 + \left(f/f_{ci}\right)^2}, \tag{2}$$

where ε_h' and G_{dc} are the limit of relative permittivity at higher frequency and direct current conductivity of the solutions, respectively. C_0 is the cell constant obtained by calibration using distilled water. It has been reported that aqueous

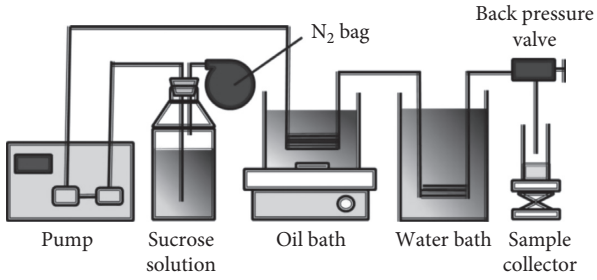

Figure 1: Schematic illustration of the reaction system for sucrose decomposition under hydrothermal conditions.

solutions have two different characteristic relaxations of water molecules: the water bound to saccharides ($i = 1$; third step, 1–3 GHz) and bulk water ($i = 2$, second step, *ca.* 20 GHz) [30, 32]. Therefore, equations (2) and (3) were assumed to be a summation of the two relaxation terms. Samples were prepared by mixing 0.5 g of disaccharide with 0–1.3 g of water. The number of water molecules to disaccharide is defined as N_w. $N_w = (m_w/M_w)/(m_d/M_d)$, where m_w and m_d are the masses of water and disaccharide (g), respectively. M_w and M_d are the molecular weights of water and disaccharide, respectively.

3. Results and Discussion

3.1. Thermal Stability of Disaccharides. In the first series of experiments, the thermal stability of the disaccharides was investigated to rule out the possibility of the thermal decomposition of the disaccharides. For this, differential scanning calorimetry (DSC) and thermal gravimetric (TG) analysis were used. Figure 2(a) shows typical DSC and TG curves for sucrose. In the temperature range between 150 and 170°C, an endothermic heat flow was observed, but no weight change was observed. The sucrose was considered to be melted in this temperature range. The weight change in sucrose was observed above 200°C from the TG curve. The DSC curve shows an endothermic adsorption in the same temperature range. These results indicated that the sucrose thermally decomposed above 220°C. The temperatures required to induce the decomposition for other disaccharides were measured to be 270°C (maltose), 24°C (trehalose), 240°C (cellobiose), 195°C (turanose), and 215°C (meribiose). For lactose, the decomposition temperature has been reported to be 220°C [33]. Thus, it is considered that the hydrolysis of disaccharides should be examined below 190°C, although data for palatinose was not obtained in this study.

3.2. Influence of Inorganic Acids on Hydrothermal Hydrolysis Behavior of Disaccharides. To select the acid in this study, sucrose was examined as a typical disaccharide. It has been reported that sucrose is susceptible to hydrolysis by acids because it has a glycosidic oxygen atom with a large electrostatic potential charge [21].

To confirm the influence of the acid species, HCl, H_2SO_4, and HNO_3 were used to induce the hydrolysis of sucrose. Each acid was mixed with sucrose to adjust the pH to 5 to initiate hydrolysis under the hydrothermal condition (185°C and 10 MPa). The change in the remaining sucrose (C/C_0) with time in the presence of each acid is shown in Figure 2(b). It is obvious that the changes in C/C_0 with time in the presence of each acid are identical. The same was true for the variation of pH (Figure 2(c)). In general, all the strong acids form H_3O^+ (H^+), known as the *leveling effect*. Therefore, the results in Figures 2(b) and 2(c) strongly indicate that the protons dissociated from the inorganic acids triggered the hydrolysis of sucrose. Thus, HCl was used for the hydrolysis of disaccharides.

3.3. Kinetic Analysis of the Hydrolysis of Disaccharides. Sucrose solutions at various pH values, adjusted by HCl, were prepared to investigate its hydrolysis under subcritical conditions (180°C and 10 MPa). The change in the remaining sucrose concentration was monitored at various pHs (Figure 3(a)). Sigmoidal curves were observed above pH 4. This indicates the presence of an induction period [34]. Following previous reports [34], we analyzed the change in the remaining sucrose (C/C_0) with time using the following equation:

$$\frac{C}{C_0} = 1 - \frac{1}{1 + \exp\left(-\left(t - t_m\right)/\tau\right)}, \tag{3}$$

where the induction time is $t_d = t_m - 2\tau$ and the apparent rate constant is $k^{app} = \tau^{-1}$. In Figure 3(a), $t_d = 25 - 160$ s and $k^{app} = 0.01 - 0.058\ s^{-1}$ were estimated from the curve fitting of equation (3) with the experimental data obtained in this study. Overall, the induction time, t_d, increased with the increasing pH. The corresponding apparent rate constant, k^{app}, also reduced with the increasing pH.

To confirm the general relationship between both, the k^{app} values were plotted against the corresponding t_d value obtained under various temperatures and pH conditions. A good correlation between both was observed at all pH values and temperatures (Figure 3(b)), which is a typical relationship often seen in the time development involving an induction period. The negatively correlated relationship between t_d and k^{app} implies a lag time for the hydrolysis of sucrose.

In a previous report, a production of organic acids such as formic acid and acetic acid associated with the hydrolysis of sucrose resulted in a pH reduction [21]. The pH variation during sucrose hydrolysis was monitored at various initial pH values. The pH converged to pH 4 regardless of the initial pH (Figure 3(c)). The reason for the convergence to the same pH appears to be due to the production of organic acids, as previously reported [21]. The pH corresponding to the induction time (t_d) is denoted as pH^{amb}. pH^{amb} was then plotted against the corresponding t_d value (Figure 3(d)). It was found that the pH^{amb} was 5 at all temperatures and initial pHs, suggesting that proton accumulation is required for the progression of sucrose hydrolysis. The pH^{amb} value for other disaccharides was also measured, as shown in Figure 4. The pH condition required to progress hydrolysis depended on the disaccharides. Overall, the pH^{amb} values

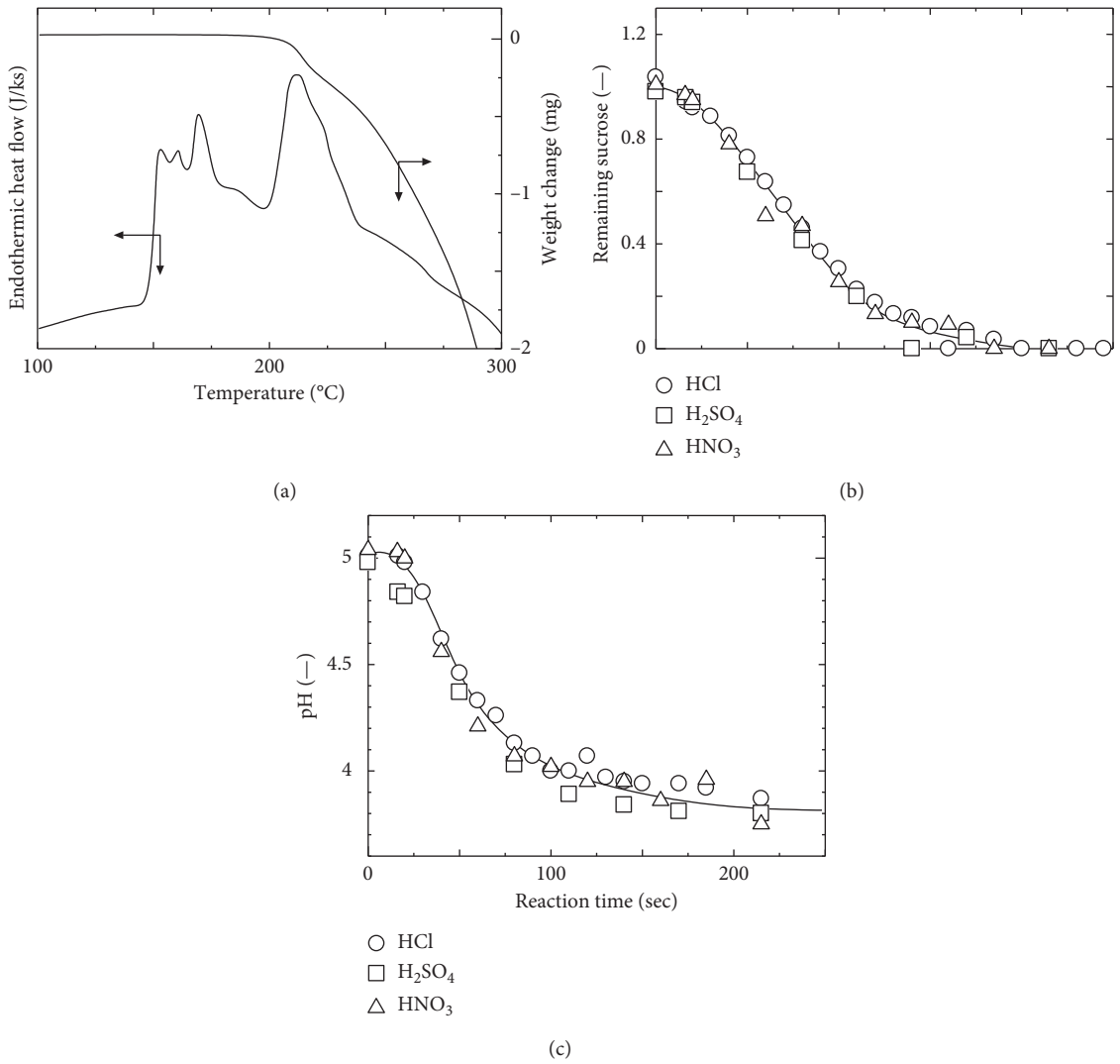

Figure 2: (a) Thermal gravimetric and differential thermogram of sucrose. Effect of acids on sucrose decomposition under the subcritical water condition. Time course of (b) remaining sucrose concentration and (c) pH. All the experiments were performed at 185°C, 10 MPa, initial pH 5, and C_0 = 0.5 wt%.

ranged between 4 and 5, suggesting that the hydrolysis of disaccharides occurred under acidic conditions in the hydrothermal reaction.

3.4. Simple Implications for the Hydrolysis Mechanism of Disaccharides. To clarify the hydrolysis mechanism of sucrose associated with the accumulation of protons, the activation energy of the sucrose hydrolysis at various pHs was investigated. Figure 5(a) shows the temperature dependencies of sucrose hydrolysis at pH 6. When the temperature was increased to 190°C, a rapid hydrolysis of sucrose was observed with a corresponding decrease in the induction period. The apparent rate constant (k^{app}) at various temperatures was estimated using equation (3) and plotted against the corresponding temperature, as shown in Figure 5(b). The slope of the plot of $\ln k^{app} - 1/T$ gives $\Delta E/R$ (Arrhenius plot), and the ΔE value was subsequently plotted against the initial pH of the sucrose solution (Figure 5(c)). Overall, the ΔE values are below 100 kJ/mol. The ΔE values for radical reactions have been reported to be about 400 kJ/mol [35]. These results indicate that the sucrose was hydrolyzed via an ionic reaction. In addition, in the range below pH 5, the ΔE value was reduced as compared with those above pH 5. The accumulation of protons appeared to be advantageous for the hydrolysis of sucrose. The same was true for other disaccharides regarding the pH dependency of the ΔE value (data not shown).

From the results, the electronic environment of the oxygen atom in the glycosidic bond of the disaccharide (where the cleavage of disaccharides occurred) played an important role in the hydrolysis reaction.

3.5. Dielectric Measurement. The hydration of disaccharides is a possible factor affecting their hydrolysis. Dielectric measurements under an alternating electric field are a

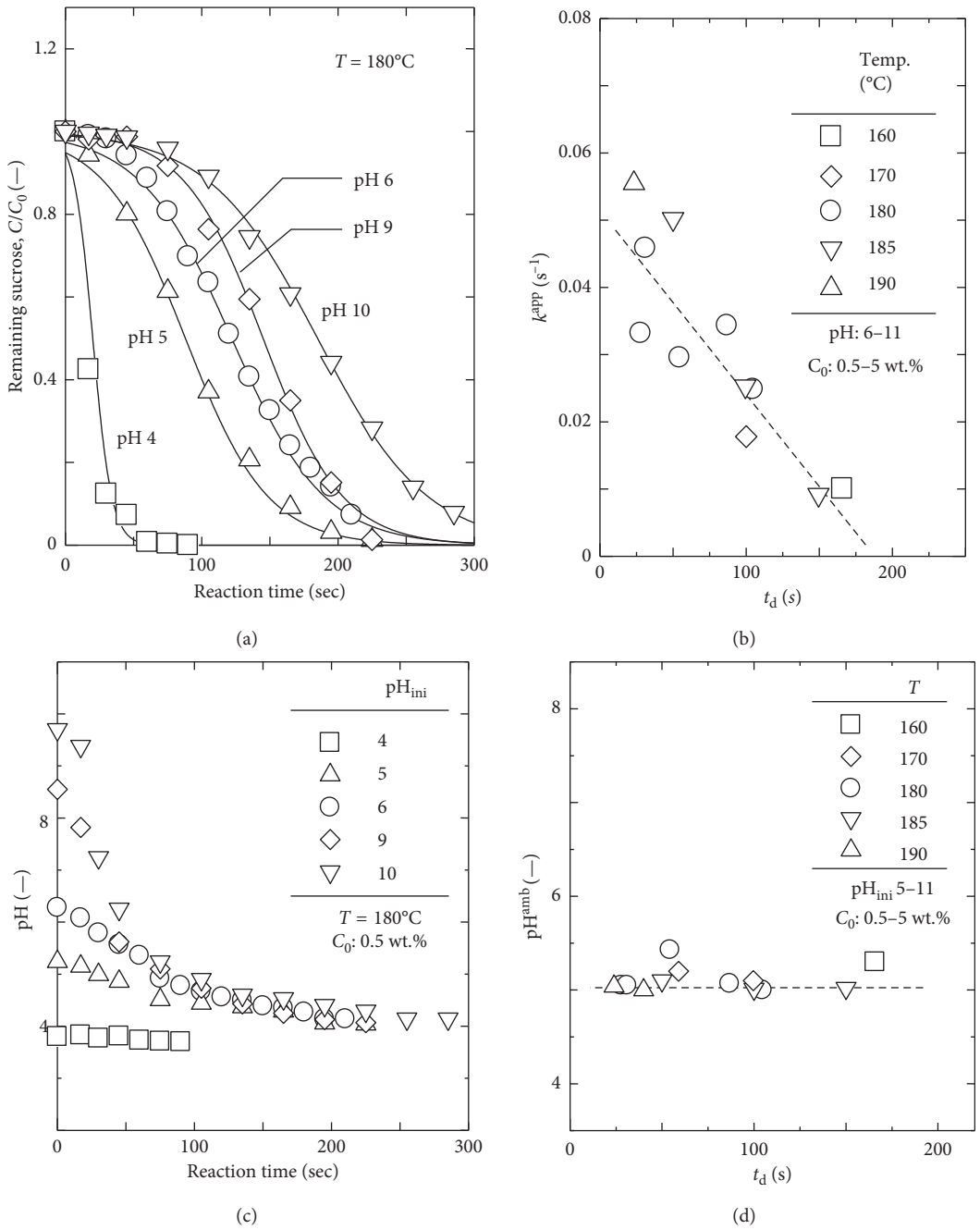

Figure 3: Kinetic pH titration. (a) Time course of remaining sucrose concentration under various pH conditions at 180°C. The experiment was performed at 180°C, 10 MPa, C_0 = 0.5 wt%, and initial pH 4–10. (b) Relationship between the induced time (t_d) and apparent rate constant (k^{app}). (c) Time course of the pH at the outlet of reaction system. (d) Relationship between t_d and the corresponding pH (pH^{amb}).

powerful tool to estimate the hydration structure [30–32]. The frequency range between 500 MHz and 20 GHz was selected because this range involves the relaxation originating from hydration [30, 32].

Typical dielectric spectra between 500 MHz and 20 GHz measured at 25°C are shown in Figures 6(a) and 6(b). In the cases of sucrose and maltose, dielectric relaxation was observed at around 1–3 and 8–20 GHz, respectively. The former relaxation was attributed to the bound water to disaccharide and the latter to that of bulk water [30, 32]. On varying the water to disaccharide content (N_w = 6.84–30.7), definite relaxation was observed for both disaccharides. The relaxation amplitude at around 1–3 GHz ($\Delta\varepsilon$) was estimated by fitting Debye-type equations (1) and (2) to the experimental data. For sucrose, the first relaxation, $\Delta\varepsilon$ = 20.3 and f = 1.2 GHz, and the second relaxation, $\Delta\varepsilon$ = 16 and f = 8 GHz, occurred at N_w = 6.84 (r^2 = 0.960); the first relaxation, $\Delta\varepsilon$ = 21.5 and f = 1.2 GHz, and the second relaxation, $\Delta\varepsilon$ = 23; and f = 8 GHz, occurred at N_w = 13.6 (r^2 = 0.955); and the first relaxation, $\Delta\varepsilon$ = 11.3 and f = 1.5 GHz, and the second

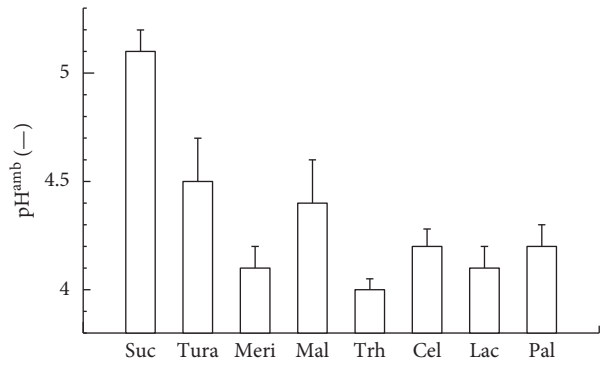

Figure 4: Specific pH value to progress the decomposition reaction of disaccharides. Suc: sucrose; Tura: turanose; Meri: meribiose; Mal: maltose; Trh: trehalose; Cel: cellobiose; Lac: lactose; Pal: palatinose. Error was calculated from the three independent experiments.

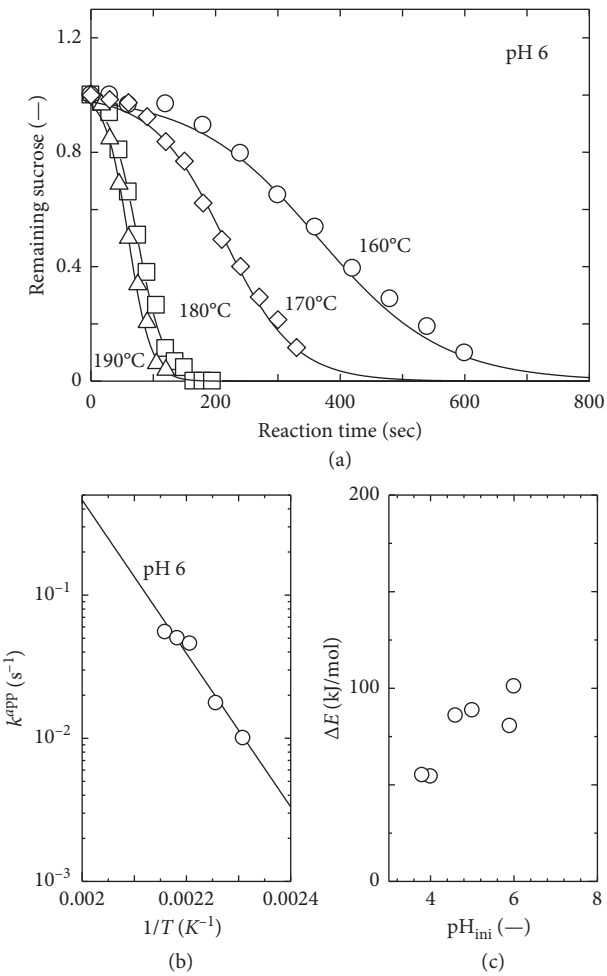

Figure 5: (a) Time course of sucrose decomposition at various temperatures. Arrhenius plot of the apparent rate constant ((b) pH 6) and (c) pH dependency of activation energy for sucrose decomposition.

relaxation, $\Delta\varepsilon = 57$ and $f = 12$ GHz, occurred at $N_w = 30.7$ ($r^2 = 0.982$). As N_w increased beyond 13.6, the characteristic frequency increased from 8 to 12 GHz, indicating the generation of free bulk water. In addition, the increase in water content increased the $\Delta\varepsilon$ value of the second relaxation. This resulted from the contribution of bulk water. The same was true for maltose.

The $\Delta\varepsilon$ value at the first relaxation, in principle, depends on the number and strength of the dipole moment derived from the bound water. The strength of the dipole moment of water reflects the extent of polarization of water. Thus, the $\Delta\varepsilon$ value as an index for the bound water was plotted against the N_w value. The $\Delta\varepsilon$ value monotonously increased up to $N_w = 10$–15 and, subsequently, decreased in the case of sucrose, turanose, and meribiose (Figure 6(c)). On the contrary, the $\Delta\varepsilon$ value monotonously increased up to $N_w = 20$–30 and then plateaued in the case of the other disaccharides (Figure 6(d)). Thus, the critical point in the $\Delta\varepsilon$ vs. N_w curve might correspond to the number of bound water molecules; thus, the critical N_w value is 15–30. However, computational studies [36, 37] have indicated that a hydration number of 13–16 is lower than the critical N_w value. This difference in the number of bound water molecules might result from the principle of the dielectric measurements: both strongly and weakly bound water are detectable. Alternatively, considering that $\Delta\varepsilon$ depends on the number and strength of dipole moment, a $\Delta\varepsilon/N_w$ value in the range between 0 and 10 might be defined as the hydration structure. The $\Delta\varepsilon/N_w$ value indicates the average strength of the dipole moment (polarization) of bound water. This definition is similar to the conventional method used to discuss the hydration of substrates, e.g., a plot of the melting enthalpy of substrates to the water content of the substrate (mol/mol) [38]. Thereby, the $\Delta\varepsilon/N_w$ values for each disaccharide are summarized in Figure 6(e). Four disaccharides (sucrose, turanose, meribiose, and maltose) had significantly higher $\Delta\varepsilon/N_w$ values than the other disaccharides. Therefore, these four disaccharides could have strongly bound hydration structures.

3.6. Implications for the pH Condition Required for the Hydrolysis of Disaccharides. It is considered that a hydration structure is formed at the hydroxyl group of monosaccharides and the glycosidic bond. The glycosidic bond is affected by hydrolysis under hydrothermal conditions. If the hydration is caused by the water bound to the glycosidic bond, the hydration structure can be considered to be related

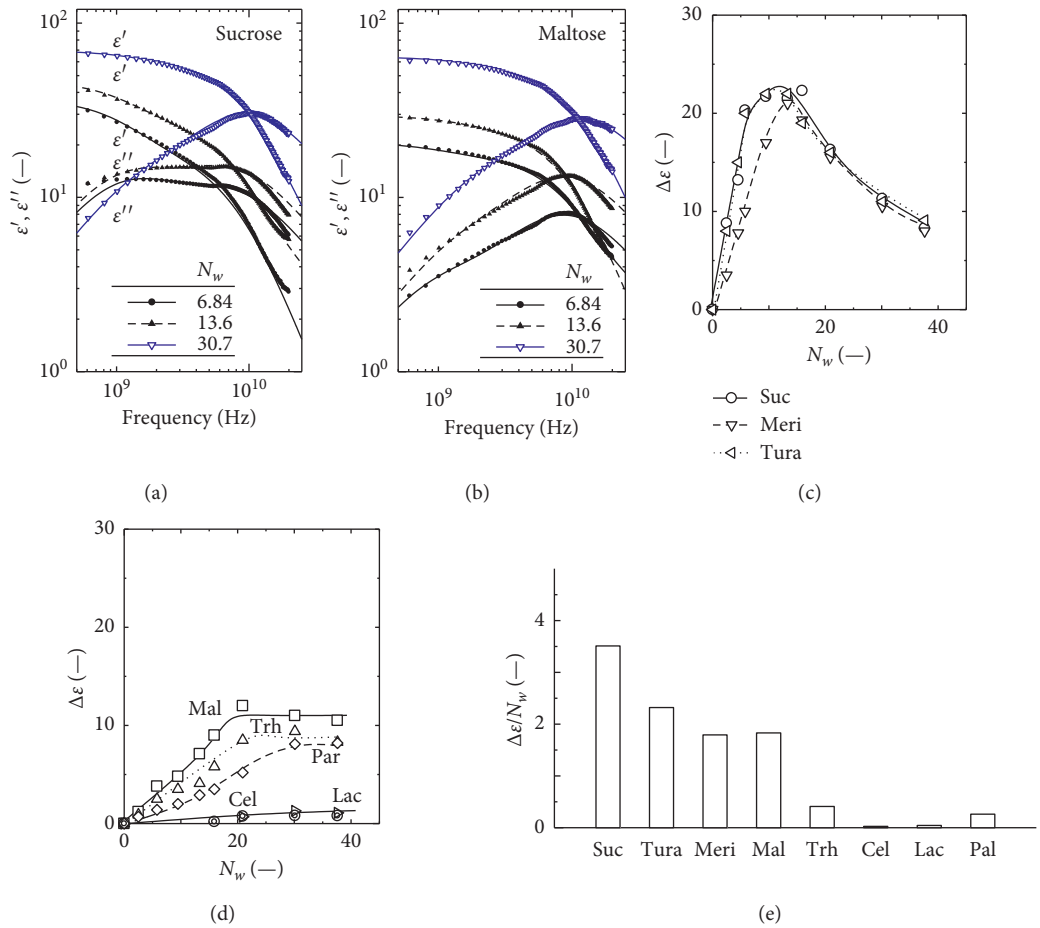

FIGURE 6: Dielectric spectra for (a) sucrose and (b) maltose in the frequency range between 500 MHz and 20 GHz. (c, d) The dielectric amplitude at first relaxation (at around 1–3 GHz) as a function of N_w. (e) Hydration index for various disaccharides. Suc: sucrose; Tura: turanose; Meri: meribiose; Mal: maltose; Trh: trehalose; Cel: cellobiose; Lac: lactose; Pal: palatinose.

to the electronic charge in the glycosidic bond (oxygen atom). Thus, theoretical calculations using the molecular orbital calculation program MOPAC 2000 were performed according to a previous report [21], and the results are summarized in Figure 7(a). Sucrose had the most negative Q value of the disaccharides used, indicating the high electron charge in the glycosidic bond of the electron-rich α-glucose-(1⟶4)-α-fructose bond [21]. Trehalose, cellobiose, lactose, and palatinose had relatively low Q values. The obtained order of Q values is likely comparable to the trend in hydrolysis (Figure 4).

To check the effect of the electronic charge of the glycosidic bond on the hydrolysis, both the pH^{amb} and $\Delta\varepsilon/N_w$ values for each disaccharide were plotted against the corresponding Q value. Figure 7(b) shows that a decrease in Q resulted in an increase in pH^{amb}, suggesting that the negative charge of the glycosidic bond is closely related to the progression of the hydrolysis reaction. The $\Delta\varepsilon/N_w$ value also indicates a negative correlation with the Q value, although some data were scattered away from the trendline (Figure 7(c)). This scattering might result from the configuration of water around the saccharides, which is dependent of the conformation of the disaccharides. Based on Figures 7(b) and 7(c), the Q value of a disaccharide could be used to determine the critical pH condition for the progression of hydrolysis.

4. Conclusion

A kinetic model taking into consideration the induction period was adopted to analyze the hydrolysis of disaccharides. Thereby, using our analysis technique, the pH value required to initiate the hydrolysis of disaccharides (pH^{amb}) can be calculated. The activation energy for the hydrolysis of disaccharides under hydrothermal conditions was calculated, and the reactions were found to be ionic reactions. Therefore, possible parameters relating to ionic reactions are (i) the hydration structure of disaccharides and (ii) the electronic charge of oxygen in the glycosidic bond. The hydration structure was determined using dielectric measurements. It was found that sucrose, turanose, and meribiose were well-hydrated relative to the other disaccharides. In addition, the calculations using MOPAC can give the Q value, and the hydration structure is roughly comparable to the Q value, although some deviations were observed. It is likely that the electronic environment of the

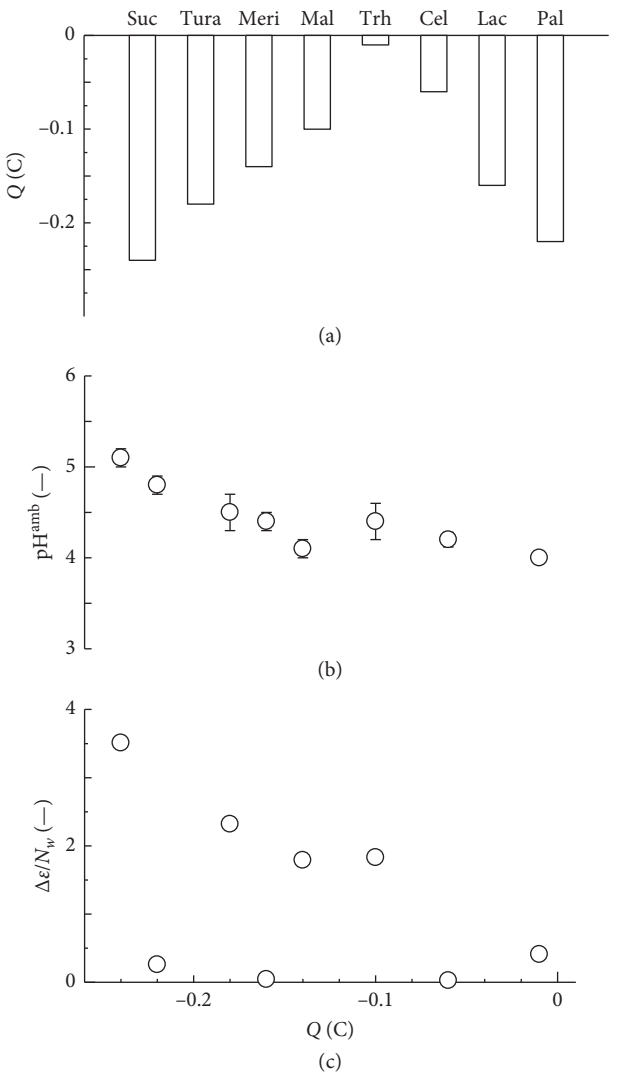

Figure 7: (a) Electronic charge around oxygen in the glycoside bond of disaccharides. Q dependency of (b) pH^{amb} and (c) $\Delta\varepsilon/N_w$. Suc: sucrose; Tura: turanose; Meri: meribiose; Mal: maltose; Trh: trehalose; Cel: cellobiose; Lac: lactose; Pal: palatinose.

oxygen atom in the glycosidic bond is related to the hydrolysis of disaccharides. Finally, the pH^{amb} value was roughly correlated with the Q value. Therefore, the method only requires knowledge of the electronic charge of the oxygen atom in the glycosidic bond of disaccharides obtained from calculation to predict the pH^{amb} of the target disaccharide. The prediction of pH^{amb} would avoid the use of excess quantities of acid to adjust the initial pH, which is of significant environmental benefit. Furthermore, a microcapillary system can be used to monitor the change in the pH with time to obtain the pH^{amb} value for the hydrothermal hydrolysis of disaccharides.

Data Availability

The data used to support the findings of this study are available from the corresponding author upon request.

Conflicts of Interest

The authors declare that there are no conflicts of interest regarding the publication of this paper.

Acknowledgments

We would like to thank Editage (http://www.editage.jp) for English language editing.

References

[1] A. A. Shra'ah and R. Helleur, "Microwave pyrolysis of cellulose at low temperature," *Journal of Analytical and Applied Pyrolysis*, vol. 105, pp. 91–99, 2014.

[2] M. Sasaki, B. Kabyemela, R. Malaluan et al., "Cellulose hydrolysis in subcritical and supercritical water," *Journal of Supercritical Fluids*, vol. 13, no. 1–3, pp. 261–268, 1998.

[3] M. Sasaki, T. Adschiri, and K. Arai, "Kinetics of cellulose conversion at 25 MPa in sub- and supercritical water," *AIChE Journal*, vol. 50, no. 1, pp. 192–202, 2004.

[4] S. Haghighat Khajavi, S. Ota, Y. Kimura, and S. Adachi, "Kinetics of maltooligosaccharide hydrolysis in subcritical water," *Journal of Agricultural and Food Chemistry*, vol. 54, no. 10, pp. 3663–3667, 2006.

[5] D. Klemm, B. Heublein, H.-P. Fink, and A. Bohn, "Cellulose: fascinating biopolymer and sustainable raw material," *Angewandte Chemie International Edition*, vol. 44, no. 22, pp. 3358–3393, 2005.

[6] M. Möller, F. Harnisch, and U. Schröder, "Hydrothermal liquefaction of cellulose in subcritical water-the role of crystallinity on the cellulose reactivity," *RSC Advances*, vol. 3, no. 27, pp. 11035–11044, 2013.

[7] W. Yang, T. Shimanouchi, S. Wu, and Y. Kimura, "Investigation of the degradation kinetic parameters and structure changes of microcrystalline cellulose in subcritical water," *Energy and Fuels*, vol. 28, no. 11, pp. 6974–6980, 2014.

[8] A. S. Amarasekara and B. Wiredu, "Degradation of cellulose in dilute aqueous solutions of acidic ionic liquid 1-(1-Propyl sulfonic)-3-methylimidazolium chloride, and p-toluene sulfonic acid at moderate temperatures and pressures," *Industrial and Engineering Chemistry Research*, vol. 50, no. 21, pp. 12276–12280, 2011.

[9] M. G. Adsul, J. E. Ghule, H. Shaikh et al., "Enzymatic hydrolysis of delignified bagasse polysaccharides," *Carbohydrate Polymers*, vol. 62, no. 1, pp. 6–10, 2005.

[10] P. Kumar, D. M. Barrett, M. J. Delwiche, and P. Stroeve, "Methods for pretreatment of lignocellulosic biomass for efficient hydrolysis and biofuel production," *Industrial and Engineering Chemistry Research*, vol. 48, no. 8, pp. 3713–3729, 2009.

[11] B. A. Z. Amin, B. Chabbert, D. Moorhead, and I. Bertrand, "Impact of fine litter chemistry on lignocellulolytic enzyme efficiency during decomposition of maize leaf and root in soil," *Biogeochemistry*, vol. 117, no. 1, pp. 169–183, 2013.

[12] Y. Yang, M. Belghazi, A. Lagadec, D. J. Miller, and S. B. Hawthorne, "Elution of organic solutes from different polarity sorbents using subcritical water," *Journal of Chromatography A*, vol. 810, no. 1-2, pp. 149–159, 1998.

[13] C. A. Eckert, D. Bush, J. S. Brown, and C. L. Liotta, "Tuning solvents for sustainable technology," *Industrial and Engineering Chemistry Research*, vol. 39, no. 12, pp. 4615–4621, 2000.

[14] D. D. Wagman, W. H. Evans, V. B. Parker et al., "The NBS tables of chemical thermodynamic properties," *Journal of Physical and Chemical Reference Data*, vol. 18, no. 4, 1982.
[15] M. Uematsu and E. U. Franck, "Static dielectric constant of water and steam," *Journal of Physical and Chemical Reference Data*, vol. 9, no. 4, pp. 1291–1306, 1980.
[16] H. Oka, S. Yamago, J. Yoshida, and O. Kajimoto, "Evidence for a hydroxide ion catalyzed pathway in ester hydrolysis in supercritical water," *Angewandte Chemie International Edition*, vol. 41, no. 4, pp. 623–625, 2002.
[17] P. Kramer and H. Vogel, "Hydrolysis of esters in subcritical and supercritical water," *Journal of Supercritical Fluids*, vol. 16, no. 3, pp. 189–206, 2000.
[18] B. Kuhlmann, E. M. Arnett, and M. Siskin, "Classical organic reactions in pure superheated water," *Journal of Organic Chemistry*, vol. 59, no. 11, pp. 3098–3101, 1994.
[19] H. P. Lesutis, R. Gläser, C. L. Liotta, and C. A. Eckert, "Acid/base-catalyzed ester hydrolysis in near-critical water," *Chemical Communications*, vol. 35, no. 20, pp. 2063-2064, 1999.
[20] C. Usuki, Y. Kimura, and S. Adachi, "Degradation of pentoses and hexouronic acids in subcritical water," *Chemical Engineering and Technology*, vol. 31, no. 1, pp. 133–137, 2008.
[21] T. Oomori, S. H. Khajavi, Y. Kimura, S. Adachi, and R. Matsuno, "Hydrolysis of disaccharides containing glucose residue in subcritical water," *Biochemical Engineering Journal*, vol. 18, no. 2, pp. 143–147, 2004.
[22] S. Haghighat Khajavi, S. Ota, R. Nakazawa, Y. Kimura, and S. Adachi, "Hydrolysis kinetics of trisaccharides consisting of glucose, galactose, and fructose residues in subcritical water," *Biotechnology Progress*, vol. 22, no. 5, pp. 1321–1326, 2008.
[23] C. Turner, P. Turner, G. Jacobson et al., "Subcritical water extraction and β-glucosidase-catalyzed hydrolysis of quercetin glycosides in onion waste," *Green Chem*, vol. 8, no. 11, pp. 949–959, 2006.
[24] S. Haghighat Khajavi, Y. Kimura, T. Oomori, R. Matsuno, and S. Adachi, "Kinetics on sucrose decomposition in subcritical water," *LWT Food Science and Technology*, vol. 38, no. 3, pp. 297–302, 2005.
[25] C. Usuki, Y. Kimura, and S. Adachi, "Isomerization of hexoses in subcritical water," *Food Science and Technology Research*, vol. 13, no. 3, pp. 205–209, 2007.
[26] T. Saito, M. Sasaki, H. Kawanabe, Y. Yoshino, and M. Goto, "Subcritical water reaction behavior of D-glucose as a model compound for biomass using two different continuous-flow reactor configurations," *Chemical Engineering and Technology*, vol. 32, no. 4, pp. 527–533, 2009.
[27] T. Shimanouchi, S. Ueno, K. Shidahara, and Y. Kimura, "Rapid conversion of glycerol to lactic acid under alkaline hydrothermal conditions, by using a continuous flow reaction system," *Chemistry Letters*, vol. 43, no. 4, pp. 535–537, 2014.
[28] T. Shimanouchi, Y. Kataoka, T. Tanifuji, Y. Kimura, S. Fujioka, and K. Terasaka, "Chemical conversion and liquid-liquid extraction of 5-hydroxymethylfurfural from fructose by slug flow microreactor," *AIChE Journal*, vol. 62, no. 6, pp. 2135–2143, 2016.
[29] T. Shimanouchi, T. Tanifuji, S. Fujioka, K. Terasaka, and Y. Kimura, "Water/methyl isobutyl ketone (MIBK) biphasic system in slug flow under high temperature and pressure conditions," *Solvent Extraction Research and Development, Japan*, vol. 21, no. 2, pp. 201–209, 2014.
[30] M. Noda, T. Shimanouchi, H. Suzuki, M. Okuyama, and R. Kuboi, "Analysis of complex permittivity of liposome for its biochemical dynamics up to 30 GHz range," *IEEE Transactions on Microwave Theory and Techniques*, vol. 54, pp. 1983–1986, 2006.
[31] T. Shimanouchi, M. Sasaki, A. Hiroiwa et al., "Relationship between the mobility of phosphocholine headgroups of liposomes and the hydrophobicity at the membrane interface: a characterization with spectrophotometric measurements," *Colloids and Surfaces B: Biointerfaces*, vol. 88, no. 1, pp. 221–230, 2011.
[32] H. T. Vu, T. Shimanouchi, D. Ishikawa et al., "Effect of liposome membranes on disaggregation of amyloid β-fibrils by dopamine," *Biochemical Engineering Journal*, vol. 71, pp. 228–236, 2013.
[33] Y. Listiohadi, J. A. Hourigan, R. W. Sleigh, and R. J. Steele, "Thermal analysis of amorphous lactose and α-lactose monohydrate," *Dairy Science and Technology*, vol. 89, no. 1, pp. 43–67, 2008.
[34] T. Shimanouchi, N. Kitaura, R. Onishi, H. Umakoshi, and R. Kuboi, "Secondary nucleation of Aβ fibrils on liposome membrane," *AIChE Journal*, vol. 58, no. 12, pp. 3625–3632, 2012.
[35] N. K. Kai, *The Chemical Handbook Standard Edition 2, Kagakubinran Kisohen 2*, Maruzen, Tokyo, Japan, 4th edition, 2001.
[36] A. Lerbert, P. Bordat, F. Affouard, M. Descamps, and F. Migliardo, "How homogeneous are the trehalose, maltose, and sucrose water solutions? An insight from molecular dynamics simulations," *Journal of Physical Chemistry B*, vol. 109, no. 21, pp. 11046–11057, 2005.
[37] S. L. Lee, P. G. Debenedetti, and J. R. Errington, "A computational study of hydration, solution structure, and dynamics in dilute carbohydrate solutions," *Journal of Chemical Physics*, vol. 122, no. 20, article 204511, 2005.
[38] D. Bach and I. R. Miller, "Hydration of phospholipid bilayers in the presence and absence of cholesterol," *Chemistry and Physics of Lipids*, vol. 136, no. 1, pp. 67–72, 2005.

Hindawi
Journal of Chemistry
Volume 2019, Article ID 8968351, 7 pages
https://doi.org/10.1155/2019/8968351

Research Article

Detection of Artificially Water-Injected Frozen *Octopus minor* (Sasaki) Using Dielectric Properties

Dongyoung Lee,[1] **Sangdae Lee**,[2] **Chang Joo Lee**,[3] **and Seung Hyun Lee**[1]

[1]*Department of Biosystems Machinery Engineering, College of Agricultural and Life Science, Chungnam National University, 99 Daehak-ro, Yuseong-gu, Daejeon 34134, Republic of Korea*
[2]*Convergence Components and Agricultural Machinery R&D Group, Korea Institute of Industrial Technology, 119 Jipyeongseonsandan 3-gil, Gimje, Jeollabuk-do 54325, Republic of Korea*
[3]*Department of Food Science and Biotechnology, College of Life Resource Science, Wonkwang University, 460 Iksandae-ro, Iksan, Jeollabuk-do 54538, Republic of Korea*

Correspondence should be addressed to Seung Hyun Lee; seunglee2@cnu.ac.kr

Received 20 September 2018; Accepted 11 November 2018; Published 2 January 2019

Guest Editor: Toshinori Shimanouchi

A few importers of marine products have practiced the fraud of artificially injecting water into *Octopus minor* for increasing their weights prior to the freezing process. These rampant practices have recently become a serious social issue and threaten public health. Therefore, it is necessary to develop the detection method for artificially water-injected frozen *Octopus minor*. This study was conducted to develop the nondestructive method for verifying adulterated *Octopus minor* by measuring dielectric properties using the coaxial probe method. Regardless of weight and measurement locations, a significant difference between ε values from normal octopuses was not observed. The ε values of *Octopus minor* were decreased in the microwave frequency range between 500 and 3000 MHz. The ε values of water-injected octopuses also showed similar trend with normal octopuses; however, the dielectric loss factor (ε'') values of adulterated octopuses were much lower than normal octopuses. After thawing normal, adulterated, and imported frozen *Octopus minor*, the ε values measured at the trunk part from these octopuses were compared and statistically analyzed. The ε'' values from normal frozen octopus were significantly different from adulterated and imported frozen octopuses. In addition, the ε'' values from the adulterated frozen octopus group that weight gain rate was less than 20% was significantly different from other adulterated octopus groups with higher weight gain rate than 20%. The ε'' values from adulterated frozen octopus groups with the range of weight gain rate between 20 and 30% were quite similar to imported frozen octopuses. Therefore, it was found that the measurement of ε'' values from *Octopus minor* has a great possibility to distinguish normal frozen octopuses and artificially water-injected frozen octopuses.

1. Introduction

Octopus minor (Sasaki, 1920), which is widely distributed along the coastal waters of Korea, China, and Japan, is one of commercially important marine species in East Asia countries [1]. Since octopus is recognized as a high nutrition and low calorie food that has the effects on lowering the cholesterol level in blood and preventing anemia, its consumption in Korea has been consistently increased; however, from 2006, domestic production of octopus in Korea has been annually decreased because of environmental destruction and overfishing. A tremendous amount of octopus was imported in Korea to meet demands from consumers, and the imported volume in 2013 was approximately 38,533 tons.

Freezing method that can retain the quality of foods is the common preservation method for octopus. Because the majority of imported octopuses are in the frozen state and their price is mainly decided by the weight, a few of importers (or distributors) of marine products have practiced excessive ice glazing of frozen fish and forced water injection into octopus for increasing weights of marine products. This rampant practice threatens public health and became a social issue in Korea. Although the Ministry of Food and Drug Safety in Korea has been inspecting for imports of octopus

from Asia countries, this inspection is entirely dependent on the ability of the inspector. Skillful inspectors of marine products have strived to distinguish normal and adulterated octopuses by using thermogravimetric analysis that can determine water content in frozen octopus; however, the precise quantitation of water content in *Octopus minor* is complicated because some specific amount of water is generally absorbed into octopus during transportation and the ice glazing process. The analysis equipment that can directly examine water content in frozen octopus is not yet existed. Therefore, the determination of water content in an imported frozen octopus is time-consuming and laborious.

In microwave and radio frequency heating, dielectric properties are the most important factor that can provide information about the interaction between electromagnetic energy in applied microwave and radio frequency and dielectric material [2]. Dielectric properties are also described in terms of complex relative permittivity and are represented as the following term [3, 4]:

$$\varepsilon = \varepsilon' - j\varepsilon'', \tag{1}$$

where ε' is the dielectric constant (the real part) that indicates the ability of the material to store energy in the applied electric field, ε'' is the dielectric loss factor (the imaginary part) that is associated with the ability of the material to dissipate energy in the applied electric field, and j is $\sqrt{-1}$.

Dielectric properties are mainly altered by several factors (i.e., density, physical structure, moisture content of the target material, frequency, and temperature), and in particular, the amount of water in the target material is the dominant factor affecting these properties [5].

There are five representative methods for measuring dielectric properties of materials: transmission line, free space, resonant cavity, parallel plate, and open-ended coaxial probe methods. Among these methods, the open-ended coaxial probe method is commonly used to measure dielectric properties of food materials because it covers broad frequency bands and pretreatment is not required for preparing samples [6]. The main advantage of this method is that dielectric properties of the target material can be easily measured by making close contact between the probe and the surface. Several studies were conducted to measure dielectric properties of frozen marine products and seafood such as tuna, shrimp, salmon, and surimi by using the open-ended coaxial probe method [7–10]. It was reported that dielectric properties of aforementioned frozen marine products were significantly changed depending on frequency, temperature, composition, and measurement location. In addition, Mendes et al. [11] attempted to develop the detection method for artificially water-added *Octopus vulgaris* by measuring their electrical conductivity and dielectric properties, and they concluded that simultaneous measurement of electrical conductivity or dielectric properties could be used to distinguish artificially water added octopus among processed octopuses. However, as far as can be determined from published literatures, there was not an attempt to determine how much water were artificially injected into octopus by measuring dielectric properties with the open-ended coaxial probe method. Therefore, this study was conducted to (1) distinguish normal and artificially water-injected *Octopus minor* (Sasaki, 1920) by measuring dielectric properties and (2) develop the nondestructive detection method verifying artificially water-injected frozen *Octopus minor* by using the open-ended coaxial probe.

2. Materials and Methods

2.1. Octopus minor. Live and frozen *Octopus minor* (Sasaki, 1920) imported from China were procured from a local seafood market. The live octopuses were randomly captured in a fish tank and packed in polystyrene boxes containing seawater and then transported to the laboratory. The imported frozen octopus block packed in a paper box consisted of 5 octopuses, and its weight was about 1 kg.

Convection oven drying method was employed to estimate moisture contents of live octopuses. Placing live octopus in the drying tray was difficult because it kept moving during the drying process; thus, live octopus was packaged in a plastic bag and then stored in 4°C refrigeration condition for 24 h. Octopus was exhausted and debilitated through this process. The weights of debilitated octopuses ($n = 35$) were measured by digital balance with 0.01 g precision (PAG2102C, OHAUS Co., USA). The octopuses were put in the convection oven and dried at 105°C for 24 h. The initial moisture content of octopus was 4.485 ± 0.593 kg of water per kg of dry matter.

2.2. Preparation of Artificially Water-Injected Frozen Octopus minor. Wells and Wells [12] reported since *Octopus vulgaris* was quite hyperosmotic compared with seawater in which it lived, osmotic uptake could occur over the general body surface. Although the species of octopus (Sasaki, 1920) used in this study was different from *Octopus vulgaris*, it was assumed that *Octopus minor* (Sasaki, 1920) was also hyperosmotic. Osmotic uptake experiment was conducted to determine the optimal concentration of sodium chloride solution for water injection into octopus to the maximum. 24 live octopuses were weighed by a digital balance and put in 24 containers (a 1 L plastic container). All containers were filled with sodium chloride solution of 700 mL with different concentrations (0% (tap water) to 2.1% (21 g/L) at increments of 0.3% (3 g/L)) and were sealed with lids. All containers were grouped by concentration of sodium chloride solution, and 8 groups of containers (3 containers for each concentration) were kept in the 4°C refrigeration condition for 24 h. Then, octopuses were removed from the solution, and their weights were measured again to determine the weight gain rate by the following equation. The experiments were conducted in triplicate:

$$\text{weight gain rate}\,(\%) = \frac{w_f - w_i}{w_i} \times 100, \tag{2}$$

where w_f is the weight of octopus immersed in the sodium chloride solution (kg) and w_i is the initial weight of octopus (kg).

After determining the optimal concentration of the sodium chloride solution, live octopuses were treated as the aforementioned method to prepare artificially water-injected frozen octopuses (adulterated octopuses). Then, adulterated octopuses were sorted by the weight gain rate (%) and divided into 5 groups, then frozen at in the chest freezer for 24 h.

Live octopuses were also frozen and were used as normal frozen octopuses (the control group) for the comparison with imported frozen octopus blocks and artificially water-injected octopus groups.

2.3. Dielectric Properties Measurement System. Dielectric probe (85070E option 050, Agilent Technologies, Santa Clara, CA) coupled with a vector network analyzer (E8361C, Agilent Technologies, Santa Clara, CA) was used for measuring dielectric properties (ε) of an octopus. The type of the dielectric probe was the performance probe operated in the frequency range between 500 MHz and 50 GHz and temperature range from −40 to 200°C. The probe was calibrated for the measurement using air, a standard shorting block, and distilled water at 10°C. The reflection coefficient (S_{11}) at the interface between the probe and the surface of octopus was measured by the network analyzer. Dielectric probe kit software (85070E software, Agilent Technologies, Santa Clara, CA) was used for the calculation of dielectric properties based on the measured reflection coefficient. As a preliminary experiment, the dielectric properties (ε) of normal octopuses and artificially water-injected octopuses were measured in the frequency range from 500 MHz to 20 GHz. Dielectric constant (ε') values from both octopus groups were constantly decreased with an increase in frequency. However, dielectric loss factor (ε'') values were sharply decreased below 3 GHz and afterward remained constant. Over 3 GHz, there was not a significant difference between dielectric loss factor (ε'') values from both octopus groups. Ionic conduction generally occurs at low frequencies, and dipole relaxation occurred at higher frequencies. Traffano-Schiffo et al. [13] reported that the ionic conductivity effect on meat can be observed below 2 GHz. In addition, Castro-Giráldez et al. [14] reported that the dielectric loss factor (ε'') measured at low frequencies (0.5 GHz), which can determine the effect of ionic conductivity, was useful in distinguishing the quality of pork meat. Therefore, the dielectric properties of octopus were measured within the frequency range between 500 MHz to 3 GHz at 101 frequency sample points. In addition, all data points (ε' and ε'') were monitored, recorded, and graphically plotted.

2.4. Dielectric Properties Measurement Procedure. The weight of live octopuses was measured, and their dielectric properties were measured at three locations, namely, mantle, trunk, and the thickest arm, as shown in Figure 1(a). Octopus secretes mucus from the skin when there is an external threat. Therefore, the mucus from the skin at the measurement location was clearly removed using paper wipers. After the measurements, live octopuses were exhausted and debilitated by using the early mentioned method and were put in the aluminum trays and frozen at −30°C for 24 h. Then, normal frozen octopuses were thawed at room temperature for 1 h, and their weights and dielectric properties were measured again. In this measurement, dielectric properties were measured only at the trunk after all water on their skin was clearly removed.

In the case of adulterated octopuses, they were sorted by weight gain rate after water injection, and all measurement procedure was the same with the aforementioned measurement procedure. Imported frozen octopuses were also thawed at room temperature for 1 h, and then, the measurement for weight and dielectric properties was performed. The experimental protocol is clearly represented in Figure 1(b).

Based on the dielectric properties measured at different stages, the penetration depth of microwave was calculated by the following equation [3]:

$$d_{\mathrm{p}} = \frac{c}{2\pi f \sqrt{2\varepsilon' \left[\sqrt{1 + \left(\varepsilon''/\varepsilon'\right)^2} - 1\right]}}, \tag{3}$$

where d_{p} is the penetration depth (m), f is the frequency (Hz), c is the speed of light in the free space (2.9979×10^8 m/s), and ε' and ε'' are the measured values of dielectric constant and dielectric loss factor of octopus, respectively.

2.5. Statistical Analysis. The result from the osmotic uptake experiment was statistically evaluated by one-way analysis of variance (ANOVA). Tukey's HSD multiple range test (p value < 0.05) was carried out using SPSS 24.0 software (SPSS Inc, Chicago, IL, USA). T-tests were conducted to compare the means of dielectric constant (ε') and loss factor (ε'') measured from normal and adulterated *Octopus minor* at different measurement locations and frequencies. Furthermore, dielectric properties measured from the normal frozen octopus group, artificially water-injected octopus groups, and imported frozen octopus group were analyzed and compared according to the procure of least squares means by using SAS (SAS 9.1; SAS Institute, Cary, NC, USA).

3. Results and Discussion

3.1. Osmotic Water Uptake of Octopus minor. Figure 2 shows the weight gain rate (%) of water-injected octopus by NaCl solutions with different concentrations. The amount of absorbed water by octopuses immersed in tap water was close to 60% of their body weight and was much larger than it by other octopuses. There was no significant difference ($p < 0.05$) in weight gain rate of octopuses immersed in NaCl solutions with different concentrations; however, the weight gain rate of octopuses was between 40% and 50%. An artificial injection of water into *Octopus minor* could be easily practiced in the environment that has lower salt concentration than seawater in which it lives. It was found that *Octopus minor* could be considered as a hyperosmotic animal. An immersion of octopus in tap water was employed to artificially inject water into octopus as much as possible.

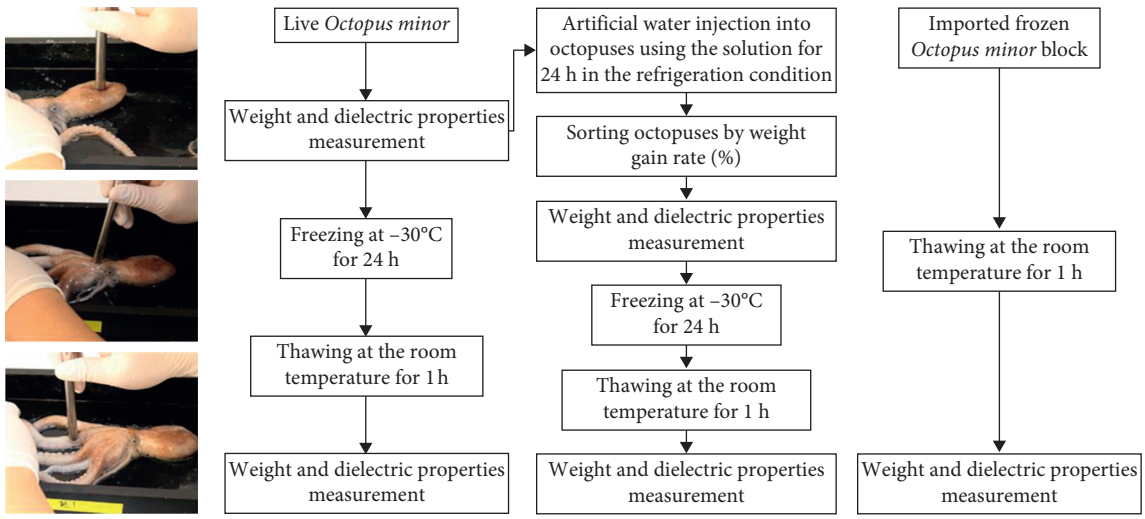

Figure 1: Dielectric properties measurement: (a) measuring location; (b) experimental protocol.

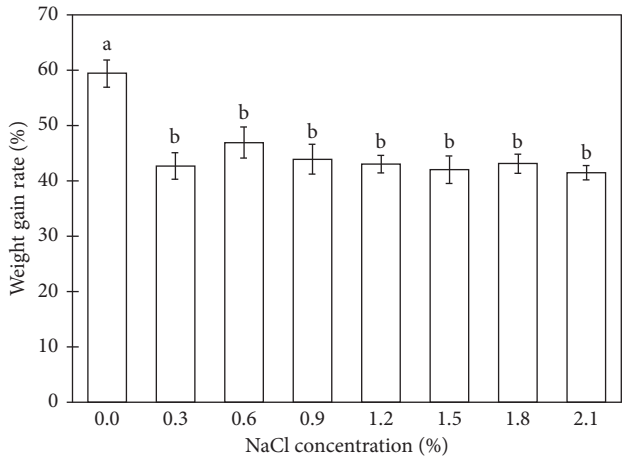

Figure 2: Weight gain rate of *Octopus minor* immersed in NaCl solutions with different concentrations.

3.2. Dielectric Properties of Octopus minor. The dielectric properties measured from live octopuses were listed in Table 1. The average weight of octopuses ($n = 300$) for dielectric properties measurement was 168.43 (±80.33) g. Dielectric constant (ε') and dielectric loss factor (ε'') of octopus measured at three locations were decreased as frequency increased. Microwave penetration depth (d_p) was also decreased with an increase in frequency. When dielectric properties of octopus arm muscle were measured *in vivo* over low frequency range between 5 Hz and 1 MHz, ε' was decreased with an increase in frequency [15]. Dielectric properties (permittivity) describe the ability of a material to polarize in response to an applied electric field [16]. Generally, as frequency increases, the net polarization of the material drops because each polarization mechanism ceases to contribute, and consequently, ε' decreased [17]. There was not a significant difference in ε' and of octopus measured at the same frequency depending on measurement locations. According to research done by Tanaka et al. [7], the effect of shrimp's measurement locations on dielectric properties was not significant. Furthermore, microwave penetration depth (d_p) from the mantle, trunk, and arm at 500 MHz was 0.0099 (±0.001) m, 0.0093 (±0.001) m, and 0.0099 (±0.001) m, respectively. Therefore, it can be considered *Octopus minor* is composed with a certain structure that uniformly absorbs microwave power.

3.3. Dielectric Properties of Adulterated Octopus minor. Dielectric constant (ε') of artificially water-injected octopuses ($n = 50$) was decreased with an increase in frequency as similar to it of normal octopus as summarized in Table 1. A significant difference between ε' and ε'' values measured from normal and adulterated octopuses was observed regardless of measurement locations at the same frequency ($p < 0.05$ in all cases). Despite the statistical result, it was not possible to clearly distinguish normal and adulterated octopuses using ε'. On the contrary, ε'' of adulterated octopuses was decreased in the frequency range from 500 MHz to 1000 MHz and increased afterward. In addition, there was a considerable change of ε'' values between normal and adulterated octopuses than ε' values. Regardless of measurement locations, the microwave penetration depths from adulterated octopuses at 500 MHz were longer than normal octopuses by at least 2 cm. In general, ε' and ε'' of foods are increased with an increase in water amount of foods because water (the dipolar molecule) dominantly affects change in dielectric properties of food. The positive correlation between ε' and water was observed; however, the correlation between ε'' and water was not clear [18]. Even though the water was artificially injected into octopuses, the uncertain correlation between ε'' and water in octopuses was observed. Salt content in food also affects the change in ε'' owing to an increase in ionic loss [19]. Salt concentration of adulterated octopuses *in vivo* might be decreased, finally resulting in decrease in ε'' of adulterated octopuses.

Table 1: Dielectric properties of normal and adulterated *Octopus minor* at different parts and frequencies.

Frequency (MHz)	Octopus	ε'			ε''		
		Mantle	Trunk	Arm	Mantle	Trunk	Arm
500	Normal	76.11^{a} (±1.94)	76.48^{a} (±1.84)	77.38^{a} (±1.41)	101.8^{c} (±16.36)	105.91^{c} (±18.24)	97.77^{c} (±8.88)
	Adulterated	77.03^{b} (±2.60)	77.35^{b} (±2.31)	76.96^{b} (±2.43)	24.17^{d} (±9.22)	21.28^{d} (±8.80)	20.51^{d} (±6.73)
1000	Normal	68.93^{a} (±1.84)	69.51^{a} (±2.24)	69.57^{a} (±1.54)	55.39^{c} (±7.63)	57.47^{c} (±8.27)	54.00^{c} (±4.28)
	Adulterated	76.09^{b} (±2.50)	77.35^{b} (±2.27)	76.79^{b} (±2.38)	16.18^{d} (±4.64)	15.08^{d} (±4.48)	15.03^{d} (±3.42)
1500	Normal	66.11^{a} (±2.18)	66.84^{a} (±2.81)	66.64^{a} (±1.65)	42.05^{c} (±5.03)	43.58^{c} (±5.55)	41.38^{c} (±3.10)
	Adulterated	75.09^{b} (±2.57)	76.43^{b} (±2.37)	75.79^{b} (±2.52)	15.44^{d} (±3.16)	15.16^{d} (±3.12)	15.30^{d} (±2.41)
2000	Normal	64.45^{a} (±2.35)	65.19^{a} (±3.08)	64.94^{a} (±1.65)	35.64^{c} (±3.88)	36.77^{c} (±4.36)	35.21^{c} (±2.74)
	Adulterated	73.78^{b} (±2.68)	74.12^{b} (±2.37)	73.11^{b} (±2.58)	15.88^{d} (±2.43)	16.01^{d} (±2.43)	16.28^{d} (±1.93)
2500	Normal	62.90^{a} (±2.46)	63.64^{a} (±3.26)	63.37^{a} (±1.79)	32.15^{c} (±3.06)	33.08^{c} (±3.66)	31.95^{c} (±2.44)
	Adulterated	72.96^{b} (±2.46)	74.12^{b} (±2.32)	73.11^{b} (±2.50)	17.26^{d} (±2.00)	17.78^{d} (±2.04)	18.05^{d} (±1.69)
3000	Normal	61.27^{a} (±2.57)	62.05^{a} (±3.35)	61.79^{a} (±1.84)	30.19^{c} (±2.65)	31.04^{c} (±3.33)	30.13^{c} (±2.34)
	Adulterated	71.73^{b} (±2.43)	72.75^{b} (±2.31)	71.57^{b} (±2.43)	18.54^{d} (±1.77)	19.29^{d} (±1.82)	19.54^{d} (±1.61)

The values having different letters are significantly different ($p < 0.05$).

There was a clear difference between ε'' values from normal and adulterated octopuses. Therefore, among dielectric properties, the ε'' value could be used as the discrimination factor to detect adulterated octopuses. Furthermore, uniform osmotic water uptake over the general surface of an octopus would be possible because there was not a significant difference in dielectric properties of adulterated octopuses regardless of measurement locations.

3.4. Dielectric Properties of Thawed Octopus minor. Figure 3 illustrates the dielectric properties of normal ($n = 100$), adulterated ($n = 140$), and imported ($n = 140$) frozen octopuses measured at the trunk location after thawing. As a preliminary experiment, dielectric properties of three different frozen octopuses were measured at three locations in the freezing range; however, the values of ε' and ε'' were very small, and the difference between dielectric properties of three different octopus groups was not observed. Mao et al. [8] and Liu and Sakai [20] reported that, below the freezing point, dielectric properties of frozen tuna and surimi were very small and there was not a significant difference depending on measurement locations.

Dielectric properties of normal and adulterated frozen octopuses were similar to the values in the freezing range. After thawing, the ε' values of adulterated frozen octopuses were slightly greater than normal frozen octopuses in all frequency ranges; however, there was not a significant difference between the two octopus groups. Even after thawing, the ε'' values of normal frozen octopuses were much greater than adulterated frozen octopus. The gap between the ε'' values of two octopus groups was narrow as frequency increased; however, the evident difference between the ε'' values of normal and adulterated frozen octopuses was observed at any specific frequency. Although it was not technically feasible to distinguish normal and adulterated frozen octopuses in the freezing range, it was possible to do two groups after thawing by using the ε'' values as the discrimination factor at low frequency. In addition, the dielectric properties (ε' and ε'') of imported frozen octopuses after thawing were quite similar to the values of adulterated frozen octopuses. It would be that *Octopus minor* absorbed water during the transport for their freezing process or water was added into octopuses to compensate for water loss during frozen storage. Therefore, the further statistical analysis was conducted to estimate the water amount added into imported frozen octopuses.

3.5. Determination of Water Amount Injected into Frozen Octopus minor after Thawing. Since there was not a significant difference between ε' values measured from adulterated and imported frozen octopuses, the ε'' values measured at the trunk part from adulterated octopuses were used as the discrimination factor. The ε'' values measured from adulterated octopuses were divided by weight gain rate (%), and the ε'' values from adulterated octopuses were classified into 5 groups for the comparison with ε'' values from imported frozen octopuses. 5 groups were less than 20% (the weight gain rate was less than 20%), 20% (20~29%), 30% (30~39%), 40% (40~49%), and 50% (over 50%). As shown in Figure 4, after 2 GHz, the ε'' values from 5 groups and the imported frozen octopus group were similar to each other group. Less than 1.5 GHz, the clear difference between 6 groups was observed. As listed in Table 2, at 500 MHz, the less 20% group was statistically quite different from other adulterated groups and the imported frozen octopus group. The 20% and 30% groups were significantly similar to the imported frozen octopus group. There was not a difference between 20% and 30% groups. Furthermore, there was no significant difference between adulterated groups when the difference in weight gain rate was at 10%. Although the clear estimation of water amount injected into octopuses was not determined by using ε'' values from adulterated and imported frozen octopuses, it was possible to clearly distinguish normal and adulterated frozen groups. In addition, the octopuses in which water was excessively injected could be distinguished from them with low weight gain rate. Therefore, the coaxial probe method has a high potential to detect an adulterated *Octopus minor*.

4. Conclusion

The detection method using a vector network analyzer and open-ended coaxial probe that can measure the sample's

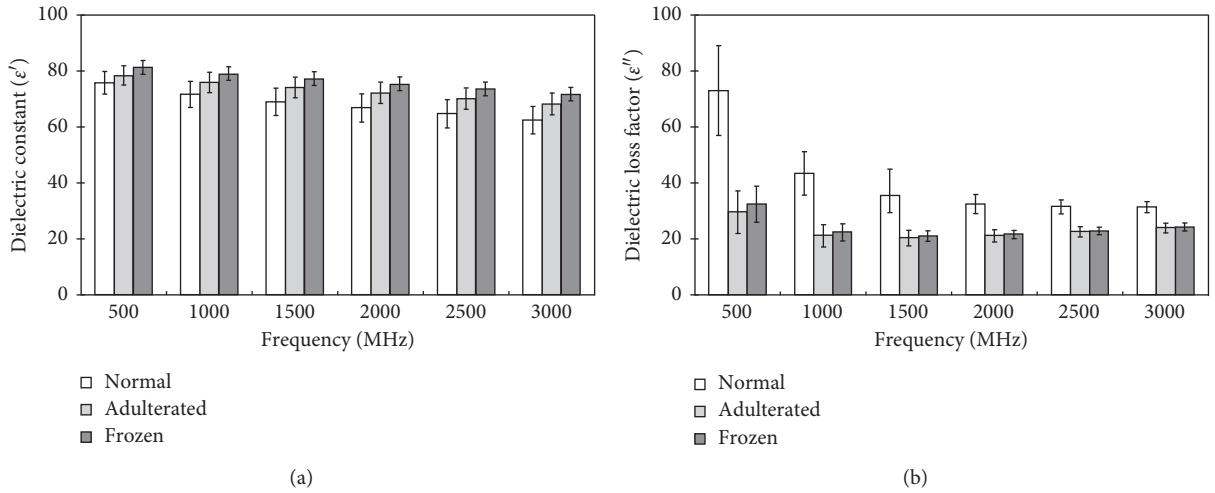

Figure 3: Dielectric properties of normal, adulterated, and imported frozen octopuses measured at the trunk part after thawing: (a) dielectric constant; (b) dielectric loss factor.

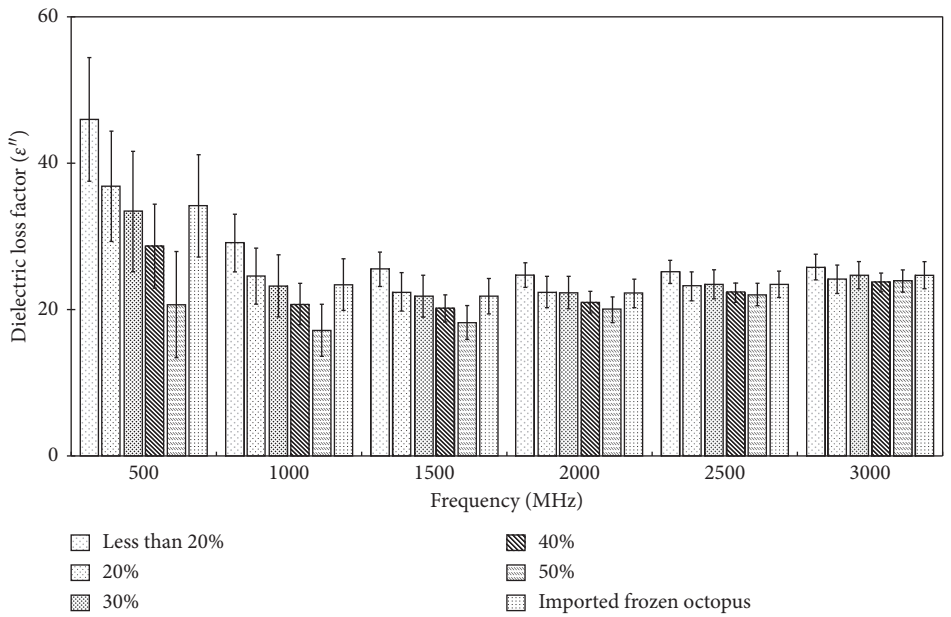

Figure 4: Dielectric loss factor adulterated and imported frozen octopuses measured at the trunk part after thawing.

Table 2: Statistical analysis of dielectric properties measured at 500 MHz and the trunk part from adulterated and imported frozen *Octopus minor* groups.

	Least squares means for the effect class					
	Less 20	20	30	40	50	Imported frozen octopus
Less than 20		4.3728* (0.0002)	5.8549* (<0.0001)	6.9993* (<0.0001)	10.8249* (<0.0001)	6.1482* (<0.0001)
20			2.2569 (0.2151)	4.1751* (0.0005)	9.2707* (<0.0001)	2.2614 (<0.0001)
30				2.3335 (0.2151)	6.5617* (<0.0001)	0.5754 (0.9926)
40					2.8037 (0.0594)	−3.0648
50						−8.8594*
Imported frozen octopus						

* p value < 0.05; the p value is indicated in parentheses.

dielectric properties by a direct contact was developed to distinguish normal octopuses and artificially water-injected octopuses. Regardless of weight and measurement locations, the dielectric properties (ε) of octopuses were decreased in the frequency range between 500 and 3000 MHz (ε': 76~61 and ε'': 101~30). In addition, artificially water-injected octopuses showed the same trend with normal octopuses (ε': 78~72 and ε'': 22~19). Among dielectric properties, the dielectric loss factor (ε'') was effective to distinguish normal and adulterated octopuses. After thawing normal, adulterated, and imported frozen octopuses, these octopus groups were easily distinguished by using the measured dielectric loss factor (ε''). At 500 MHz, the dielectric loss factor (ε'') from imported frozen octopuses was similar to the octopuses in which the weight gain rate was between 20 and 39%. The octopus group with less than 10% weight gain rate was significantly different from other adulterated frozen octopus groups. The statistical analysis of the dielectric loss factor of adulterated and imported frozen samples determined that it was possible to detect extremely water-injected octopus. Therefore, by measuring the dielectric loss factor of frozen *Octopus minor* after thawing, the adulterated frozen *Octopus minor* could be detected in a short time.

Data Availability

The data used to support the findings of this study are available from the corresponding author upon request.

Conflicts of Interest

The authors declare that there are no conflicts of interest regarding the publication of this article.

Acknowledgments

This work was carried out with the support of research fund provided by Ministry of Food and Drug Safety (Imported Food Safety Policy Bureau, Imported Food Inspection Management Division) in 2016.

References

[1] J. H. Kang, Y. K. Kim, J. Y. Park, C. M. An, and J. C. Jun, "Development of microsatellite markers to genetically differentiate populations of *Octopus minor* from Korea and China," *Molecular Biology Reports*, vol. 39, no. 8, pp. 8277–8286, 2012.

[2] M. E. Sosa-Morales, L. Valerio-Junco, A. López-Malo, and H. S. García, "Dielectric properties of foods: reported data in the 21st century and their potential applications," *LWT-Food Science and Technology*, vol. 43, no. 8, pp. 1169–1179, 2010.

[3] Y. Wang, T. D. Wig, J. Tang, and L. M. Hallberg, "Dielectric properties of foods relevant to RF and microwave pasteurization and sterilization," *Journal of Food Engineering*, vol. 57, no. 3, pp. 257–268, 2003.

[4] V. Komarov, S. Wang, and J. Tang, "Permittivity and measurements," *IEEE Transactions on Microwave Theory and Techniques*, vol. 47, no. 11, pp. 2123–2130, 1999.

[5] M. S. Venkatesh and G. S. V. Raghavan, "An overview of microwave processing and dielectric properties of agri-food materials," *Biosystems Engineering*, vol. 88, no. 1, pp. 1–18, 2004.

[6] T. P. Marsland and S. Evans, "Dielectric measurements with an open-ended coaxial probe," *IEE Proceedings H (Microwaves, Antennas and Propagation)*, vol. 134, no. 4, pp. 341–349, 1987.

[7] F. Tanaka, P. Mallikarjunan, and Y.-C. Hung, "Dielectric properties of shrimp related to microwave frequencies: from frozen to cooked stages," *Journal of Food Process Engineering*, vol. 22, no. 6, pp. 455–468, 1999.

[8] W. Mao, M. Watanabe, and N. Sakai, "Dielectric properties of surimi at 915 MHz and 2450 MHz as affected by temperature, salt and starch," *Fisheries Science*, vol. 69, no. 5, pp. 1042–1047, 2003.

[9] Y. Wang, J. Tang, B. Rasco, F. Kong, and S. Wang, "Dielectric properties of salmon fillets as a function of temperature and composition," *Journal of Food Engineering*, vol. 87, no. 2, pp. 236–246, 2008.

[10] Y. Llave, Y. Terada, M. Fukuoka, and N. Sakai, "Dielectric properties of frozen tuna and analysis of defrosting using a radio-frequency system at low frequencies," *Journal of Food Engineering*, vol. 139, pp. 1–9, 2014.

[11] R. Mendes, O. Schimmer, H. Vieira, J. Pereira, and B. Teixeira, "Control of abusive water addition to *Octopus vulgaris* with non-destructive methods," *Journal of the Science of Food and Agriculture*, vol. 98, no. 1, pp. 369–376, 2018.

[12] M. J. Wells and J. Wells, "Water uptake in a cephalopod and the function of the so-called 'pancreas'," *Journal of Experimental Biology*, vol. 145, no. 1, pp. 215–226, 1989.

[13] M. V. Traffano-Schiffo, M. Castro-Giraldez, R. J. Colom, and P. J. Fito, "Study of the application of dielectric spectroscopy to predict the water activity of meat during drying process," *Journal of Food Engineering*, vol. 166, pp. 285–290, 2015.

[14] M. Castro-Giráldez, M. C. Aristoy, F. Toldrá, and P. Fito, "Microwave dielectric spectroscopy for the determination of pork meat quality," *Food Research International*, vol. 43, no. 10, pp. 2369–2377, 2010.

[15] F. X. Hart, R. B. Toll, N. J. Berner, and N. H. Bennett, "The low-frequency dielectric properties of octopus arm muscle measured in vivo," *Physics in Medicine and Biology*, vol. 41, no. 10, pp. 2043–2052, 1996.

[16] Z. Ahmad, "Polymeric dielectric materials," in *Dielectric Material*, pp. 3–26, IntechOpen, London, UK, 2012.

[17] M. Russel, S. Zhenxiang, L. Changrui et al., "Development of a detection method based on dielectric spectroscopy for real-time monitoring of meta-cresol contamination in beach-sand," *Sensors and Actuators A: Physical*, vol. 268, pp. 16–26, 2017.

[18] S. Ryynänen, "The electromagnetic properties of food materials: a review of the basic principles," *Journal of Food Engineering*, vol. 26, no. 4, pp. 409–429, 1995.

[19] J. G. Lyng, J. M. Arimi, M. Scully, and F. Marra, "The influence of compositional changes in reconstituted potato flakes on thermal and dielectric properties and temperatures following microwave heating," *Journal of Food Engineering*, vol. 124, pp. 133–142, 2014.

[20] C. Liu and N. Sakai, *Dielectric Properties of Tuna at 2450 MHz and 915 MHz as a Function of Temperature*, Japanese Society for Food Science and Technology, Tokyo, Japan, 1999.

Hindawi
Journal of Chemistry
Volume 2019, Article ID 4180708, 7 pages
https://doi.org/10.1155/2019/4180708

Research Article

Ethylene Vinyl Alcohol Copolymer (EVOH) as a Functional Barrier against Surrogate Components Migrating from Paperboard

Caroline Maes,[1,2] **Giberto Mitsuyoshi Yuki Junior**,[3] **Cynthia Teniers**,[1] **Wout Luyten**,[1] **Geert Herremans**,[1] **Roos Peeters**,[2] **Pieter Samyn**,[4] **Robert Carleer**,[4] **and Mieke Buntinx**[2]

[1]*Kuraray-Eval Europe NV, Haven 1053 Nieuwe Weg 1, Bus 10, 2070 Zwijndrecht, Belgium*
[2]*Hasselt University, Packaging Technology Center IMO-IMOMEC, Wetenschapspark 27, 3590 Diepenbeek, Belgium*
[3]*Université de Pau et des Pays de l'Adour, École Nationale Supérieure en Génie des Technologies Industrielles, 64000 Pau, France*
[4]*Hasselt University, Applied and Analytical Chemistry IMO-IMOMEC, Agoralaan Building D, 3590 Diepenbeek, Belgium*

Correspondence should be addressed to Mieke Buntinx; mieke.buntinx@uhasselt.be

Received 21 September 2018; Accepted 25 October 2018; Published 1 January 2019

Guest Editor: Kyung-Min Park

Ethylene vinyl alcohol copolymer (EVOH) is a key material of interest as a functional barrier against substances migrating from recycled paperboard, due to its outstanding barrier properties. Three multilayer films containing two different grades of EVOH, L171B (3 μm) and F171B (3 and 5 μm), were benchmarked against a multilayer film containing polyamide 6/6.6 copolymer (PA 6/6.6, 3 μm) and monolayer polyethylene terephthalate (PET, 12 μm). The 5 films were evaluated as barrier materials against 5 surrogate substances simulating different migrants potentially present in recycled paperboard: *n*-heptadecane (C17) as a mineral oil-saturated hydrocarbon (MOSH), 4-methylbenzophenone (MBP) as a photoinitiator, di-*n*-propyl phthalate (DPP) as a plasticiser, and anthracene (ANT) and perylene (PER) as mineral oil aromatic hydrocarbons (MOAHs). The test was accelerated at 60°C for 25 days, which is equivalent to a shelf life of 2 years at 25°C. All films containing 3 or 5 μm EVOH were found to be good barriers, showing no breakthrough values over 1% of the initial concentration found in the paperboard, and they could easily compete with 12 μm PET. The multilayer with 3 μm PA 6/6.6 showed higher breakthrough values for both MBP and DPP than the other materials although still below the 1% threshold value. However, ANT showed substantial breakthrough values of nearly 2%, indicating that PA 6/6.6 might not offer enough protection against low-weight MOAH components.

1. Introduction

Mineral oil hydrocarbons (MOHs) contamination in food has become a major concern in the past decade when it was brought to light that these substances might be potentially harmful for the human health. Both the German Federal Institute for Risk Assessment (BfR) [1] and the European Food Safety Authority (EFSA) [2] published a scientific opinion on the potential health risks of MOHs present in food due to contamination in the food chain.

In terms of MOHs contamination and toxicology, the EFSA [2] distinguishes two main groups: mineral oil-saturated hydrocarbons (MOSHs), which can be *n*-alkanes, branched alkanes and cycloalkanes, and mineral oil aromatic hydrocarbons (MOAHs), which are polyaromatic hydrocarbons, mainly alkylated. MOSHs from C_{16} to C_{35} may accumulate and cause microgranulomas in the lymph nodes, spleen, liver, and other tissues [2]. For MOAHs, there are only few toxicological data available; however, MOAHs with 3 or more nonalkylated and minor alkylated aromatic rings are suspected for being mutagenic and carcinogenic and are therefore of concern [2]. Due to these findings, the EFSA also recommends that the revision of the acceptable daily intake (ADI) of some food-grade MOSHs is necessary.

Migration from recycled paperboard was found to be one of the main sources for this contamination. Several

studies reported severe migration of both MOSHs and MOAHs from paperboard packaging into foodstuff which was not only limited to the primary but also originated from the secondary and even the tertiary packaging [3–7]. Lorenzini et al. [7] found that about 60–80% of the $<n\text{-}C_{24}$ fraction of MOSHs/MOAHs present in the paperboard was transferred to the food inside the package. Vollmer et al. [6] confirmed these findings and also reported that 10–20% of the migrated fraction were MOAHs.

Regulation (EC) No. 1935/2004 [8] states that food contact materials (FCMs) should not transfer any of their constituents to food in quantities that may endanger human health and bring about unacceptable changes in the composition of the food or a deterioration in the organoleptic characteristics thereof. Unfortunately, so far, no harmonised European Regulation for paperboard packaging exists. Recently, Commission Recommendation (EU) 2017/84 [9] has been issued to monitor the presence of MOHs and their sources in 2017 and 2018. The results of this study are expected in 2019. Several countries already took the lead by establishing their own recommendation or regulation; for instance, in Austria, the Federal Ministry of Health states in Recommendation BMG-75210/0018-II/B/13/2012 [10] that if food is packaged in recycled paperboard, it should be protected by a functional barrier. Switzerland has a similar approach in its "Bedarfsgegenständeverordnung" 817.023.21 [11], which states that recycled paperboard should not be in contact with food, unless measures are taken, e.g. by means of a barrier layer.

Even though there is no specific regulatory obligation on the European level, it is now generally recommended to minimise the transfer of MOHs and other harmful components migrating from paperboard packaging [1, 2, 12, 13]. The most widely accepted solution is the integration of a functional barrier in the primary packaging concept, where it can limit the migration from primary, secondary, and tertiary packaging as well as the cross-contamination from other products and the environment [5]. A functional barrier can either limit the maximum migration into food to a quantity below the specific migration limit (SML) or can prolong the time of breakthrough when migrated components are first detected, to a time beyond the shelf life [14].

Ethylene vinyl alcohol copolymer (EVOH) (see the structure in Figure 1) is a key material of interest due to its outstanding barrier properties as reported by Maes et al. [15]. The random copolymer consists of ethylene units, which contribute to processability and flexibility, and vinyl alcohol units, which are responsible for the high barrier properties. EVOH has one of the lowest oxygen permeability rates (P_{O_2}) amongst polymers, and it shows excellent barrier properties against other gases, such as nitrogen and carbon dioxide. In addition, it also prevents the scalping of aromas and flavours in food packaging [16–18]. EVOH also offers a good barrier against fuels and other chemicals, such as benzene, toluene, ethylbenzene and xylene isomers (BTEX), agrochemicals including fumigants, and others. In the automotive sector, EVOH is already widely used in applications like fuel tanks [15].

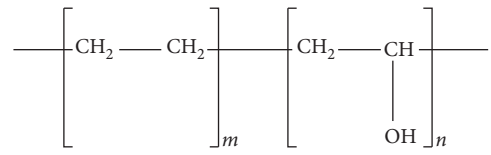

Figure 1: Structure of ethylene vinyl alcohol copolymer (EVOH).

Maes et al. [19] already demonstrated that EVOH offers good protection against mineral oil migration. The breakthrough time of a mineral oil mixture (Gravex 913) was determined for two EVAL™ EVOH grades, E105B and F171B, using the method developed by Fiselier and Grob [14]. The multilayer films containing 5.2 and 4.4 μm EVOH, respectively, showed breakthrough times of, respectively, >7.1 and >10.6 years [19].

More recent studies are focussing on the use of surrogate substances instead of a mineral oil mixture to assess the functional barrier against mineral oil and other contaminants originating from recycled paperboard [20, 21]. This approach allows careful evaluation of known components with different polarity and boiling points instead of total migration. Based on these studies, the Schweizerisches Verpackungsinstitut (SVI) published a guideline for the evaluation of the barrier efficiency of internal bags for food packaging in recycled paperboard [22]. Because the shelf life of most dry foods is several years, a test at regular storage conditions (25°C) would take too long; however, the test can be accelerated by increasing the temperature. The acceleration factor can be calculated using the Arrhenius equation (Equation 1) as described in Commission Regulation (EU) No. 10/2011 [9], which suggests an activation energy (E_a) of 80 kJ/mol as a worst-case scenario. A test performed at 60°C would be accelerated by factor 30 compared to a test at 25°C, reducing the test time for a shelf time of two years to 25 days:

$$t_2 = t_1 \cdot e\left[-\frac{E_a}{R} \cdot \left(\frac{1}{T_1} - \frac{1}{T_2}\right)\right]. \quad (1)$$

In this paper, EVOH was evaluated as a functional barrier against 5 surrogate substances simulating a MOSH, two MOAHs, a plasticiser, and a printing ink component, migrating from recycled paperboard.

2. Materials and Methods

2.1. Chemicals and Materials. Methyl tert-butyl ether (MTBE, 100%) and methanol (MeOH, 98.5%) were obtained from VWR International S.A.S. (Fontenay-sous-Bois, France). Anthracene (ANT, 99%) and bicyclohexyl (CyCy, 99%) were from Acros Organics (Geel, Belgium). Di-*n*-propyl phthalate (DPP, 98%), *n*-heptadecane (C17, 99%), 4-methylbenzophenone (MBP, 98%), and Sudan red II (1(2,4-dimethylphenylazo)-2-naphthol) all were supplied by Alfa Aesar-Thermo Fisher GmbH (Kandel, Germany). Finally, perylene (PER, synthesis grade) was obtained from Merck KGaA (Darmstadt, Germany).

For this study, five different film samples were evaluated. Four of these films were multilayer structures which were

produced on a Dr. Collin 5-layer blown film line by the TS Department of EVAL Europe N.V., and one was a monolayer polyethylene terephthalate (PET) film (12 μm) obtained through the EVAL R&D Department of Kuraray Co. Ltd. in Japan. The general structure of the multilayer films was LDPE/tie/barrier/tie/LDPE. The barrier layer was either EVAL™ EVOH-grade F171B (32 mol% ethylene) of either 5 or 3 μm thickness, 3 μm EVAL™ EVOH-grade L171B (27 mol% ethylene), or 3 μm polyamide 6/6.6 copolymer (PA 6/6.6). The different samples are shown in Table 1. Both structures of PA 6/6.6 and PET are given in Figure 2.

The paperboard used as a donor was of virgin grade (290 g/m^2) which was provided by Smurfit Kappa Van Mierlo Offset Packaging (Turnhout, Belgium). The receptor material was obtained from BGB Analytik AG (Boeckten, Switzerland) and was made of copy paper (115 g/m^2) soaked in 20% polydimethylsiloxane (PDMS), which was cured and cleaned for 8 h at 130°C and 0.1 bar.

2.2. Spiking of the Donors. The spike solution was prepared using *n*-heptadecane (C17), 4-methylbenzophenone (MBP), and di-*n*-propyl phthalate (DPP) as surrogate components and Sudan red II for visual control of equal distribution in the paperboard as listed by Biedermann-Brem et al. [21] and in the guideline provided by the SVI [22]. As shown in Table 2, C17, MBP, and DPP, respectively, represent an MOSH, photoinitiator, and plasticiser, respectively. Yet MOAH components are of the greatest concern; therefore, anthracene (ANT) and perylene (PER) were added to simulate MOAH components (Table 2). All components were dissolved in MTBE at a concentration of 250 mg/L.

The donor paperboard (A5) was soaked in this solution until it was completely saturated; afterwards, it was dried by holding it in a vertical position underneath the fume hood to allow the MTBE to evaporate. Several boards were then tightly wrapped together in aluminium foil and placed in an oven at 40°C for 2 weeks for conditioning. This condition was chosen based on experiments of Biedermann-Brem et al. to allow the polar components to penetrate the paperboard more deeply. This allowed a more gradual release of the components from the paperboard mimicking a more realistic migration scenario [21, 23].

2.3. Preparation of the Test Packs. After conditioning, the donor paperboard was sampled for the determination of the initial concentrations by removing a piece of 9 cm × 2 cm for extraction and subsequent analysis by gas chromatography using a quadrupole mass spectrometer (GC-MS) as detector. The remaining donor was then covered in aluminium foil on the top side and folded around the border with approximately 1 cm overlap on all edges of the bottom side. This resulting donor pack was then taped on top of the test film sample, which had larger dimensions. To ensure the donor was wrapped tightly, the excess of the film sample was folded around the donor pack and taped on top. Finally, the receptor (A5) was secured on the other side of the film sample (Figure 3). Afterwards, the test pack was completely covered in aluminium foil. To ensure the receptor was free of possible contaminations, it was first heat-treated at 150°C for 30 minutes prior to using it in the test pack.

All test packs were put in the oven simultaneously and loaded with a heavy object (e.g. a glass plate) to decrease the air exchange between the packs. The test packs were kept in the oven for 25 days at 60°C, which covers a period of 2 years of shelf life at 25°C, using an acceleration factor of 30 as calculated by the Arrhenius equation. The receptor was sampled at regular intervals by cutting a piece of 9 cm × 2 cm keeping a distance of 1 cm from the border and the previous sampling to avoid the effect of sideways migration due to the absence of the receptor material in the vicinity area. Even though this effect was not found to be considerable, it was found to be a best practice [21]. Each film sample was tested in duplicate.

2.4. Extraction and GC-MS Analysis. The samples were extracted using a MTBE/MeOH (95/5 v/v) solution. The 9 cm × 2 m samples of the donor and receptor were cut into smaller pieces and then extracted with, respectively, 10 and 2 mL of the extraction solution. To each of these extracts, 10 μL of the internal standard solution was added, prepared by dissolving 100 mg CyCy in 10 mL MTBE of which 300 μL was then diluted in 10 mL MTBE. The film samples were extracted in the same way as the receptor to check whether there were possible interferences with the analysis of the surrogate substances. The vials containing the samples with extraction solution were put in an oven overnight at 40°C to facilitate the extraction process after the addition of CyCy as the internal standard. Biedermann-Brem et al. found that the extraction was most challenging for the most polar component (MPB) after it has penetrated the board deeply. However, after a night at 40°C, the extraction was virtually complete [23].

The extracts were analysed by injecting 1 μL into a Trace Ultra 1310 GC coupled to an ISQ LT Quadrupole MS in a splitless mode at a constant helium flow of 1.2 mL/min. The column used was a 30 m × 0.25 mm i.d. × 0.25 μm film thickness DB5-MS capillary column. The oven temperature was first kept at 30° C for 5 minutes after injection. Then, at a 10°C/min ramp, the temperature was raised till 330°C, which was maintained for 2 minutes. 6 calibration solutions were prepared to which 10 μL of the internal standard was added to determine the exact amount of the surrogate components in the sample extracts. For each test pack, the amount of migration for each of the 5 substances that passed through the barrier into the receptor was determined. This amount was expressed as a percentage breakthrough value of the initial concentration that was found in the donor paperboard.

2.5. O_2GTR Measurements. The oxygen transmission rate (O_2GTR) of all five film samples was determined using a MOCON OX-TRAN® 2/21 at 20°C and 65% RH in accordance with ASTM F1927. For the PET and PA 6/6.6 film, the use of a mask was necessary to reduce the test surface area from the standard 50 cm^2 to 5 cm^2 to remain within the detection range of the coulometric detector.

Table 1: Film samples and their characteristics.

Barrier material	Ethylene content (mol%)	Average layer distribution LDPE/tie/barrier/tie/LDPE (μm)	Oxygen barrier at 20°C and 65% RH	
			O_2GTR ($cm^3/(m^2 \cdot day \cdot atm)$)	P_{O_2} ($cm^3 \cdot \mu m/(m^2 \cdot day \cdot atm)$)
F171B	32	21/4/5/5/20	0.7	3.2
		21/5/3/5/20	1.7	5.4
L171B	27	22/5/3/5/21	0.7	2.0
PA 6/6.6	/	20/5/3/4/18	479	1629
PET	/	12	91	60

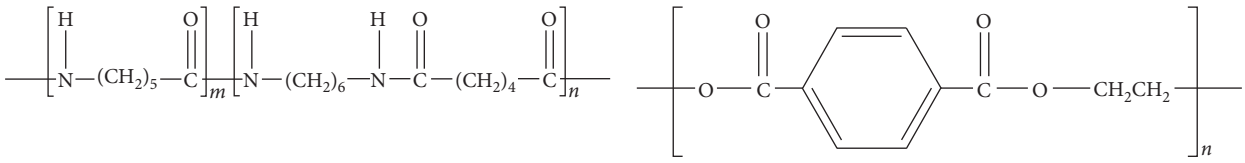

(a) (b)

Figure 2: Structure of polyamide 6/6.6 copolymer (PA 6/6.6) (a) and polyethylene terephthalate (PET) (b).

3. Results and Discussion

3.1. Breakthrough of Surrogate Components. In Figure 4, the breakthrough values of the five surrogate components are given in percent of the initial concentration found in the spiked donor for all films after 25 days at 60°C, which translates into a shelf life of 2 years at 25°C. The guideline provided by the Swiss Packaging Institute states that the barrier is good when the values remain below 1% of the initial concentration at the end of the shelf life [22]. This criterion was based on GC analysis of recycled paperboard extracts initiated by the German Federal Ministry of Food, Agriculture and Consumer Protection (BMELV) and its outcome that no nonevaluated substances in the critical volatility range (C_{14}–C_{25}) exceeded 10 mg/kg paperboard. The BMELV specified a threshold of toxicological relevance of 0.01 mg/kg in food, which corresponds to the detection limit that is widely applied by the EU [24]. Taking into account the typical mass ratio of food to paperboard of 10, this leads to the threshold value of 1% of the substances initially found in the paperboard [23].

The results in the graph clearly show that the multilayer films with the two different EVAL™ grades, 5 and 3 μm F171 and 3 μm L171, are sufficient and can easily compete with a monolayer 12 μm PET film. For the EVAL™ and PET films, C17 shows the highest migration potential, which is likely due to its low boiling point (302°C) and selectivity of the polymer matrix. Biedermann-Brem and Grob found that polyvinyl alcohol had a higher selectivity for C17 than for MBP and DPP, making it less resistant to C17, resulting in a higher breakthrough percentage than the other two components [20].

The multilayer film containing 3 μm of PA 6/6.6, however, shows higher values for MBP and DPP compared to the other films, but these values are still below the 1% threshold value. It is likely that these components might have caused a plasticising effect on the PA 6/6.6 matrix, which could be less present in PET and EVOH due to stronger inter- and intramolecular bonds caused by the presence of more functional groups [25, 26]. PA 6/6.6 has longer polar chains and is therefore to be expected that the free space between the chains allows larger molecules to pass through. C17 did not show higher breakthrough values than the other two materials, which indicates a strong change in selectivity as was shown by Biedermann-Brem and Grob [20]. ANT is an apolar molecule that shows breakthrough values of nearly 2% after 25 days at 60°C. The threshold value of 1% for ANT was reached after only 5 days at 60°C in the PA 6/6.6 film, which is approximately 150 days at 25°C, indicating that 3 μm PA 6/6.6 does not provide sufficient protection against low-weight MOAH components for products that require a shelf life over 150 days. This effect was possibly strengthened by the plasticising effect of the polar components or interaction between the components DPP, MBP, and ANT such as copermeation. Zhou et al. reported this effect for limonene and ethyl butyrate, where the presence of ethyl butyrate increased the permeation of limonene through a high-density polyethylene (HDPE) film [27]. But further research is needed to confirm these findings.

The component PER did not break through in any of the films, which is most likely due to its higher boiling point of 494°C opposed to C17 (302°C), MBP (326°C), DPP (340°C), and ANT (340°C), making it less susceptible for migration from the cardboard, as transport of the molecules occurs in the gas phase and requires a minimum vapour pressure [7, 14].

3.2. Relationship Breakthrough Values and O_2GTR. The O_2GTR values are given in Table 1 as well as the P_{O_2} normalised to a barrier thickness of 1 μm. The films containing EVOH have very low O_2GTR values, which are two orders of magnitude lower than the PET film, which is also still considered as a good barrier. The PA 6/6.6 has an O_2GTR value significantly higher than that of the other two materials, and this was also reflected in the breakthrough values of

Table 2: Components used in the spike solution and their physical and chemical properties. For each substance, the structure, CAS Registry Number, polarity, partition coefficient for octanol/water (log $P_{o/w}$), molar weight (Mw), boiling point (Bp), and simulant group are given.

	Name	Structure	CAS	Polarity	Log $P_{o/w}$	Mw (Da)	Bp (°C)	Simulant group
C17	*n*-Heptadecane		629-78-7	Nonpolar	9.8	240	302	MOSH
MBP	4-Methyl benzophenone	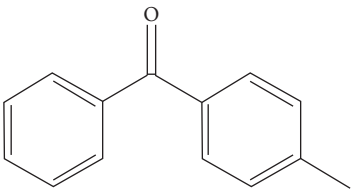	134-84-9	Polar	3.4	196	326	Photoinitiator
DPP	Di-*n*-propyl phthalate	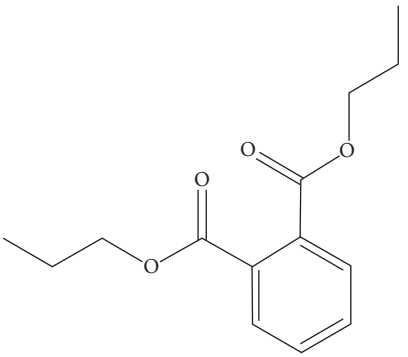	131-16-8	Polar	3.8	250	340	Plasticiser
ANT	Anthracene	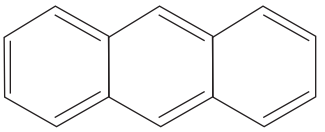	120-12-7	Nonpolar	4.56	178	340	MOAH
PER	Perylene	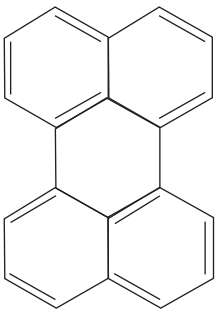	198-55-0	Nonpolar	5.74	252	494	MOAH
—	Sudan red II		3118-97-6	—	—	—	—	Visual inspection
MTBE	Methyl tert-butyl ether		1634-04-4	—	—	—	55.2	Solvent

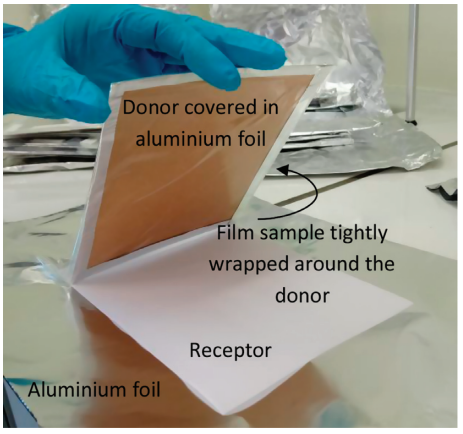

Figure 3: Test pack before being enclosed in aluminium foil.

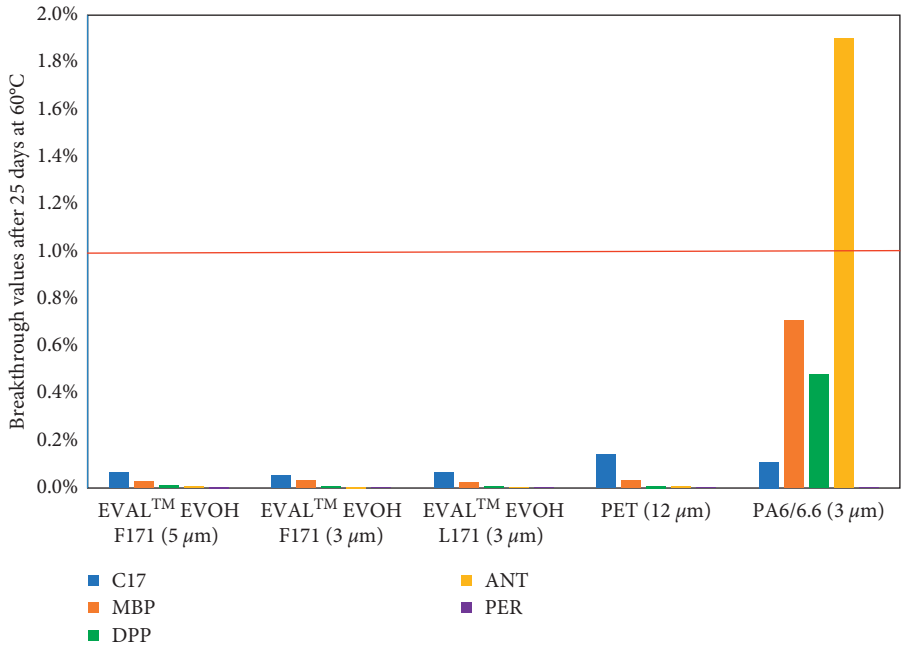

Figure 4: Breakthrough values of *n*-heptadecane (C17), 4-methyl benzophenone (MBP), di-*n*-propyl phthalate (DPP), anthracene (ANT), and perylene (PER) after 25 days at 60°C.

MBP, DPP, and ANT. However, a clear correlation between O_2GTR and the migration of the surrogate components was not visible, as the PA 6/6.6 had similar breakthrough values for C17 as PET and EVOH, which both outperformed the PA 6/6.6 as an oxygen barrier.

4. Conclusion

The results show that both EVAL™ F171B (3 and 5 μm) and L171B (3 μm) have good barrier properties against the surrogate components migrating from recycled paperboard. They can easily compete with PET (12 μm), while clearly outperforming PA 6/6.6 at the same thickness.

When applying the 1% threshold value for breakthrough, both EVOH grades can comfortably protect the food for a shelf life of over 2 years at 25°C against mineral oil migration. Additionally, EVOH also offers good barrier properties against oxygen, nitrogen, carbon dioxide, odours, aroma, flavours, and others, making it a multifunctional solution.

Data Availability

The data used to support the findings of this study are available from the corresponding author upon request.

Conflicts of Interest

This study was done via a collaboration between University Hasselt and Kuraray EVAL Europe, which was partly supported by the agency Flanders Innovation & Entrepreneurship via a VLAIO Baekeland mandate (PhD in collaboration with the industry). The main author was employed at EVAL Europe during her PhD and is affiliated to both University Hasselt and Kuraray EVAL Europe.

Acknowledgments

The authors would like to thank Dr. Thomas Gude from SQTS for his valuable input, as well as An Grieten and Kevin Mertens from the Smurfit Kappa group, who so kindly provided us with paperboard samples. Special thanks are due to Jan Czech from the research group Applied and Analytical Chemistry and Dimitri Adons from the Packaging Technology Center for their support. The authors would also like to thank David Smits, Philip Willems, Miche Gruythuysen, Ellen Verachtert, and Clara Vlaeminck from EVAL Europe NV for their contribution. The authors acknowledge support from the agency Flanders Innovation & Entrepreneurship via the VLAIO Baekeland mandate of Caroline Maes (IWT 150253).

References

[1] Bundesinstitut für Risikobewertung (BfR), *Stellungnahme Nr. 008/2010: Übergänge von Mineralöl aus Verpackungsmaterialien auf Lebensmittel*, Bundesinstitut für Risikobewertung (BfR), Berlin, Germany, 2009.

[2] EFSA, EFSA Panel on Contaminants in the Food Chain (CONTAM), "Scientific Opinion on Mineral Oil Hydrocarbons in Food," *EFSA Journal*, vol. 10, no. 6, p. 185, 2012.

[3] M. Biedermann, K. Fiselier, and K. Grob, "Aromatic hydrocarbons of mineral oil origin in foods: method for determining the total concentration and first results," *Journal of Agricultural and Food Chemistry*, vol. 57, no. 19, pp. 8711–8721, 2009.

[4] M. Biedermann, Y. Uematsu, and K. Grob, "Mineral oil contents in paper and board recycled to paperboard for food

packaging," *Packaging Technology and Science*, vol. 24, no. 2, pp. 61–73, 2011.

[5] M. Biedermann, J.-E. Ingenhoff, M. Barbanera, D. Garbini, and K. Grob, "Migration of mineral oil into noodles from recycled fibres in the paperboard box and the corrugated board transport box as well as from printing inks: a case study," *Packaging Technology and Science*, vol. 24, no. 5, pp. 281–290, 2011.

[6] A. Vollmer, M. Biedermann, F. Grundböck et al., "Migration of mineral oil from printed paperboard into dry foods: survey of the German market," *European Food Research and Technology*, vol. 232, no. 1, pp. 175–182, 2010.

[7] R. Lorenzini, K. Fiselier, M. Biedermann, M. Barbanera, I. Braschi, and K. Grob, "Saturated and aromatic mineral oil hydrocarbons from paperboard food packaging: estimation of long-term migration from contents in the paperboard and data on boxes from the market," *Food Additives and Contaminants: Part A*, vol. 27, no. 12, pp. 1765–1774, 2010.

[8] *Regulation (EC) No 1935/2004 of The European Parliament and of The Council of 27 October 2004 on Materials and Articles Intended to Come into Contact with Food and Repealing Directives 80/590/EEC and 89/109/EEC*, 2004, https://eur-lex.europa.eu/legal-content/EN/TXT/?qid=1542700905837&uri=CELEX:02004R1935-20090807.

[9] *Commission Regulation (EU) No 10/2011 of 14 January 2011 on Plastic Materials and Articles Intended to Come into Contact with Food*, 2011, https://eur-lex.europa.eu/legal-content/EN/TXT/?qid=1542701000844&uri=CELEX:02011R0010-20180914.

[10] Bundesministerium für Gesundheit, *Empfehlung BMG-75210/0018-II/B/13/2012: Verwendung von Recyclingkarton zur Lebensmittelverpackung*, Bundesministerium für Gesundheit, Berlin, Germany, 2012.

[11] EDI, *Verordnung des EDI über Materialien und Gegenstände, die dazu bestimmt sind, mit Lebensmitteln in Berührung zu KommenIssuing Organization*, Das Eidgenössische Departement des Innern (EDI), Washington, DC, USA, 2016, https://www.admin.ch/opc/de/classified-compilation/20143393/index.html.

[12] T. Bode, *Mineralöle in Lebensmitteln—Ergebnisse des Foodwatch-Tests*, (V.i.S.d.P.) Foodwatch e. V., Berlin, Germany,-November 2018, https://www.foodwatch.org/uploads/media/Testergebnisse_Mineraloele_in_Lebensmitteln.pdf.

[13] Foodwatch e. V., *Gift aus der Verpackung—Mineralöl und Andere Chemikalien in Lebensmitteln*, Foodwatch e. V., Berlin, Germany, November 2018, https://www.foodwatch.org/uploads/media/2015-10_Mineraloel_in_Lebensmitteln_Hintergrund_11.pdf.

[14] K. Fiselier and K. Grob, "Barriers against the migration of mineral oil from paperboard food packaging: experimental determination of breakthrough periods," *Packaging Technology and Science*, vol. 25, no. 5, pp. 285–301, 2012.

[15] C. Maes, W. Luyten, G. Herremans, R. Peeters, R. Carleer, and M. Buntinx, "Recent updates on the barrier properties of ethylene vinyl alcohol copolymer (EVOH): a review," *Polymer Reviews*, vol. 58, no. 2, pp. 209–246, 2018.

[16] K. K. Mokwena and J. Tang, "Ethylene vinyl alcohol: a review of barrier properties for packaging shelf stable foods," *Critical Reviews in Food Science and Nutrition*, vol. 52, no. 7, pp. 640–650, 2012.

[17] R. B. Armstrong, M. Asme, M. Spe, and M. Igs, "Improving indoor air quality by reducing radon and vapor intrusion through the use of ethylene vinyl alcohol (EVOH)," in *Proceedings of International Radon Symposium*, Columbus Ohio, 2010.

[18] G. Lopez-Carballo, D. Cava, J. M. Lagarón, R. Catalá, and R. Gavara, "Characterization of the interaction between two food aroma components, alpha-pinene and ethyl butyrate, and ethylene-vinyl alcohol copolymer (EVOH) packaging films as a function of environmental humidity," *Journal of Agricultural and Food Chemistry*, vol. 53, no. 18, pp. 7212–7216, 2005.

[19] C. Maes et al., "Cardboard packaging with ethylene vinyl alcohol copolymer (EVOH) as a functional barrier against mineral oil migration," in *Proceedings of 28th IAPRI Symposium on Packaging 2017: Unlocking the Full Potential of Packaging Across the Value-Chain*, The Olympic Museum, Lausanne, Switzerland, May 2017.

[20] S. Biedermann-Brem and K. Grob, "Barriers against the migration from recycled paperboard into food: measuring efficiency by surrogate components," *Packaging Technology and Science*, vol. 27, no. 9, pp. 713–726, 2014.

[21] S. Biedermann-Brem, M. Biedermann, and K. Grob, "Taped barrier test for internal bags used in boxes of recycled paperboard: update of the method," *Packaging Technology and Science*, vol. 30, no. 3, pp. 91–102, 2017.

[22] SVI Schweizerisches Verpackungsinstitut, *SVI Guideline—Specification and Testing of Barrier Efficiency of Internal Bags for Food Packaging in Recycled Paper-Board*, SVI Schweizerisches Verpackungsinstitut, Bern, Switzerland, 2016.

[23] S. Biedermann-Brem, M. Biedermann, and K. Grob, "Taped barrier test for internal bags used in boxes of recycled paperboard: the role of the paperboard and its consequence for the test," *Packaging Technology and Science*, vol. 30, no. 3, pp. 75–89, 2017.

[24] BMELV German Federal Ministry of Food Agriculture and Consumer Protection, *Ausmaß der Migration Unerwünschter Stoffe aus Verpackungsmaterialien aus Altpapier in Lebensmittel, Project 2809HS012*, BMELV German Federal Ministry of Food Agriculture and Consumer Protection, Bonn, Germany, 2012.

[25] A. R. De Anda, L. A. Fillot, S. Rossi, D. Long, and P. Sotta, "Influence of the sorption of polar and non–polar solvents on the glass transition temperature of polyamide 6,6 amorphous phase," *Polymer Engineering and Science*, vol. 51, no. 11, pp. 2129–2135, 2011.

[26] J. M. Lagarón, E. Giménez, R. Gavara, and J. J. Saura, "Study of the influence of water sorption in pure components and binary blends of high barrier ethylene–vinyl alcohol copolymer and amorphous polyamide and nylon-containing ionomer," *Polymer*, vol. 42, no. 23, pp. 9531–9540, 2001.

[27] Q. X. Zhou, B. Guthrie, and K. R. Cadwallader, "Development of a system for measurement of coupling dynamic vapour sorption with purge-and-trap/fast gas chromatography," *Packaging Technology and Science*, vol. 17, no. 4, pp. 175–185, 2004.

Hindawi
Journal of Chemistry
Volume 2018, Article ID 7575201, 6 pages
https://doi.org/10.1155/2018/7575201

Research Article

Microfluidic Preparation of Liposomes Using Ethyl Acetate/*n*-Hexane Solvents as an Alternative to Chloroform

Eunhye Yang,[1] Hyunjong Yu,[1] Jun-Young Park,[1] Kyung-Min Park,[2] and Pahn-Shick Chang[1,3,4]

[1]*Department of Agricultural Biotechnology, Seoul National University, Seoul 08826, Republic of Korea*
[2]*Department of Food Science and Biotechnology, Wonkwang University, Iksan 54538, Republic of Korea*
[3]*Center for Food and Bioconvergence, Seoul National University, Seoul 08826, Republic of Korea*
[4]*Research Institute of Agriculture and Life Sciences, Seoul National University, Seoul 08826, Republic of Korea*

Correspondence should be addressed to Kyung-Min Park; kmpark79@wku.ac.kr and Pahn-Shick Chang; pschang@snu.ac.kr

Received 6 September 2018; Revised 30 October 2018; Accepted 21 November 2018; Published 18 December 2018

Academic Editor: José L. Arias Mediano

Although liposomes have been used as a nutrient delivery carrier in the pharmaceutical, cosmetic, and food industries, they still suffer from the critical issue caused by the use of halogenated solvents (e.g., chloroform), which may be harmful to humans. Nonhalogenated solvents have been screened as candidate substitutes for chloroform based on their physicochemical properties. However, none of the candidates examined to date could form stable inverted micelles when used alone. Here, to obtain physicochemical properties similar to chloroform, combined mixtures were prepared using various ratios of each candidate. Based on the results of random combination trials with numerous candidates, ethyl acetate: *n*-hexane = 4 : 1(v/v) was selected as the optimum ratio because it could form stable inverted micelles and a transparent liposome solution without phase separation. The ethyl acetate and *n*-hexane mixture are a potential substitute for chloroform, which may resolve concerns regarding the toxicity of residual halogenated solvents in lipid nanovesicles.

1. Introduction

Lipid nanovesicles have been used extensively in the cosmetics, food, and pharmaceutical industries to increase stability, dispersibility, flavor or taste masking, and bioavailability of functional materials [1]. Their basic structures consist of spherical vesicles with an aqueous core surrounded by a hydrophobic lipid bilayer. Due to their inherent structures, both hydrophobic and hydrophilic bioactive materials can be simultaneously incorporated into a single lipid nanovesicle. This characteristic makes lipid nanovesicles attractive for use in various industries.

Liposomes are the best-studied lipid nanovesicles, with a lipid bilayer formed by phospholipids as the main building blocks [2]. They have also been developed for actual food applications, including encapsulation of iron (ferrous sulfate) [3], lactoferrin [4], and ascorbic acid [5] in milk. Although liposomes have potential for use as delivery systems, there are still some problems associated with the organic solvents used in their preparation [6]. Among the various organic solvents available, chloroform has often been used due to its low boiling point and high evaporation rate. However, it cannot be completely removed from final products by changing manufacturing practices because of physical or chemical barriers. In addition to having no therapeutic value, organic solvents may be associated with chronic health effects, especially halogenated solvents [7], as they affect the central nervous system, kidney, and liver and cause dermatitis and irritation of the skin, eyes, upper respiratory tract, and mucous membranes [8, 9]. In addition, encapsulated products may show accelerated decomposition due to these solvents [10].

To resolve this problem, various approaches have been reported using nonhalogenated and less hazardous solvents,

such as isopropyl alcohol [11] and ethanol [12]. Unfortunately, the methods are restricted to a small scale, such as injection methods, as their nature makes it difficult to evaporate these solvents to establish mass-production systems.

This study was performed to identify a substitute nonhalogenated solvent that could be applied to the production of liposomes from the laboratory scale to the pilot scale. The novel water/oil/water (W/O/W) emulsion method using a microfluidizer [13] was used in this study due to its advantages, including simplicity, low polydispersity, continuous flow of solvent without danger of clogging, suitability for heat-sensitive materials, and ease of scaling up to larger volumes, all of which make it well-suited to many food manufacturing processes. Finally, to assess various applications of liposomes prepared using nonhalogenated solvents, branched-chain amino acids (BCCAs) [14, 15] and curcumin [16, 17] were encapsulated as a hydrophilic material and a hydrophobic material, respectively.

2. Materials and Methods

2.1. Materials. Phosphatidylcholine (soybean lecithin) was purchased from Ilshin Wells (Seoul, Korea). β-Sitosterol (>99.0%), isopropanol, curcumin, and a ninhydrin assay kit were purchased from Sigma-Aldrich Co. (St. Louis, MO). Organic solvents, including chloroform, acetone, ethyl acetate, and *n*-hexane, were purchased from Daejung Chemical & Metals Co. (Siheung, Gyeonggi-do, Korea). Branched-chain amino acids (BCAAs, leucine : isoleucine : valine = 2 : 1 : 1 (w/w/w)) were kindly provided by Daesang Co. (Icheon, Gyeonggi-do, Korea). Ethylene glycol and stannous chloride ($SnCl_2$) were purchased from Acros Organics (Waltham, MA) and Daejung Chemical & Metals Co., respectively. All chemicals except BCAAs (food grade) were of reagent grade.

2.2. Preparation of Liposomes by the W/O/W Emulsion Method Using a Microfluidizer. Figure 1 shows a schematic diagram of the double emulsion (W/O/W) method using a microfluidizer. Lecithin (1 g) and β-sitosterol (0.125 g) were dissolved in 200 mL of each organic solvent and subsequently stirred for 5 minutes to form clear solutions. Then, 100 mL distilled water with BCAAs or curcumin was added to the mixture and sonicated with a 20 kHz probe-type ultrasonicator (ULH-700S; Jeiotech, Korea) for 5 minutes to form inverted micelles; each cycle consisted of 1 second pulse-on and 4 seconds pulse-off with 210 W sonication power at 4°C. Inverted micellar solution was injected into a microfluidizer adjusted to a pressure of 15,000 psi for 10 passage times to form small and even inverted micelles. Samples were retrieved from the microfluidizer after which two volumes of distilled water with 5 g of sucrose were added, and the mixture was sonicated. The microfluidizer was primed with distilled water. The sample mixture was microfluidized by passage five times at a pressure of 5,000 psi. After the microfluidization process, a homogeneous white opaque W/O/W double emulsion was formed with the organic phase filling the small space between the lipid layers. The W/O/W emulsion solutions were placed in glass beakers and magnetically stirred at 400 rpm to evaporate organic solvents. The emulsion solution prepared with chloroform used as the positive control was treated for 24 hours, and the emulsion solutions prepared with combinations of ethyl acetate/*n*-hexane were treated for 48 hours at room temperature. By the time evaporation was complete, the phospholipids had formed a typical liposomal bilayer and the solution was transparent.

2.3. Analysis of Liposomes

2.3.1. Dynamic Light Scattering (DLS). The size distribution and polydispersity index (PdI) of the liposomes were measured using a Zetasizer Nano ZS (Malvern Instruments, Worcestershire, UK). Samples in a volume of 0.5–1.0 mL were applied to disposable plastic cuvettes, and each measurement was conducted in triplicate. Sample measurement conditions were refractive index, 1.330; viscosity, 0.8872 conventional; equilibration time, 1 minute; measurement temperature, 25°C; and measurement angle, 173° backscattering.

2.3.2. Transmission Electron Microscopy (TEM). For visualization using TEM, uranyl acetate was used as a negative staining reagent for the liposomes [6]. The overall procedures were as follows. The vesicle sample (10 μL) was dropped onto a Formvar-coated silicon monoxide grid (200 mesh). After 1 minute, uranyl acetate solution (2%(w/v)) was loaded onto the grid for 1 minute, followed by direct washing of the grid with double-distilled water. The grid was dried completely at ambient temperature before visualization of the vesicles by TEM (120 keV; JEOL Ltd., Tokyo, Japan).

2.3.3. Encapsulation Efficiency

(1) Ninhydrin Analysis. For ninhydrin reagent preparation, ninhydrin powder (200 mg) was dissolved in 7.5 mL ethylene glycol and vortexed for 2 minutes, followed by mixing with 2.5 mL 4N sodium acetate buffer (pH 5.5). Stannous chloride solution was prepared by dissolving $SnCl_2$ powder (50 mg) in 500 μL ethylene glycol. Finally, the stannous chloride solution (250 μL) was mixed with the previous solution just before the reaction [18]. The BCAA sample (20 μL) and ninhydrin reagent (100 μL) were loaded together into 2 mL microtubes and vortexed for 5 seconds. The microtubes were heated in a boiling water bath for 10 minutes, followed by immediate cooling on ice for at least 2 minutes. Then, 1 mL 50% (v/v) ethanol solution was applied to the microtubes and vortexed for 5 seconds. The absorbance of each sample was measured spectrophotometrically at 570 nm using a UV-Vis spectrophotometer (UV-2450; Shimadzu, Kyoto, Japan).

(2) Curcumin Content. The absorbance of each sample was measured spectrophotometrically at 570 nm using a UV-Vis

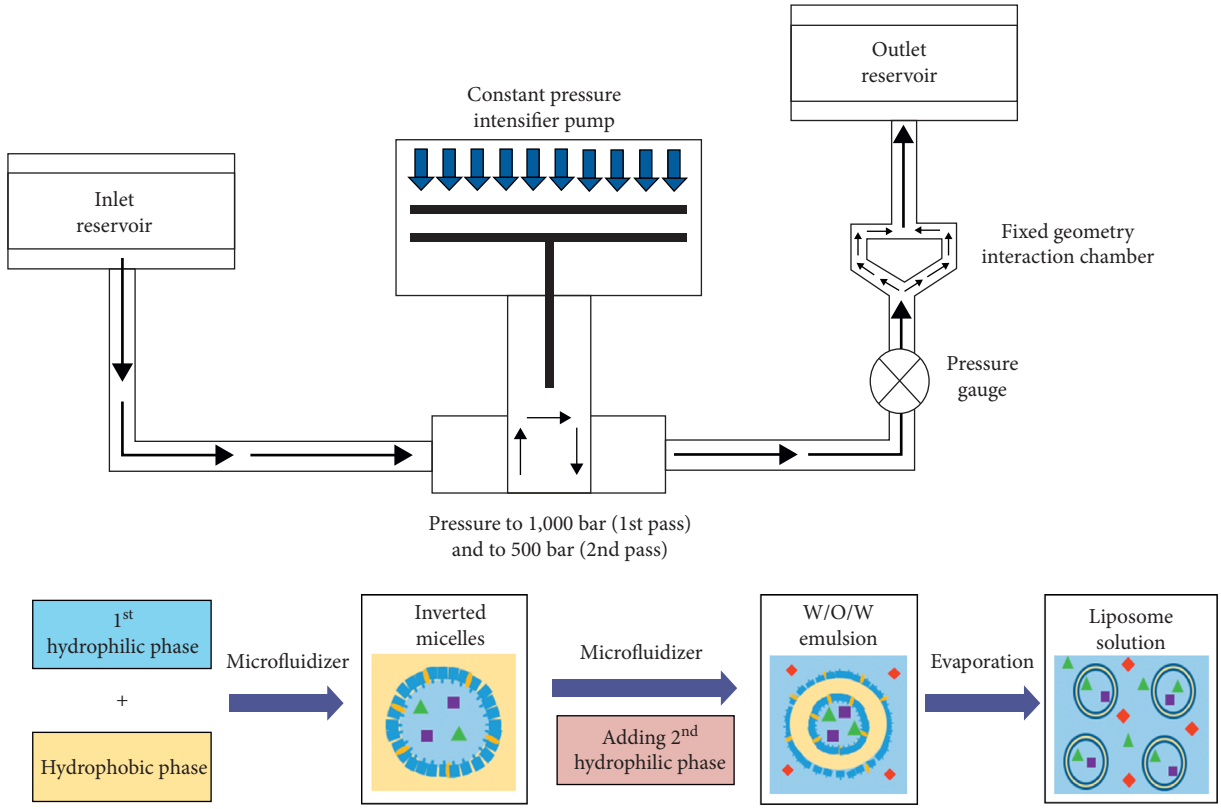

Figure 1: Schematic diagram of the double emulsion (water/oil/water) method using microfluidizer.

spectrophotometer (UV-2450; Shimadzu, Kyoto, Japan), and curcumin content was calculated based on the calibration curve of curcumin in water.

(3) Encapsulation Efficiency. The samples (approximately 3.5 mL) were loaded into ultrafiltration tubes and then centrifuged at 4,000 × g for 10 minutes. The retentant and the filtrate were collected, and their volumes were measured using a pipette. In addition, the material concentration of the retentant and the filtrate was measured using a UV-Vis spectrophotometer after treatment with Triton X-100. The encapsulation efficiency (%) was calculated using the following equation:

$$\text{encapsulation efficiency (EE)} = 100 \times \frac{\text{total material} - \text{free material}}{\text{total material}}, \quad (1)$$

where the total material is the sum of the material in the retentant and the filtrate and the free material is the amount of material in the filtrate.

3. Results and Discussion

3.1. Selection of Nonhalogenated Solvents. Solvents were first selected from the nonhalogenated solvents that are frequently used for extraction of functional materials. They were then filtered out according to the permissible daily exposure limit, as determined by the Ministry of Food and Drug Safety (MFDS) guidelines, in milligrams. Finally, candidates (acetone, isopropyl alcohol, *n*-hexane, and ethyl acetate) were selected based on having solvent properties similar to chloroform, including high polarity and high vapor pressure. The availability of these candidates to liposomes was assessed by examining whether phase separation occurred at the stage of inverted micelle production for 24 hours at room temperature.

When *n*-hexane and ethyl acetate were used as solvents, respectively, the inverted micelle phases immediately separated (within 1 hour) into micelle-poor and micelle-rich phases that formed densely packed aggregates, and most micelles were destroyed (Figure 2) as *n*-hexane has lower polarity (polarity index = 0.1) and ethyl acetate higher solubility in water (8.7 g/100 mL) than chloroform (polarity index = 4.1 and solubility in water = 0.81 g/100 mL). When isopropyl alcohol and acetone were used as solvents, they were found to be miscible in water. This property prevented them forming a lipid bilayer for W/O/W emulsion in the second stage and dispersal like micelles.

To obtain the desired physicochemical properties, ethyl acetate and *n*-hexane were combined in various ratios based on the properties of the solvents (Table 1). Ethyl acetate: *n*-hexane = 4 : 1 (v/v) was selected as the optimum ratio because it formed stable inverted micelles without phase separation for 24 hours and produced the most transparent liposome solution (Figure 3).

3.2. Preparation of Liposomes Loaded with Hydrophilic/Hydrophobic Materials. Liposomes prepared by the double emulsion method using the mixed solvent to dissolve

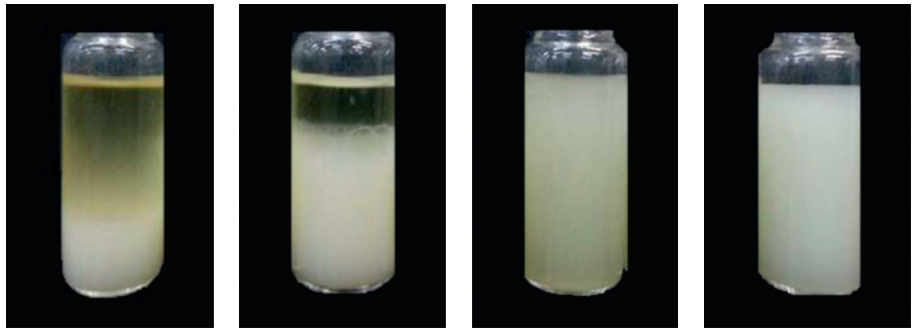

(a) (b) (c) (d)

Figure 2: Inverted micelles prepared using nonhalogenated solvents to dissolve phospholipids. (a) *n*-hexane; (b) ethyl acetate; (c) acetone; (d) isopropyl alcohol.

Table 1: Physicochemical properties of chloroform and nonhalogenated solvents.

	Chloroform	*n*-Hexane	Ethyl acetate	Acetone	Isopropanol	Methanol	Diethyl ether	Methyl acetate	Benzene
Polarity index	4.10	0.10	4.40	5.10	3.90	5.10	2.80	4.40	3.00
Solubility in water (g/100 mL)	0.82	0.00	8.70	Miscible	Miscible	Miscible	6.90	24.40	0.18
Viscosity (cP)	0.57	0.33	0.45	0.32	2.30	0.55	0.22	0.36	0.61
Vapor pressure (kPa)	25.90	17.60	9.73	30.60	6.02	13.02	58.66	23.06	12.70
Lecithin solubility	S	S	S	S	S	I	S	I	S
Allowable concentration (g/kg)	Prohibited	0.01	0.05	0.03	0.05	0.05	Prohibition	Prohibition	Prohibition

S, soluble; I, insoluble.

Figure 3: Inverted micelles (a) (layer separation) and liposomes (b) (transparency) prepared using mixtures with different volumetric ratios of ethyl acetate to *n*-hexane.

lipid loaded with the hydrophilic material, BCAA, were small and monodispersed (PdI = 0.177 and diameter = 98.68 nm). TEM was used to characterize the morphology of the liposomes. The size of the liposomes was about 100 nm, which was consistent with the value determined by DLS (Figure 4). The image shows that liposomal bilayers formed from the double emulsions by solvent evaporation. However, the encapsulation efficiency of liposomes prepared using mixed solvents (23.12%) was lower than that of liposomes prepared using chloroform (42.40%). As mixed solvents have lower vapor pressure, they require a longer evaporation time than that of chloroform (48 hours vs. 24 hours, respectively). Prepared using the same method, liposomes loaded with the hydrophobic material, curcumin, were also small and monodispersed (PdI = 0.119 and diameter = 88.1 nm). TEM analysis showed the size of the liposomes to be about 100 nm, which was consistent with the value determined by DLS (Figure 5). The morphology of liposomes with curcumin produced from the double emulsion solution was similar to that of the liposomes with the hydrophilic material. In contrast to the hydrophilic material, the encapsulation efficiency of the curcumin-loaded liposomes prepared using mixed solvents (98.0%) was similar to that of liposomes prepared using chloroform (99.0%). These observations implied that

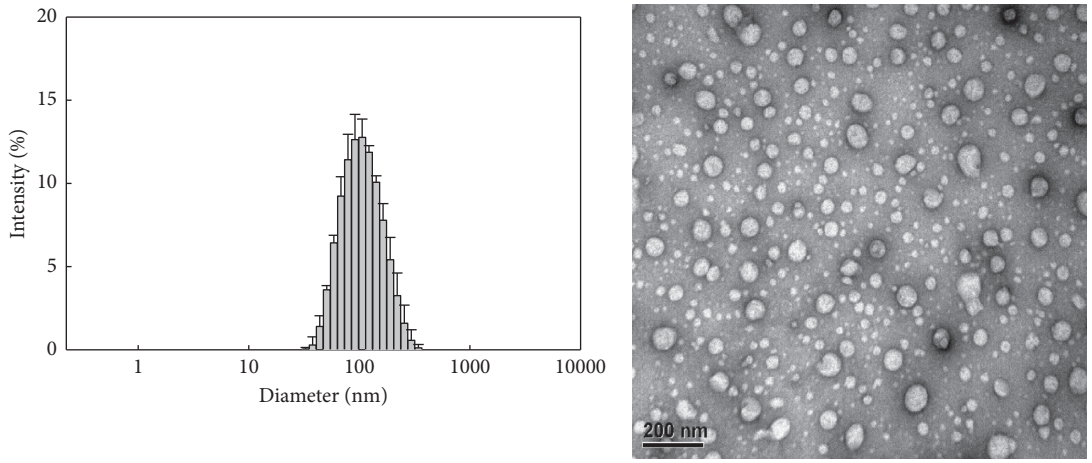

Figure 4: Size distribution (a) and TEM visualization (b) of BCAA-loaded liposomes prepared using nonhalogenated solvent (ethyl acetate : *n*-hexane = 4 : 1 (v/v)).

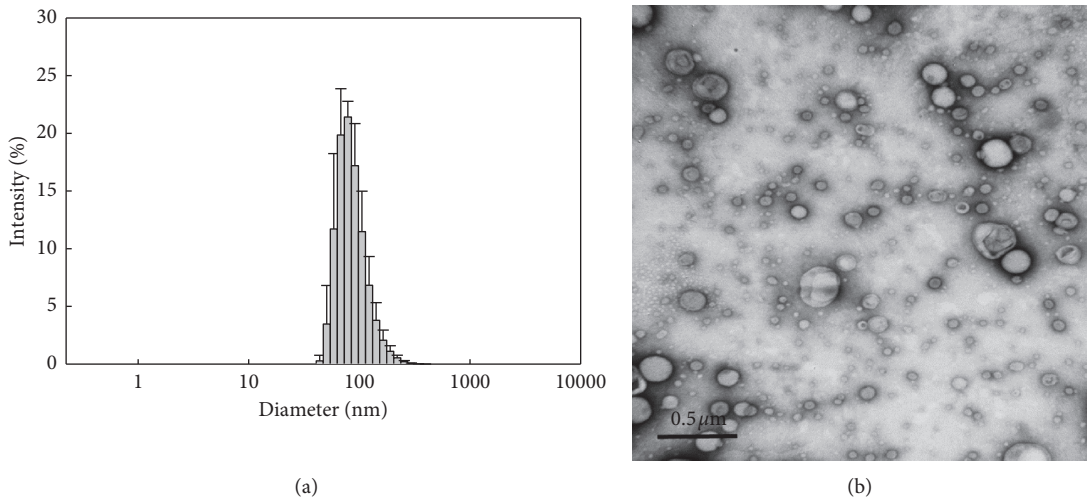

Figure 5: Size distribution (a) and TEM visualization (b) of curcumin-loaded liposomes prepared using nonhalogenated solvent (ethyl acetate : *n*-hexane = 4 : 1(v/v)).

hydrophobic materials are less affected by evaporation time than that of hydrophilic materials.

4. Conclusion

Candidate solvents (acetone, isopropyl alcohol, *n*-hexane, and ethyl acetate) were selected from among food-compatible and nonhalogenated solvents based on their solvent properties similar to those of chloroform, such as high polarity and high vapor pressure. Individual nonhalogenate solvents did not form stable inverted micelles when used alone. To obtain the desired physicochemical properties, ethyl acetate and *n*-hexane were combined in various ratios. A ratio of ethyl acetate: *n*-hexane = 4 : 1(v/v) was selected because it formed stable inverted micelles without phase separation. This study implies that combinations of nonhalogenated solvents could be promising substitutes for chloroform, which may be harmful to human health.

Data Availability

The data used to support the findings of this study are available from the corresponding author upon request.

Conflicts of Interest

The authors declare that they have no conflicts of interest.

Authors' Contributions

Eunhye Yang and Hyunjong Yu contributed equally to this work.

Acknowledgments

This paper was supported by Wonkwang University in 2018.

References

[1] A. Akbarzadeh, R. Rezaei-Sadabady, S. Davaran et al., "Liposome: classification, preparation, and applications," *Nanoscale Research Letters*, vol. 8, no. 1, 102 pages, 2013.

[2] D. Pentak, "Alternative methods of determining phase transition temperatures of phospholipids that constitute liposomes on the example of DPPC and DMPC," *Thermochimica Acta*, vol. 584, pp. 36–44, 2014.

[3] S. Xia and S. Xu, "Ferrous sulfate liposomes: preparation, stability and application in fluid milk," *Food Research International*, vol. 38, no. 3, pp. 289–296, 2005.

[4] H. Onishi, "Lactoferrin delivery systems: approaches for its more effective use," *Expert Opinion on Drug Delivery*, vol. 8, no. 11, pp. 1469–1479, 2011.

[5] B. Farhang, Y. Kakuda, and M. Corredig, "Encapsulation of ascorbic acid in liposomes prepared with milk fat globule membrane-derived phospholipids," *Dairy Science & Technology*, vol. 92, no. 4, pp. 353–366, 2012.

[6] T. T. Pham, C. Jaafar-Maalej, C. Charcosset, and H. Fessi, "Liposome and niosome preparation using a membrane contactor for scale-up," *Colloids and Surfaces B: Biointerfaces*, vol. 94, pp. 15–21, 2012.

[7] S. Naeem, L. V. Kiew, L. Y. Chung, K. S. Fui, and M. B. Misran, "A comparative approach for the preparation and physicochemical characterization of lecithin liposomes using chloroform and non-halogenated solvents," *Journal of Surfactants and Detergents*, vol. 18, no. 4, pp. 579–587, 2015.

[8] P. Perocco, S. Bolognesi, and W. Alberghini, "Toxic activity of seventeen industrial solvents and halogenated compounds on human lymphocytes cultured in vitro," *Toxicology Letters*, vol. 16, no. 1-2, pp. 69–75, 1983.

[9] L. M. Tormoehlen, K. J. Tekulve, and K. A. Nañagas, "Hydrocarbon toxicity: a review," *Clinical Toxicology*, vol. 52, no. 5, pp. 479–489, 2014.

[10] A. M. Ruder, "Potential health effects of occupational chlorinated solvent exposure," *Annals of the New York Academy of Sciences*, vol. 1076, no. 1, pp. 207–227, 2006.

[11] P. Gentine, A. Bubel, C. Crucifix, L. Bourel-Bonnet, and B. Frisch, "Manufacture of liposomes by isopropanol injection: characterization of the method," *Journal of Liposome Research*, vol. 22, no. 1, pp. 18–30, 2011.

[12] M. Pons, M. Foradada, and J. Estelrich, "Liposomes obtained by the ethanol injection method," *International Journal of Pharmaceutics*, vol. 95, no. 1–3, pp. 51–56, 1993.

[13] T. Lajunen, K. Hisazumi, T. Kanazawa et al., "Topical drug delivery to retinal pigment epithelium with microfluidizer produced small liposomes," *European Journal of Pharmaceutical Sciences*, vol. 62, pp. 23–32, 2014.

[14] S. S. N. Ling, E. Magosso, N. A. K. Khan, K. H. Yuen, and S. A. Barker, "Enhanced oral bioavailability and intestinal lymphatic transport of a hydrophilic drug using liposomes," *Drug Development and Industrial Pharmacy*, vol. 32, no. 3, pp. 335–345, 2008.

[15] X. Xu, M. A. Khan, and D. J. Burgess, "Predicting hydrophilic drug encapsulation inside unilamellar liposomes," *International Journal of Pharmaceutics*, vol. 423, no. 2, pp. 410–418, 2012.

[16] W. S. Orr, J. W. Denbo, K. R. Saab et al., "RETRACTED: liposome-encapsulated curcumin suppresses neuroblastoma growth through nuclear factor-kappa B inhibition," *Surgery*, vol. 151, no. 5, pp. 736–744, 2012.

[17] A. P. Ranjan, A. Mukerjee, L. Helson, R. Gupta, and J. K. Vishwanatha, "Efficacy of liposomal curcumin in a human pancreatic tumor xenograft model: inhibition of tumor growth and angiogenesis," *Anticancer Research*, vol. 33, no. 9, pp. 3603–3609, 2013.

[18] B. Starcher, "A ninhydrin-based assay to quantitate the total protein content of tissue samples," *Analytical Biochemistry*, vol. 292, no. 1, pp. 125–129, 2001.

Hindawi
Journal of Chemistry
Volume 2018, Article ID 2981596, 8 pages
https://doi.org/10.1155/2018/2981596

Research Article

Transglycosylation Properties of a Novel α-1,4-Glucanotransferase from *Bacteroides thetaiotaomicron* and Its Application in Developing an α-Glucosidase-Specific Inhibitor

Hye-Jeong Choi, Dam-Seul Ko, Na-Ri Kim, Woo-Jae Choung, Ye-Seul Koo, Da-Woon Jeong, and Jae-Hoon Shim

Department of Food Science and Nutrition and Center for Aging and Health Care, Hallym University, Hallymdaehak-gil 1, Chuncheon, Gangwon-do 24252, Republic of Korea

Correspondence should be addressed to Jae-Hoon Shim; jhshim@hallym.ac.kr

Hye-Jeong Choi and Dam-Seul Ko contributed equally to this work.

Received 11 September 2018; Accepted 8 November 2018; Published 17 December 2018

Guest Editor: Toshinori Shimanouchi

In this study, α-glucanotransferase from *Bacteroides thetaiotaomicron* was expressed in *Escherichia coli* and characterized. Conserved amino-acid sequence alignment showed that *Bacteroides thetaiotaomicron* α-glucanotransferase (BtαGTase) belongs to the glycoside hydrolase family 77. The enzyme exhibited optimal catalytic activity at 60°C and pH 3.0. BtαGTase catalyzed transglycosylation reactions that produced only glycosyl or maltosyl transfer products, which are preferable for the generation of transglycosylated products with high yield. The 1-deoxynojirimycin (DNJ) glycosylation product G1-DNJ was generated using BtαGTase, and the inhibitory effect of G1-DNJ was analyzed. A kinetic study of inhibition revealed that G1-DNJ inhibited α-glucosidase to a greater extent than did DNJ but did not show any inhibitory effects towards α-amylase, suggesting that G1-DNJ is a potential candidate for the prevention of diabetes.

1. Introduction

Bacteroides thetaiotaomicron is a human colonic gram-negative obligate anaerobe found in high numbers in the human intestine that can ferment a wide diversity of polysaccharides [1]. Members of this genus require carbohydrates as a source of carbon and energy. Polysaccharides are the essential source of carbohydrates for these bacteria in the human intestine [2]. Carbohydrates are fermented by *Bacteroides* and other intestinal bacteria, resulting in the production of volatile fatty acids that are reabsorbed by the large intestine and used by the host as an energy source; these constitute a significant proportion of the host's daily energy requirements. *B. thetaiotaomicron* contains a system that enables the broad utilization of starch and various genes involved in starch binding and application [3]. Wexler reported that its 172 glycohydrolases and 163 homologs of starch-binding proteins enable this organism to utilize a wide variety of dietary carbohydrates available in the gut [4].

The glycoside hydrolase family GH77 is a monospecific family consisting of 4-α-glucanotransferase (α-GTase, EC 2.4.1.25) and defined by an established classification system based on the sequences of all active carbohydrate enzymes from the Carbohydrate-Active Enzyme (CAZy) database [5]. α-GTase catalyzes the transfer of α-1,4-glucan to an acceptor, which is usually the 4-hydroxyl group of another α-1,4-glucan or glucose [6]. In this reaction, hydrolysis of the α-1,4 linkage and subsequent synthesis of a new α-1,4 linkage occur repeatedly within the same glucan molecule or between different molecules [7]. Effective donors of

maltooligosaccharides include amylopectin and soluble starch, which together with glucose also serve as acceptors [8]. These enzymes are found in microorganisms and plants, in which they are involved in maltooligosaccharide metabolism or glycogen and starch metabolism, respectively [6]. While the *Bacteroides thetaiotaomicron* GH77 family contains only one of these enzymes, other GH families contain many carbohydrate-related enzymes.

α-GTase transglycosylation activity is useful in carbohydrate chemistry. Starches that are modified by α-GTases show novel rheological and nutritional properties, such as thermoreversible gelation, fat-replacing properties, and hypocholesterolemic and hypoglycemic effects [9]. α-GTases from different bacteria have successfully modified the properties of various food materials, including increased water solubility, stability, functional effects, and taste [10]. In addition, intramolecular glucan transferase produces cyclic glucans (cycloamyloses) with a higher degree of polymerization compared with cyclodextrins [9]. 1-Deoxynojirimycin (DNJ), an aza-sugar, has structural characteristics similar to those of cyclic monosaccharides; however, the oxygen is substituted with a nitrogen atom. DNJ prevents glucose from entering the bloodstream from the intestines by inhibiting the activities of α-amylase and α-glucosidase [11, 12]. Intestinal α-glucosidase is one of the glucosidases of the small intestinal epithelium [13]. α-Glucosidase hydrolyzes α-1-4-linked D-glucose from the nonreducing end of α-glucoside, which is the last step in the digestion of disaccharides and polysaccharides [14]. Thus, inhibition of intestinal α-glucosidases would prevent the rapid digestion of carbohydrate and, consequently, the sharp postprandial rise in blood glucose [13]. However, antidiabetic drugs that prevent carbohydrate digestion have gastrointestinal side effects, such as abdominal distention and flatulence. These side effects may be caused by the inhibition of α-amylase, which leads to the accumulation of undigested carbohydrates in the intestines [15, 16]. Therefore, antidiabetic drugs that specifically inhibit α-glucosidase are required.

In this study, we cloned a novel α-GTase of the GH77 family from *Bacteroides thetaiotaomicron* (BtαGTase) and examined its reaction pattern using diverse substrates. Additionally, we applied the transglycosylation activity of BtαGTase to DNJ to develop a prospective candidate for the prevention of diabetes.

2. Materials and Methods

2.1. Chemicals and Reagents. *Bacteroides thetaiotaomicron* VPI-5482 was obtained from the Korean Collection for Type Cultures (KCTC). Luria-Bertani (LB) medium was purchased from BD (Franklin Lakes, NJ, USA). NaCl was purchased from GeorgiaChem (Suwanee, GA, USA). Kanamycin monosulfate was purchased from Duchefa Biochemie (Haarlem, the Netherlands). *Escherichia coli* MC1061 (F±, *ara*D139, *rec*A13, D [*ara*ABCleu] 7696, *gal*U, *gal*K, Δ*lac*X74, *rps*L, *thi*, *hsd*R2, and *mcr*B) was used as the parental strain for DNA manipulation and transformation. α-Glucosidase from *Saccharomyces cerevisiae*, α-amylase from porcine pancreas, glucose (G1), maltose (G2), maltotriose (G3), maltotetraose (G4), maltopentaose (G5), maltohexaose (G6), maltoheptaose (G7), DNJ, $Zn(C_2H_2O_2)_2$, *p*-nitrophenyl-α-D-glucopyranoside (*p*NPG), and ammonium hydroxide were purchased from Sigma-Aldrich (St. Louis, MO, USA). Soluble starch, $MnCl_2$, and $CuCl_2$ were purchased from Showa Chemical (Showa, Japan). Amylose (potato starch) was purchased from ICN Biomedicals (Tokyo, Japan). $Co(NO_3)_2$ and $CaCl_2$ were purchased from Junsei Chemical (Tokyo, Japan). $FeCl_2$ and $MgCl_2$ were purchased from Shinyo Pure Chemicals (Tokyo, Japan). EDTA was purchased from Promega (Madison, WI, USA). *p*-Nitrophenyl-α-D-maltoside (pNPG2) was purchased from Gold Biotechnology (Olivette, MO, USA).

2.2. Cloning and Sequence Analysis. The gene encoding *bt_2146* was separated from the genomic DNA of *B. thetaiotaomicron*, and the target DNA was amplified by polymerase chain reaction (PCR) using two primers (bt-F, 5′-AAAA*CCATGG*CCACTGTATCATTTAAC-3′ and bt-R, 5′-AAAA*CTCGAG*TTTCTTGGGAGCTCTGCC-3′) containing the *Nco*I and *Xho*I restriction enzyme sites, respectively. The PCR conditions were as follows: denaturation for 1 min at 98°C, followed by 30 cycles of 10 s at 98°C, annealing for 30 s at 53°C, and extension for 1 min 30 s at 72°C.

2.3. Expression and Purification of a Recombinant Protein. *E. coli* transformants were cultured in LB medium (10 g/L Bacto Tryptone, 5 g/L yeast extract, and 5 g/L NaCl) supplemented with kanamycin (50 μg/mL) for 30 h at 30°C with shaking at 150 rpm. The cells were harvested by centrifugation (7,000 ×g, 20 min, 4°C) and suspended in lysis buffer (300 mM NaCl, 50 mM Tris-HCl buffer (pH 7.5), and 10 mM imidazole). Cells were disrupted using a sonicator in ice-cold water (output 12, 5 min, 4 times; XL-2000; Qsonica, LLC, Newtown, CT, USA). The cell extract was subsequently centrifuged (7,000 ×g, 20 min, 4°C) and the supernatant collected. The supernatant was purified by nickel-nitrilotriacetic acid (Ni-NTA) affinity chromatography using washing (0.9 M NaCl, 0.05 M Tris-HCl buffer (pH 7.5), and 0.02 M imidazole) and elution (0.9 M NaCl, 0.05 M Tris-HCl buffer (pH 7.5), and 0.25 M imidazole) buffers. The purified enzyme, BtαGTase, was visualized by sodium dodecyl sulfate polyacrylamide gel electrophoresis (SDS-PAGE). The BtαGTase concentration was determined from 2 μL drops of protein solution using the NanoDrop 2000c spectrophotometer (Thermo Fisher Scientific, Waltham, MA, USA) at 280 nm with the appropriate extinction coefficient for BtαGTase (227,128 $cm^{-1}\,M^{-1}$).

2.4. Sequence Analysis. The characterized α-GTase sequences of GH77 family members were obtained from the CAZy database (http://www.cazy.org/). Sequence alignment was performed using the Alignment X software, a component of Vector NTI Suite 5.5 (InforMax, Bethesda, MD, USA). In addition, a phylogenetic tree was constructed using MEGA6 software based on the neighbor-joining tree method (1,000 bootstrap samples) [17].

2.5. Enzymatic Assay. BtαGTase enzymatic activity was measured in an amylose and maltose mixture (0.02% (w/v) amylose solution and 0.05% (w/v) maltose solution in 50 mM citric-NaOH (pH 3.0) at 60°C) as described previously by Lee et al. [7]. After preheating at 60°C for 5 min, the enzyme activity was measured using Lugol's solution. The standard curve consisted of ~0.000391–0.025% (w/v) amylose solution, and one unit of BtαGTase activity was defined as the amount of enzyme that hydrolyzed 1 μg/mL reducing amylose 1 min after transfer to G2. Absorbance was measured at 620 nm using a spectrophotometer (Multiskan FC; Thermo Fisher Scientific).

2.6. Effects of Temperature and pH on Enzyme Activity and Stability. The optimal temperature for BtαGTase activity was determined using amylose and G2 as substrates in 50 mM citric-NaOH (pH 3.0) buffer, and Lugol's solution was used to measure the activity at various temperatures (40–70°C). Similarly, the effect of pH on BtαGTase activity was measured at various pH values (2.5–6) using 50 mM citric-NaOH (pH 2.5–3.5) and 50 mM sodium acetate (pH 3.5–6.0).

2.7. Effects of Metal Ions on Enzyme Activity. To evaluate the effects of metal ions on the activity of the purified enzyme, the reaction mixture was preincubated at 50°C for 10 min at 5 mM final concentrations of $MgCl_2$, $MnCl_2$, $CaCl_2$, $CoCl_2$, $CuCl_2$, $FeCl_3$, $ZnCl_2$, and EDTA. The relative activity of BtαGTase was measured under standard conditions (50°C, pH 3.0) using Lugol's solution. The enzyme activity in the absence of metal ions was considered to be 100%.

2.8. Analysis of the Reaction Products Using Thin-Layer Chromatography (TLC). The TLC was performed using a K5F silica-gel plate (Whatman, Maidstone, UK). After the samples were spotted, the silica-gel plate was dried and placed in developing solvent (*n*-butanol:ethanol:water, 5 : 5 : 3, v/v/v). To analyze the reaction products, the TLC plate was dried, saturated in dipping solution (0.33% w/v N-[1-naphthyl]-ethylenediamine and 5% (v/v) H_2SO_4 in methanol), and heated at 110°C for 10 min.

2.9. Preparation of the Transglycosylation Product. For the transglycosylation reaction, a substrate solution containing 1.5% (w/v) DNJ and 1% (w/v) soluble starch was prepared in 50 mM sodium acetate buffer (pH 6.0). BtαGTase was added to this substrate solution and was incubated for 7 h before terminating the enzyme reaction by boiling the solution for 10 min.

2.10. Purification of the Transglycosylation Product Using Preparative-High Performance Liquid Chromatography (Prep-HPLC). The DNJ transglycosylation product was purified using LC-Forte/R preparative-high-performance liquid chromatography (prep-HPLC; YMC Korea, Seongnam, Korea) equipped with a Triart-C18 column (250 × 20 mm; YMC Korea) and an ultraviolet detector (200 and 210 nm). For the isocratic solvent system, 0.1% ammonium in deionized water was used at a flow rate of 12.0 mL/min at room temperature, and 1 mL of the sample was injected.

2.11. High-Performance Anion Exchange Chromatography Analysis (HPAEC). The HPAEC analysis was performed using a CarboPac™ PA1 column (4 × 250 mm; Dionex, Sunnyvale, CA, USA) and a pulsed aerometric detector (ED40; Dionex). For the analysis, 20 μL of the sample was injected and eluted with multiple gradients of 600 mM sodium acetate in 150 mM NaOH at a flow rate of 1 mL/min. The linear gradients of sodium acetate were as follows: 0–2% for 0–20 min, 2–40% for 20–58 min, 40–100% for 58–68 min, 100% for 68–70 min, and 100–0% for 70–78 min.

2.12. Matrix-Assisted Laser Desorption/Ionization Time-of-Flight (MALDI-TOF) Mass Spectrometry Analysis of G1-DNJ. The molecular mass of G1-DNJ was determined using the MALDI-TOF mass spectrometer (Voyager DE-STR; Applied Biosystems, Foster City, CA, USA). The sample in methanol was mixed with the matrix, α-cyano-4-hydroxycinnamic acid (CHCA), at a 1 : 1 ratio. The mixture (1 μL) was applied to a MALDI-TOF mass spectrometry probe and dried slowly at room temperature. An accelerating voltage of 20,000 V was used.

2.13. Inhibition Kinetics of α-Glucosidase and α-Amylase. To determine the inhibition mechanism, a modified Dixon plot was produced [18]. The inhibitory mode of DNJ and the DNJ transfer product (G1-DNJ) against α-glucosidase and α-amylase were analyzed using the substrates *p*NPG and *p*NPG2, respectively. The increase in absorption due to the hydrolysis of *p*NPG substrates was observed at 405 nm using an enzyme-linked immunosorbent assay (ELISA) plate reader (Multiskan FC; Thermo Fisher Scientific). The reaction mixture containing 100 μL of the substrate, 50 mM sodium acetate buffer (pH 7.0), 50 mM potassium phosphate buffer (pH 6.9, 40 μL), and various concentrations of inhibitor (0.1–1 μmol) dissolved in 20 μL distilled water was preheated for 5 min before adding the enzyme (40 μL).

3. Results

3.1. Cloning and Expression of Alpha-Glucanotransferase str. IM2 in E. coli. The α-glucanotransferase-encoding gene *bt_2146* was amplified successfully from *B. thetaiotaomicron* using PCR (Figure S1 in Supplementary Data). The amplified gene (~2.7 kb) was ligated into the pTKNd119 vector. The resulting recombinant plasmid, pTKNdBtαgtase, was transformed into *E. coli* MC1061, and the expressed enzyme was subsequently purified by Ni-NTA affinity chromatography. The expression of BtαGTase was analyzed by SDS-PAGE (Figure S2 in Supplementary Data). The predicted size of the expressed enzyme was 105 kDa. Table 1 shows the purification results.

Table 1: Purification of the BtαGTase enzyme.

Step	Volume (mL)	Enzyme activity (U)	Protein concentration (mg/mL)	Protein amount (mg)	Specific activity (U/mg)	Yield (%)	Purification fold
Cell extract	104	3.57	169.44	17621.76	0.20×10^{-3}	100	1.00
Ni-NTA	1.5	2.03	2.26	3.39	0.59	56.8	2953.20

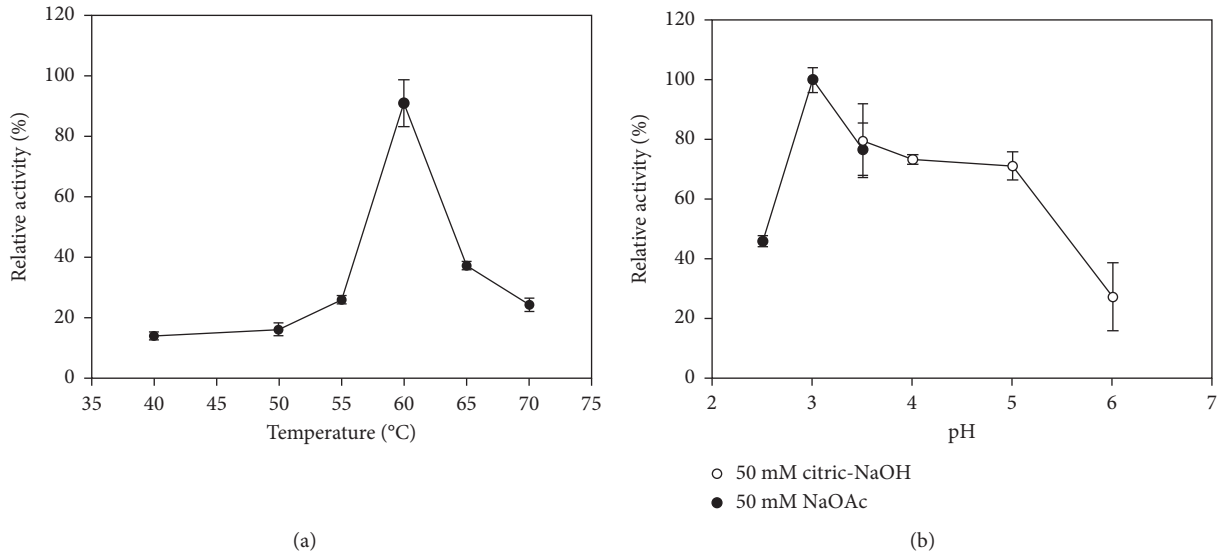

Figure 1: Effect of temperature and pH on *Bacteroides thetaiotaomicron* α-glucanotransferase (BtαGTase) enzyme activity. (a) The optimal temperature and (b) pH were measured using 0.02% amylose and 0.05% maltose as substrates.

3.2. Characterization of Recombinant BtαGTase. The optimal temperature and pH of BtαGTase enzymatic activity, measured using amylose and G2 as substrates, were 60°C and pH 3.0, respectively (Figure 1). BtαGTase showed transglycosylation activity toward α-1,4 linked substrates including G2, G3, G4, G5, G6, and G7 (Figure 2). As shown in Figure 3, some metal ions, including Ca^{2+}, Mg^{2+}, and Cu^{2+}, increased BtαGTase activity; however, other metal ions including Mn^{2+}, Co^{2+}, Zn^{2+}, Fe^{3+}, and EDTA decreased BtαGTase activity.

3.3. Preparation of the DNJ Transfer Product. As shown in Figure 4, DNJ and soluble starch were reacted with BtαGTase, and the enzyme reaction was analyzed by HPAEC. The enzyme reaction product was purified using prep-HPLC and analyzed by HPAEC and MALDI/TOF-MS (Figures 5 and 6). With a molecular mass of 349.33 Da, the transfer product was identified as a glucosyl DNJ (G1-DNJ).

3.4. Kinetic Study of the Inhibitory Activity of DNJ and G1-DNJ. The inhibitory effects of DNJ and G1-DNJ against α-glucosidase and α-amylase were analyzed in a kinetic study. As shown in Figure 7(a), both the DNJ and G1-DNJ plots showed a series of lines converging on the same point above the *x*-axis, indicating that DNJ and G1-DNJ have competitive inhibitory effects on α-glucosidase. The K_i value of G1-DNJ was lower than that of DNJ, suggesting that

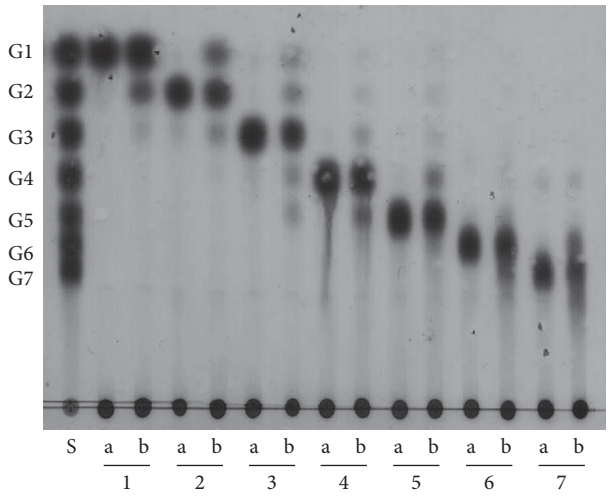

Figure 2: Thin-layer chromatography (TLC) analysis of the transferred products of the BtαGTase reaction. TLC analysis of the hydrolytic products generated by BtαGTase. S, standard (G1–G7); lane 1, glucose (G1); lane 2, maltose (G2); lane 3, maltotriose (G3); lane 4, maltotetraose (G4); lane 5, maltopentaose (G5); lane 6, maltohexaose (G6); and lane 7, maltoheptaose (G7). a, before the reaction; b, after the reaction. Hydrolysis was performed at 60°C at pH 3.0 for 12 h.

G1-DNJ is a better inhibitor of α-glucosidase (Table 2). In the α-amylase inhibition assay, the DNJ plot showed a competitive inhibitory pattern, while the G1-DNJ plot did

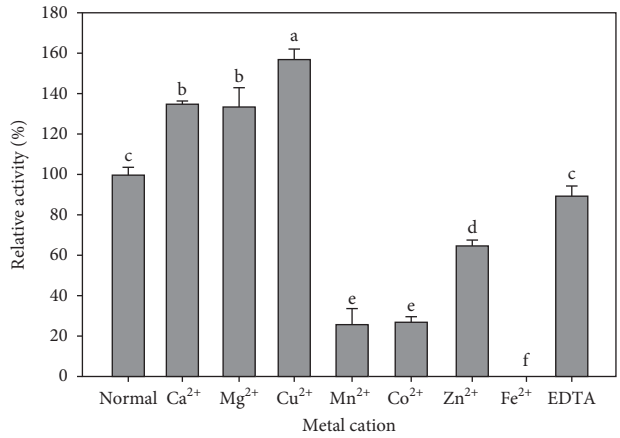

Figure 3: Effect of metal ions on BtαGTase enzyme activity. The purified enzyme was preincubated with various metal ions for 10 min, and the enzyme activity was subsequently measured under standard conditions using G2 and amylose as substrates.

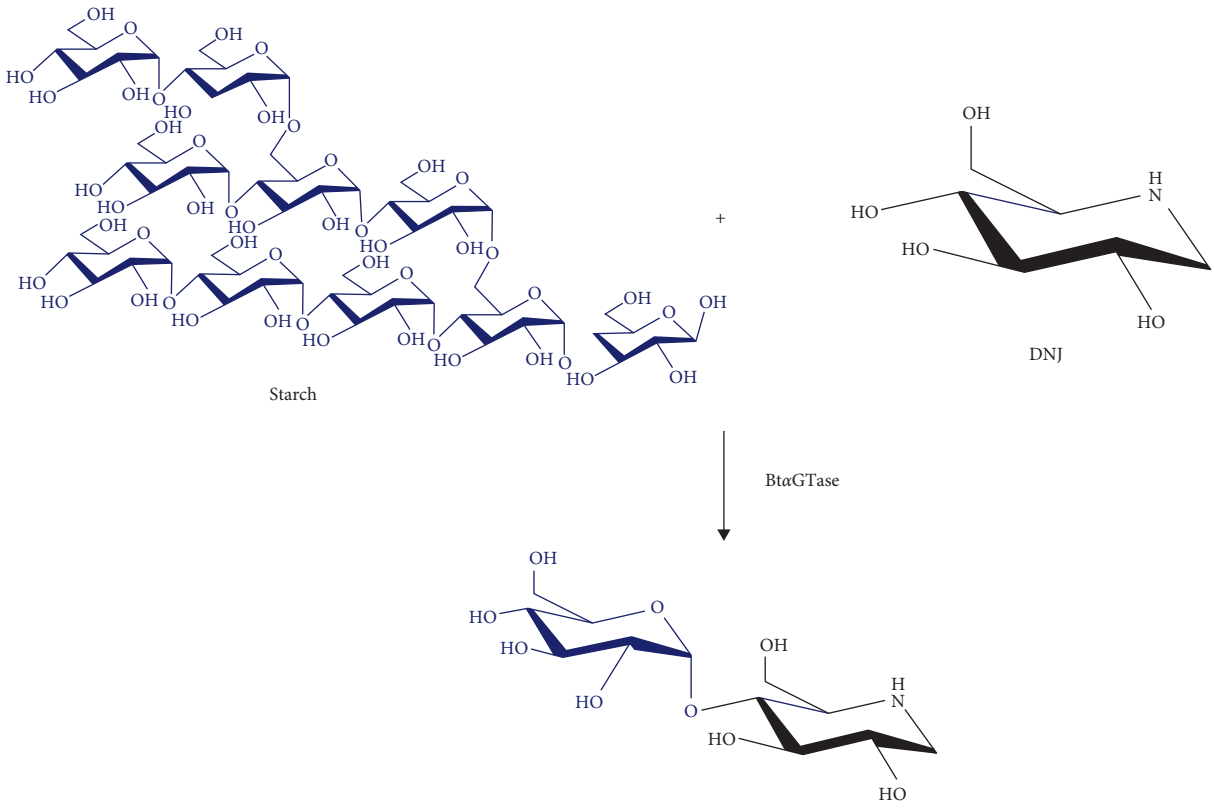

Figure 4: Production of 1-deoxynojirimycin (DNJ) glycosides using BtαGTase from DNJ and starch.

not demonstrate any convergence of lines, indicating that G1-DNJ does not have an inhibitory effect on α-amylase (Figure 7(b)).

4. Discussion

αGTase belongs to the α-amylase superfamily [8, 19]. This enzyme catalyzes disproportionation reactions, which hydrolyze α-glycosidic linkage and subsequently synthesize new α-glycosidic linkage within the same or different glucan molecules [7, 8]. Recently, the use of α-GTase has received considerable attention, specifically for the development of many starch products such as cycloamylose, cyclic cluster dextrin, slowly digestible starch, and thermoreversible starch [20–23]. In our study, a novel α-GTase from *B. thetaiotaomicron* was cloned and characterized. An amino acid sequence alignment indicated that BtαGTase contained conserved regions and three catalytic sites that belong to the GH77 family (Supplementary Data 4). Interestingly, BtαGTase demonstrated low disproportionation activity, resulting in only one or two types of transfer products using various maltooligosaccharides as acceptor molecules

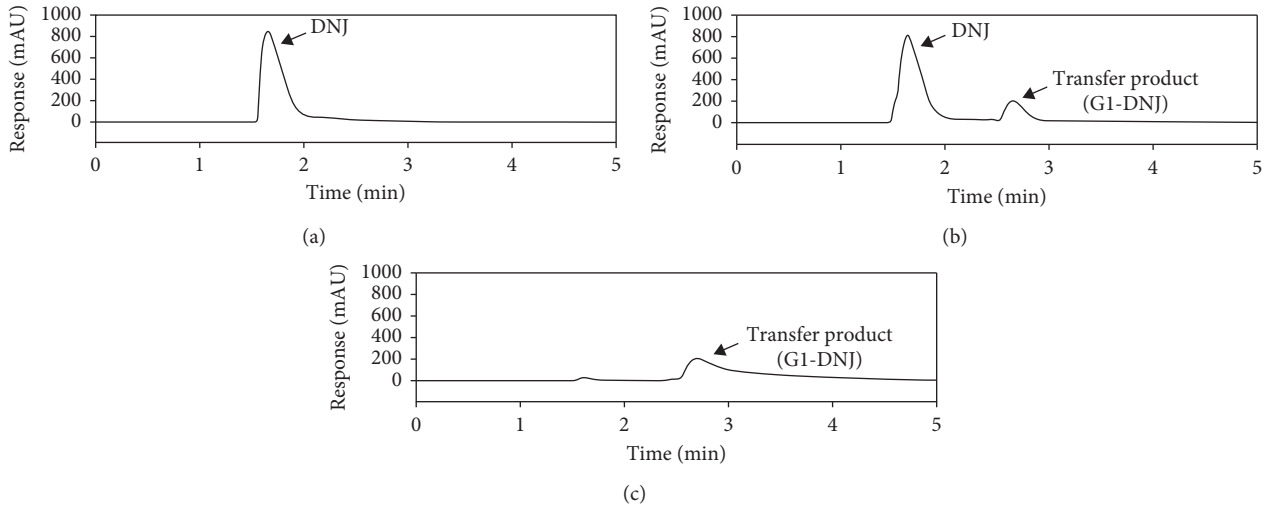

Figure 5: High-performance anion exchange chromatography analysis (HPAEC) chromatograms of DNJ and the transglycosylation product. (a) Before the reaction. (b) After the reaction. (c) The purified transglycosylation product (G1-DNJ).

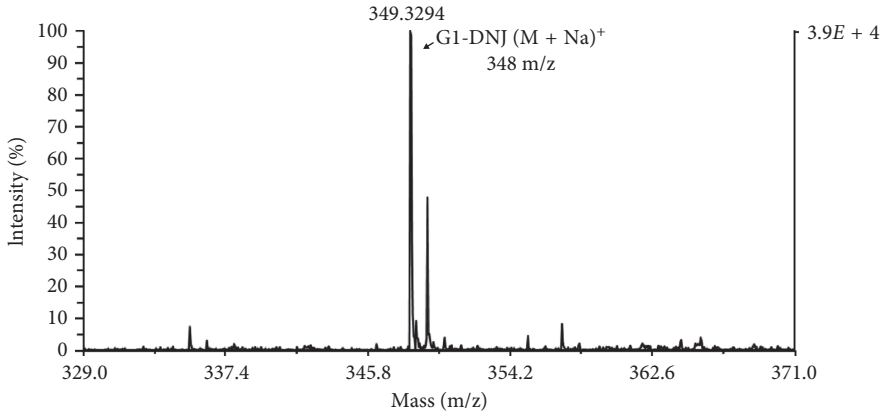

Figure 6: Matrix-assisted laser desorption/ionization time-of-flight (MALDI-TOF) mass spectrum of the DNJ transglycosylation product. The purified glycosylation transfer product was determined using MALDI-TOF mass spectrometry. The molecular weight of the glucoside was one glucose residue larger than that of DNJ. G1-DNJ was observed at m/z 348.3294 $(M + Na)^+$.

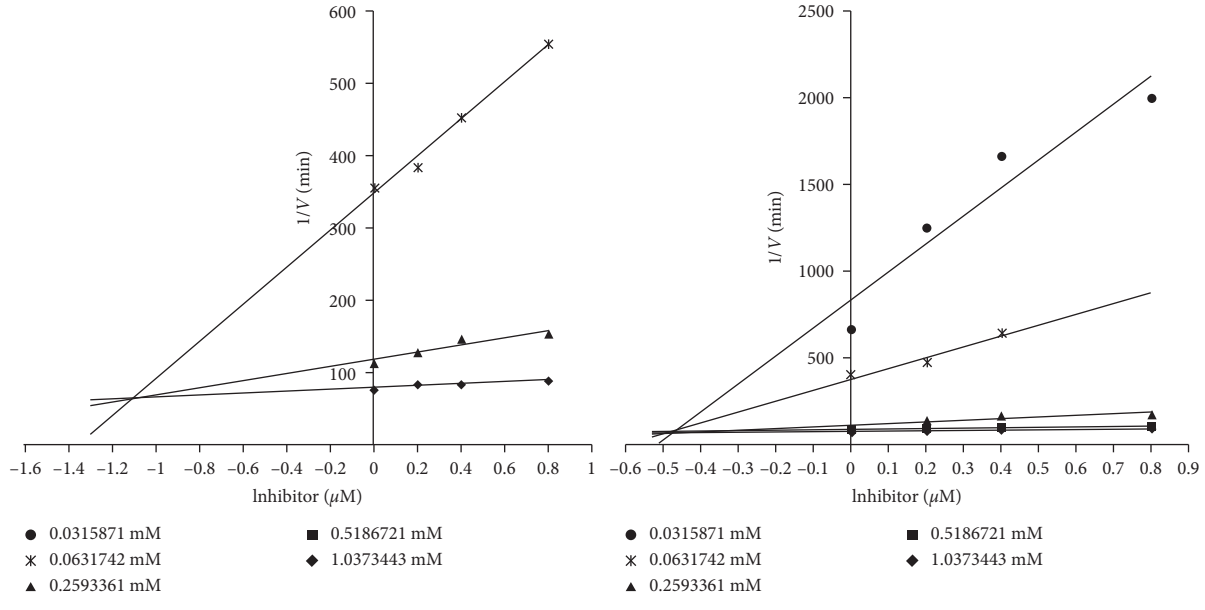

(a)

Figure 7: Continued.

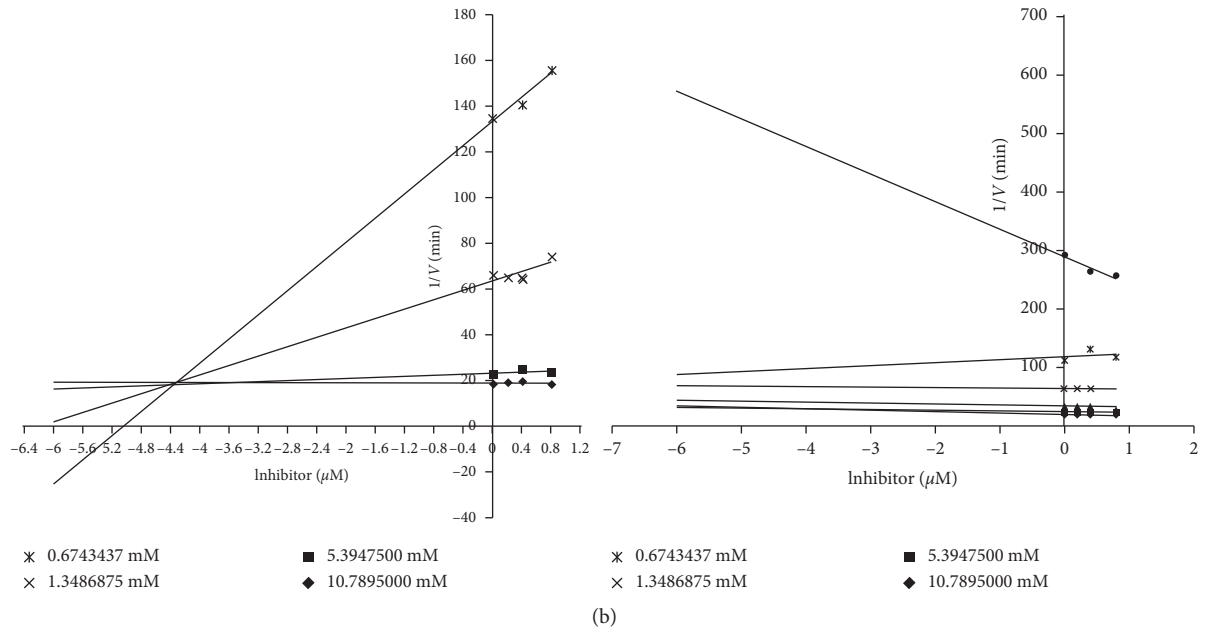

Figure 7: Dixon plots showing the inhibitory effects of the DNJ transglycosylation product on α-glucosidase (a) and α-amylase (b) activity. The reaction rate of the enzyme was measured in the presence of DNJ (left) and G1-DNJ (right).

Table 2: Kinetic study of enzyme inhibition by DNJ and G1-DNJ.

Inhibitor	Enzyme	K_i (μM)	Inhibition type
DNJ	α-Glucosidase	1.1	Competitive
	α-Amylase	4.4	Competitive
G1-DNJ	α-Glucosidase	0.48	Competitive
	α-Amylase	—	—

(Figure 2). Although BtαGTase is not able to elongate several glucosyl units, this low disproportionation activity could be advantageous for the preparation of a single glucosyl-transfer product and to enhance the availability of the acceptor molecule. In addition, the production of various products from an enzyme reaction is not beneficial for the purification of a specific product. Therefore, BtαGTase may be a valuable enzyme for transglycosylation reactions.

Generally, antidiabetic drugs used to treat type II diabetes mellitus, such as acarbose and DNJ, inhibit the activities of α-amylase and α-glucosidase [11]. Inhibition of α-amylase leads to the accumulation of undigested carbohydrates in the intestines, which may cause abdominal distention and flatulence [15, 16]. In this study, the transfer product G1-DNJ inhibited only α-glucosidase (Table 2, Figure 7), which may reduce the side effects of other antidiabetic drugs.

In conclusion, we assessed the properties and industrial applicability of BtαGTase. This enzyme is a novel α-glucanotransferase of the glycoside hydrolase family GH77, and its transglycosylation properties render it efficient in preparing molecules with the transfer of single-glucosyl residues. G1-DNJ, prepared using BtαGTase, showed stronger inhibitory effects than those of DNJ, but it did not affect α-amylase activity, suggesting that this molecule may be a potential drug candidate for the treatment of type II diabetes mellitus.

Data Availability

The data used to support the findings of this study are available from the corresponding author upon request.

Conflicts of Interest

The authors declare that they have no conflicts of interest.

Acknowledgments

This study was partly based on H.-J. Choi's thesis (Hallym University). This research was supported in part by the Basic Science Research Program (NRF-2017-R1D1A1A09000746) of the National Research Foundation, funded by the Korean Government and the Main Research Program (E0164800-03) of the Korea Food Research Institute (KFRI), and funded by the Ministry of Science and ICT. The authors appreciate the support provided by Hallym Research Fund (HRF-201702-007).

Supplementary Materials

Figure S1: generation of the DNA construct for BtαGTase expression. (A) The bt_2146 gene was amplified by polymerase chain reaction (PCR). Lane S, DNA marker; lane 1, amplified BtαGTase gene. (B) The pKTNd_bt2146 construct was generated by ligating bt_2146 into the pTKNd vector. Figure S2: Sodium dodecyl sulfate polyacrylamide gel electrophoresis (SDS-PAGE) of BtαGTase at each purification step. Lane S, protein size standards; lane 1, cellular protein from the crude extract; lane 2, soluble fraction;

lane 3, insoluble fraction; and lane 4, purified BtαGTase. Figure S3: Lineweaver-Burk plots showing the inhibitory effects of DNJ and G1-DNJ on the α-glucosidase (a) and α-amylase (b) activity. Figure S4: sequence alignment of conserved regions between BtαGTase and related glycoside hydrolase family GH77 members. BtαGTase, α-glucanotransferase from *Bacteroides thetaiotaomicron*; SpαGTase, α-glucanotransferase from *Streptococcus pneumoniae*; TsαGTase, α-glucanotransferase from *Thermus scotoductus*; TbαGTase, α-glucanotransferase from *Thermus brockianus*; TaαGTase, α-glucanotransferase from *Thermus aquaticus*; Ss-αGTase, α-glucanotransferase from *Synechocystis* sp.; SmαGTase, α-glucanotransferase from *Streptococcus mutans* UA159; StαGTase, α-glucanotransferase from *Solanum tuberosum*; CbαGTase, α-glucanotransferase from *Clostridium butyricum*; CrαGTase, α-glucanotransferase from *Chlamydomonas reinhardtii*; AtαGTase, α-glucanotransferase from *Arabidopsis thaliana*; Ac-11bαGTase, α-glucanotransferase from *Acidothermus cellulolyticus*; Ecs-k12αGTase, α-glucanotransferase from *Escherichia coli* str. K-12; Tt-hb8αGTase, α-glucosidase from *Thermus thermophilus*; and Sd2-40αGTase, α-glucanotransferase from *Saccharophagus degradans*. Closed circles at the conserved regions III, IV, and V represent the catalytic sites in family GH77 members. (*Supplementary Materials*)

References

[1] K. A. Smith and A. A. Salyers, "Characterization of a neopullulanase and an alpha-glucosidase from *Bacteroides thetaiotaomicron* 95-1," *Journal of Bacteriology*, vol. 173, no. 9, pp. 2962–2968, 1991.

[2] K. L. Anderson and A. A. Salyers, "Biochemical evidence that starch breakdown by *Bacteroides thetaiotaomicron* involves outer membrane starch-binding sites and periplasmic starch-degrading enzymes," *Journal of Bacteriology*, vol. 171, no. 6, pp. 3192–3198, 1989.

[3] A. Lammerts van Bueren, A. Saraf, E. C. Martens, and L. Dijkhuizen, "Differential metabolism of exopolysaccharides from probiotic *Lactobacilli* by the human gut symbiont *Bacteroides thetaiotaomicron*," *Applied and Environmental Microbiology*, vol. 81, no. 12, pp. 3973–3983, 2015.

[4] H. M. Wexler, "*Bacteroides*: the good, the bad, and the nitty-gritty," *Clinical Microbiology Reviews*, vol. 20, no. 4, pp. 593–621, 2007.

[5] A. Kuchtová and Š. Janeček, "In silico analysis of family GH77 with focus on amylomaltases from *borreliae* and disproportionating enzymes DPE2 from plants and bacteria," *Biochimica et Biophysica Acta (BBA)-Proteins and Proteomics*, vol. 1854, no. 10, pp. 1260–1268, 2015.

[6] T. Kaper, B. Talik, T. J. Ettema, H. Bos, M. J. E. C. van der Maarel, and L. Dijkhuizen, "Amylomaltase of *Pyrobaculum aerophilum* IM2 produces thermoreversible starch gels," *Applied and Environmental Microbiology*, vol. 71, no. 9, pp. 5098–5106, 2005.

[7] B. H. Lee, D. K. Oh, and S. H. Yoo, "Characterization of 4-α-glucanotransferase from *Synechocystis* sp. PCC 6803 and its application to various corn starches," *New Biotechnology*, vol. 26, no. 1-2, pp. 29–36, 2009.

[8] T. Takaha, M. Yanase, S. Okada, and S. M. Smith, "Disproportionating enzyme (4-α-glucanotransferase; EC 2.4.1.25) of potato. Purification, molecular cloning, and potential role in starch metabolism," *Journal of Biological Chemistry*, vol. 268, no. 2, pp. 1391–1396, 1993.

[9] M. S. Kim, J. H. Jang, and Y. W. Kim, "Overproduction of a thermostable 4-α-glucanotransferase by codon optimization at N-terminus region," *Journal of the Science of Food and Agriculture*, vol. 93, no. 11, pp. 2683–2690, 2013.

[10] D. Li, S. A. Roh, J. H. Shim et al., "Glycosylation of genistin into soluble inclusion complex form of cyclic glucans by enzymatic modification," *Journal of Agricultural and Food Chemistry*, vol. 53, no. 16, pp. 6516–6524, 2005.

[11] Y. Narita and K. Inouye, "Kinetic analysis and mechanism on the inhibition of chlorogenic acid and its components against porcine pancreas α-amylase isozymes I and II," *Journal of Agricultural and Food Chemistry*, vol. 57, no. 19, pp. 9218–9225, 2009.

[12] S. Takasu, I. S. Parida, S. Onose et al., "Evaluation of the anti-hyperglycemic effect and safety of microorganism 1-deoxynojirimycin," *PLoS One*, vol. 13, no. 6, Article ID e0199057, 2018.

[13] Y. Yao, X. Cheng, and G. Ren, "α-Glucosidase inhibitory activity of protein-rich extracts from extruded adzuki bean in diabetic KK-Ay mice," *Food and Function*, vol. 5, no. 5, pp. 966–971, 2014.

[14] J. Yan, G. Zhang, J. Pan, and Y. Wang, "α-Glucosidase inhibition by luteolin: kinetics, interaction and molecular docking," *International Journal of Biological Macromolecules*, vol. 64, pp. 213–223, 2014.

[15] Y. T. Deng, S. Y. Lin-Shiau, L. F. Shyur, and J. K. Lin, "Pu-erh tea polysaccharides decrease blood sugar by inhibition of α-glucosidase activity in vitro and in mice," *Food and Function*, vol. 6, no. 5, pp. 1539–1546, 2015.

[16] W. Zhang, D. Kim, E. Philip et al., "A multinational, observational study to investigate the efficacy, safety and tolerability of acarbose as add-on or monotherapy in a range of patients: the GlucoVIP study," *Clinical Drug Investigation*, vol. 33, no. 4, pp. 263–274, 2013.

[17] A. I. ElSayed, M. Boulila, and P. Rott, "Molecular evolutionary history of Sugarcane yellow leaf virus based on sequence analysis of RNA-dependent RNA polymerase and putative aphid transmission factor-coding genes," *Journal of Molecular Evolution*, vol. 78, no. 6, pp. 349–365, 2014.

[18] S. Dhital, M. J. Gidley, and F. J. Warren, "Inhibition of α-amylase activity by cellulose: kinetic analysis and nutritional implications," *Carbohydrate Polymers*, vol. 123, pp. 305–312, 2015.

[19] M. J. E. C. van der Maarel, B. van der Veen, J. C. M. Uitdehaag, H. Leemhuis, and L. Dijkhuizen, "Properties and applications of starch-converting enzymes of the α-amylase family," *Journal of Biotechnology*, vol. 94, no. 2, pp. 137–155, 2002.

[20] H. Jiang, M. Miao, F. Ye, B. Jiang, and T. Zhang, "Enzymatic modification of corn starch with 4-α-glucanotransferase results in increasing slow digestible and resistant starch," *International Journal of Biological Macromolecules*, vol. 65, pp. 208–214, 2014.

[21] H. Leemhuis, J. M. Dobruchowska, M. Ebbelaar et al., "Isomalto/malto-polysaccharide, a novel soluble dietary fiber made via enzymatic conversion of starch," *Journal of Agricultural and Food Chemistry*, vol. 62, no. 49, pp. 12034–12044, 2014.

[22] C. J. Paul, H. Leemhuis, J. M. Dobruchowska et al., "A GH57 4-α-glucanotransferase of hyperthermophilic origin with potential for alkyl glycoside production," *Applied Microbiology and Biotechnology*, vol. 99, no. 17, pp. 7101–7113, 2015.

[23] Y. Xu, X. Zhou, Y. Bai et al., "Cycloamylose production from amylomaize by isoamylase and *Thermus aquaticus* 4-α-glucanotransferase," *Carbohydrate Polymers*, vol. 102, pp. 66–73, 2014.

Hindawi
Journal of Chemistry
Volume 2018, Article ID 1285823, 9 pages
https://doi.org/10.1155/2018/1285823

Research Article

Application of Food-Grade Proteolytic Enzyme for the Hydrolysis of Regenerated Silk Fibroin from *Bombyx mori*

Ji An Joung, Mi Na Park, Ji Young You, Bong Joon Song, and Joon Ho Choi

Department of Food Science and Biotechnology, Wonkwang University, Iksan 54538, Republic of Korea

Correspondence should be addressed to Joon Ho Choi; jhchoi1124@wku.ac.kr

Received 24 August 2018; Accepted 8 October 2018; Published 8 November 2018

Guest Editor: Sang-Hyun Park

In vitro biodegradation of *Bombyx mori* silk fibroin (SF) was studied using food-grade proteolytic enzymes to replace acid hydrolysis. Based on the residual protein quantity and yield of amino acids (AAs) after enzymatic hydrolysis, we evaluated the proteolytic enzyme process of SF. FoodPro and Alcalase that are classified as alkaline proteases are selected as two of the best candidate enzymes for hydrolysis of SF. The activity of these enzymes exhibits a broad range of pH (6.5 to 9.0) and temperature (50°C to 65°C). The single enzyme treatment of SF using FoodPro exhibited a hydrolytic efficiency of 20–25%, and >2 g/L AAs were released after reaction for 3 h. A 2-stage enzymatic treatment using a combination of FoodPro and Flavourzyme in a sequence for a reaction time of 6 h was developed to enhance the efficiency of the proteolytic process. The yield of AAs and residual protein quantity in the enzymatic hydrolysates obtained from FoodPro-treated regenerated SF in the 1st step was 2,040 ± 23.7 mg/L and 70.6%, respectively. The yield of AAs was > two-fold (4,519 ± 42.1 mg/L), whereas the residual protein quantity decreased to 55.1% after the Flavourzyme treatment (2nd step) compared to those of the single FoodPro treatment. In the mixed treatment by simultaneously using FoodPro and Flavourzyme, approximately 45% of SF was degraded and 4.5 g/L of AAs were released within 3 h of reaction time. The regenerated SF and its enzymatic hydrolysates were characterized by performing UV-visible spectra, gel electrophoresis, and size-exclusion chromatography analyses. In the 2-stage treatment using FoodPro initially and subsequently Flavourzyme, the aggregates and high molecular weight proteins of SF were dissociated and degraded into the low molecular weight proteins/peptides (10–15 kDa and 27 kDa). SF hydrolysates as functional food might be enzymatically produced using the commercial food-grade proteolytic enzymes.

1. Introduction

The silk fibroin (SF) from *Bombyx mori* (silkworm) cocoons present as a double-stranded fibroin fiber that is coated with adhesive sericin proteins. The raw silk fiber is composed of 20–30% sericin and 70–80% SF with trace amounts of waxes and carbohydrates [1]. Pure SF is separated from sericin by the degumming procedure [2], and a variety of aqueous or organic solvent processing methods are used to generate silk biomaterials for a wide range of applications [3–6]. The predominant protein of silk, i.e., fibroin, is a hydrophobic structural protein that is insoluble in hot water and consists of heavy and light chains with 390 kDa and 25 kDa molecular weights (MW), respectively, linked by a disulfide bond [7, 8]. The SF heavy chain is rich in hydrophobic β-sheets that form blocks linked by small hydrophilic linkers or spacers. The predominant regions of SF primarily consist of approximately 76% of amino acids (AAs) with nonpolar side chains. The main AAs of SF are glycine (43.7%) and alanine (28.8%) that form the dominant crystalline β-sheet regions that act as reinforcements and contribute to the strength and stiffness of silk [9, 10]. Although silk is defined as a nondegradable material by the United States Pharmacopeia owing to a negligible loss in tensile strength *in vivo,* the enzymatic degradation behaviors of SF as biomaterials have been reviewed for the medical application *in vivo* [11, 12].

The *in vitro* biodegradation of *B. mori* SF was studied using proteolytic enzymes (collagenase F, α-chymotrypsin I-S, and protease type XXI) to degrade SF fibers and films [13]. The enzymatic hydrolysis of SF was performed using

α-chymotrypsin, collagenase IA, and protease XIV in SF yarns [14], protease XIV in porous SF sheets [15–17], collagenase IA and protease XXIII in 3D-scaffolds SF [18–20], proteinase K, protease XIV, α-chymotrypsin, collagenase, and matrix metalloproteinase in SF hydrogels and films [21], and actinase in SF solution [22]. Due to the unique chemical, mechanical, and biocompatibility properties, *B. mori* SF was investigated as a biomaterial and functional food source for years. Fibroin-derived bioactive proteins/peptides and hydrolysates were developed as the functional components of foods, cosmetics, pharmaceutical preparations, and alternative sources of food additives to improve human health [23]. The applications of SF in processed foods were proposed, and currently, the three forms of SF (solution, gel, and powder) are commercially available [24]. The SF hydrolysates that are prepared by performing acid hydrolysis or enzymatic hydrolysis consist of a mixture of AAs and oligopeptides that are known to exhibit beneficial effects on animal models. The bioactive peptides derived from SF are reported to reduce blood cholesterol level, increase antigenotoxicity, inhibit angiotensin-converting enzyme activity, enhance insulin sensitivity and glucose metabolism, improve alcohol metabolism, and stimulate osteoblastic differentiation [23, 25–28].

Fibroinase is a native silk digestion enzyme characterized as a cysteine proteinase and digests fibroin and sericin [29, 30]. Alcalase [25–27], actinase [22], and alkaline protease [31] were used to prepare the bioactive peptides and enzymatic hydrolysates (EHs) from SF/silkworm powder. The fibroin solubilization conditions affected the MW distribution of EHs produced using Alcalase supplied from Novozymes [32]. Additionally, actinase was introduced to hydrolyze regenerated silk fibroin (RSF) at 37°C for 12 h [22]. The silkworm powder was modified by enzymatic treatment using alkaline protease (FoodPro), and the MW of silk protein was decreased [31]. To prepare SF hydrolysates, enzymatic hydrolysis is more efficient than acid hydrolysis with aspect to the recovery yield and quality of products. However, very few previous studies reported the production of SF hydrolysates using commercial food-grade enzymes. Therefore, we performed the enzymatic hydrolysis of SF using commercial food-grade enzymes and characterized these EHs.

2. Materials and Methods

2.1. Materials. Degummed SF fiber acquired from a Korean sericulture farm (Kimjae, South Korea) was provided by SSBIO PHARM Co., Ltd. (Cheonan, South Korea). Commercial food-grade proteolytic enzymes, FoodPro® and Alphalase® (DuPont Industrial Biosciences, Brabrand, Denmark), Collupulin™ MG (DSM Food Specialties, Alexander Fleminglaan, Netherlands), Alcalase®, Neutrase®, Protamex®, and Flavourzyme® (Novozymes A/S, Bagsvaerd, Denmark), Promod™ 192P, 279MDP, and 278MDP (Biocatalysts Ltd., Wales, UK), and Bromelain (PT Bromelain Enzyme, Lampung, Indonesia) were purchased and stored at 4°C until their use in experimental reactions. Anhydrous citrate and Na_2HPO_4 to prepare citrate-phosphate buffer (CPB) [33], $CaCl_2$ and 95% ethanol to prepare SF solubilization reagent, and other chemicals were of reagent-grade and purchased from Samchun Pure Chemical Co., Ltd. (Gyeonggi-do, South Korea). Standard protein, i.e., albumin from bovine serum (BSA) and Folin and Ciocalteu's phenol reagent to perform quantification of protein concentration and ninhydrin reagent and glycine to analyze the AAs were purchased from Sigma-Aldrich (St. Louis, MO, USA). The Precision Plus Protein™ standards and Silver Stain Plus™ kit to perform SDS-PAGE and silver staining, respectively, were purchased from BIO-RAD Laboratories (Hercules, CA, USA).

2.2. Preparation of RSF Solution. Degummed SF fiber was dissolved in Ajisawa's reagent [34] composed of $CaCl_2$: ethanol : distilled water in 1 : 2 : 8 molar ratio at 121°C for 15 min, thus yielding a 20% (W/V) solution. This solution was dialyzed against deionized water using a cellulose membrane dialysis tube (MW cut-off 14,000 kDa, Sigma-Aldrich) for >3 days to remove excess salt and ethanol. The RSF solution was centrifuged to remove insoluble materials, and final concentration was determined as 130–180 g/L using the Lowry method [35] with 73–76% recovery yield. RSF solutions at various pH levels were prepared using CPB. The pH-conditioned RSF solutions were stored at room temperature for 48 h to achieve homogeneity. The premature precipitates in RSF solutions were removed by centrifugation at 13,000 rpm for 10 min (Smart-R17, Hanil Scientific Inc., Gimpo, South Korea).

2.3. Estimation of Specific Activities of Proteolytic Enzymes. The proteolytic activity of enzymes was determined using casein as a substrate by performing Sigma's nonspecific protease activity assay [36] with a minor modification. Casein solution (5 mL; 0.65% (W/V)) was mixed with the enzyme solutions (1 mL) of various concentrations. After 10 min incubation at 37°C, 0.4 M trichloroacetic acid (5 mL) was added to terminate the reaction. The reaction mixture was incubated at 37°C for 30 min and centrifuged to remove insoluble precipitates. The supernatant (1 mL) was mixed with 0.55 M sodium carbonate (5 mL) and subsequently 0.5 mM Folin and Ciocalteu's phenol reagent (1 mL). After 30 min incubation at 37°C, the absorbance at 660 nm was measured using a spectrophotometer (Optizen POP, Mecasys Co., Daejeon, South Korea). Based on the standard curve obtained using L-tyrosine, the proteolytic activity was determined in terms of units (U), that is, the quantity of tyrosine equivalents in micromoles released from casein per min. The specific pH of each enzymatic reaction was regulated using 0.25 M CPB at corresponding pH. The protein concentrations of proteolytic enzyme solutions were determined using the Lowry method. The proteolytic activity of enzymes was expressed as specific activity in terms of U/mg-protein.

2.4. Proteolytic Hydrolysis of RSF. Enzymatic reaction was performed using RSF solution along with food-grade

enzymes at specific conditions. Each sample acquired from the reaction mixture was boiled at 100°C for 10 min to inactivate the enzyme and centrifuged at 13,000 rpm for 10 min to remove the insoluble precipitate. The supernatant of each sample was used to measure the protein and AAs concentrations by performing the Lowry method and ninhydrin reaction, respectively [37]. The protein and AAs concentrations were expressed in terms of BSA and glycine equivalent, respectively. The protein concentration of SF solution used for enzymatic reaction was approximately 30 g/L. The efficiency of protein degradation by enzymatic hydrolysis was expressed as the percentage of remaining protein using the following equation: residual protein (%) = $(P_f/P_i) \times 100$ where P_i is the initial concentration of the sample and P_f is the protein concentration of reaction mixture at a specific condition. To screen the proteolytic enzymes to perform SF hydrolysis, each enzyme (6 U) was incubated with 330 mg of RSF for 3 h. The effects of temperature and pH on the reactions involving the candidate enzymes (FoodPro and Alcalase) were determined by performing a combination reaction using enzyme (5 U) and SF (400 mg) for 5 h. The effect of substrate-to-enzyme ratio was determined using the initially selected enzyme, i.e., FoodPro, and an enzyme concentration of 5 U was used during the subsequent enzymatic treatment experiments. To enhance the efficiency of enzymatic hydrolysis by performing the 2-stage treatment, SF was initially allowed to react with FoodPro and then with any other selected proteolytic enzyme.

2.5. Gel Electrophoresis. The MW of SF and its EHs were determined by performing sodium dodecyl sulfate polyacrylamide gel electrophoresis (SDS-PAGE) using 4–20% Mini-PROTEAN® TGX™ precast protein gel (BIO-RAD). The total protein samples of RSF, initial EHs obtained using FoodPro, and final EHs obtained using Flavourzyme were loaded at protein concentration values of 28–84, 19–57, and 15–45 μg/well, respectively. The samples were resolved in SDS-PAGE with Precision Plus Protein standards as MW markers and stained using a Silver Stain Plus kit (BIO-RAD).

2.6. Size-Exclusion Chromatography (SEC). The high-performance liquid chromatography system combined with a photodiode array detector (Atlus™, PerkinElmer, Waltham, MA, USA) and 5Diol-300-II size-exclusion column (COSMOSIL, 7.5 mm ID × 300 mm, 300 Å pore size, Nacalai Tesque, Inc., Kyoto, Japan) was used to perform SEC. The protein quantities used during analyses were 700 μg RSF, 250 μg EHs obtained after 1st step using FoodPro, and 200 μg EHs obtained after 2nd step using Flavourzyme. 0.25 M CPB (pH 6.0) was used as the mobile phase at a flow rate of 1 mL/min, and the eluted protein concentration was measured at 280 nm at 30°C.

2.7. Statistical Analysis. All the experiments were performed in triplicates, and results were represented as mean value ± standard deviation. Analysis of variance was conducted, and the mean variations were analyzed using Duncan's multiple range test ($p < 0.05$). The statistical analyses were conducted using the Statistical Package for the Social Sciences (SPSS) for Windows 12.0 software (SPSS Inc., Chicago, IL, USA).

3. Results and Discussion

3.1. pH Dependency of RSF Solubility in Aqueous Solution. pH affects the charges of carboxyl as well as amino groups in RSF, enables electrostatic interactions, and promotes intramolecular or intermolecular interactions such as hydrophobic interactions and hydrogen bonding. The effect of pH on the RSF solubility in aqueous solution was determined using 0.25 M CPB solutions with pH range 3.0–9.0. The protein concentration of each sample equilibrated at a specific pH for 48 h was determined before and after centrifugation (Figure 1). The protein concentration in RSF solution prior to centrifugation was relatively stable (26.8 ± 0.81 g/L) at pH between 5.0 and 9.0. After centrifugation, the stable protein concentration (26.7 ± 0.14 g/L) was obtained at a narrow pH range 5.0–6.5. Some of the soluble RSF was coagulated in alkaline condition; therefore, the soluble protein concentration after centrifugation decreased at pH > 7. In pH < 5 condition, the soluble protein concentration after centrifugation decreased owing to colloidal precipitation. The stable protein concentration was maintained at pH between 5.0 and 6.5 that might be associated with the spinning process (decrease from 6.9 to 4.8 along the path) in the silk glands [38]. A similar effect of pH on RSF solubility was reported in a study that indicated pH dependency between the shear sensitivity of SF and β-sheet crystallization [39].

3.2. Screening of Candidate Proteolytic Enzyme to Hydrolyze RSF. The specific activities of food-grade proteolytic enzymes and results of enzymatic hydrolysis at particular pH and temperature conditions are summarized in Table 1. The reaction conditions such as pH and temperature of each enzyme were selected based on the manufacturer's recommendations. FoodPro and Alcalase are classified as endotype and alkaline proteases that exhibit higher specific activity values than other proteolytic enzymes. An equal unit of each enzyme was used to screen the candidate proteolytic enzyme to perform RSF hydrolysis. FoodPro, Alcalase, Protamex, and/or Alphalase were potential candidates to efficiently hydrolyze SF owing to the concentration of AA in the EHs which was >2,000 mg/L. Flavourzyme is classified as mixed endotype/exotype and was not selected as the SF started to precipitate after 1 h reaction time. With an increase in the AA concentrations in EHs, the residual protein (%) decreased to approximately 80% in Alcalase-, FoodPro-, Protamex-, and Alphalase-treated SF. The AA concentrations in EHs represent not only free AAs but also peptides because the ninhydrin reaction is used to determine free amino and amine groups in AAs, peptides, and proteins [40]. Alcalase and FoodPro were selected as candidate proteases to hydrolyze SF. These two enzymes are produced by *Bacillus* strains, known as serine proteases, and classified

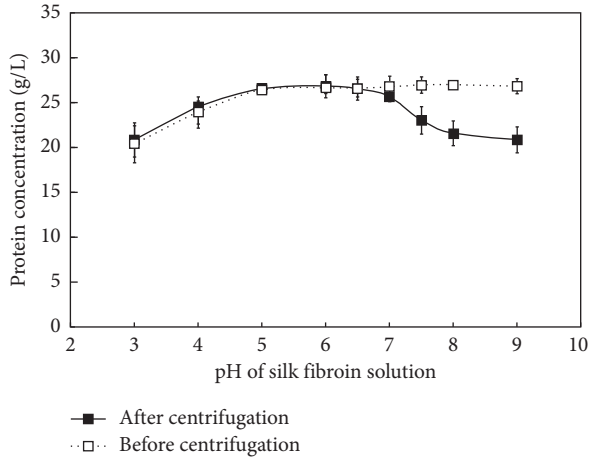

Figure 1: Effect of pH on the solubility of regenerated silk fibroin in 0.25 M citrate-phosphate buffer.

as alkaline proteases. Although fibroinase is the native silk-digesting enzyme, it was identified as a cysteine protease [29, 30]; Collupulin and Bromelain are classified as cysteine proteases, and they exhibited low activities in enzymatic hydrolysis of SF in our study.

3.3. Effects of Temperature, pH, and Substrate-to-Enzyme Ratio on RSF Hydrolysis. The effect of temperature on the candidate enzymes was determined by performing the reactions at range 50°C–65°C and pH 8.0 (Table 2). The proteolytic activities of Alcalase and FoodPro were efficient at a broad temperature range between 50°C and 60°C and drastically decreased at >65°C. The optimal temperature to conduct RSF hydrolysis was determined as 60°C. The effect of pH on the efficiency of enzymatic hydrolysis of SF was determined at pH range 6.5–9.0 and 60°C (Table 3). The proteolytic activities of Alcalase and FoodPro were effective at a broad pH range 6.5–9.0, and the optimal pH was determined as 8.0. Finally, FoodPro was selected as the proteolytic enzyme to perform the 1st step of 2-stage RSF hydrolysis. To determine the efficiency of enzymatic hydrolysis, the substrate-to-enzyme ratio was estimated using a fixed quantity of RSF (400 mg) and FoodPro (1, 5, 10, or 25 U) at pH 8.0 and 60°C (Figure 2). A decrease in residual protein (%) and an increase in AAs of EHs were proportional to an increase in FoodPro concentration ranging from 1 to 10 U per RSF (400 mg).

3.4. Enhancement of Efficiency in Enzymatic Hydrolysis. The enzymatic hydrolysis using FoodPro was almost saturated after 3 h of reaction and did not extend during a prolonged reaction time. To improve the efficiency of enzymatic hydrolysis in RSF, a 2nd enzyme (5 U) was introduced after 3 h of reaction initiation using FoodPro. The 2nd enzymatic treatment was conducted for additional 3 h of reaction time at specific conditions, and the results are summarized in Table 4. The AAs in the EHs obtained from 1st step FoodPro-treated RSF was 2,040 ± 23.7 mg/L, and it increased > two-fold (4,519 ± 42.1 mg/L) during the subsequent Flavourzyme treatment (2nd step). The drastic increase in AA concentration in EHs might be associated to the characteristics of Flavourzyme that exhibits mixed activities of endotype and exotype enzymes. The residual protein was 70.6 ± 5.39% after FoodPro treatment (1st step), and it further decreased to 55.1 ± 5.28% during Flavourzyme treatment (2nd step). Therefore, RSF was efficiently hydrolyzed by the 2-stage enzymatic treatment by sequentially using FoodPro and Flavourzyme at the 1st and 2nd step, respectively, within 6 h of reaction time. To reduce the enzymatic reaction time, the AAs and protein yields of mixed proteolytic enzyme treatment by simultaneously using the combination of FoodPro and Flavourzyme were compared to those of the 2-stage enzymatic treatment (Figure 3). In the mixed proteolytic enzyme treatment, the enzymatic hydrolysis was conducted at 60°C and pH 7.0. The residual protein and AAs concentration in EHs during the mixed proteolytic enzyme treatment for 3 h were 54.4 ± 2.35% and 4,663 ± 23.0 mg/L, respectively. Additionally, enzymatic hydrolysis in the mixed proteolytic enzyme treatment was not extended at prolonged reaction time up to 6 h. Therefore, the RSF in aqueous solution was hydrolyzed by mixed proteolytic enzyme treatment which reduced the reaction time compared to that by the 2-stage enzymatic treatment by sequentially using FoodPro and Flavourzyme.

3.5. Characterization of RSF and Its EHs Using UV-Visible Spectra. To characterize RSF and its EHs, UV-visible spectra analysis was performed using the same concentrations of samples, and results are presented in Figure 4. All the samples with 2.0 g/L concentration exhibited a characteristic protein absorption band in UV-visible spectra. The absorption intensities at 280 nm increased after enzymatic treatments, indicating that the hydrophobic and self-assembled regimes in RSF protein were initially relaxed, and subsequently the degradable protein/peptide content increased compared to those of untreated RSF. Moreover, similar changes were reported using alkaline protease-treated silkworm powder in UV-visible spectra analysis [31].

3.6. MW Determination of RSF and Its EHs Using SDS-PAGE. The MWs of RSF and its EHs were analyzed by performing SDS-PAGE using 4–20% gradient gel (Figure 5). The RSF exhibited a broad MW distribution ranged from 60 to 150 kDa, and the protein bands were visible at approximately 10–22 kDa. The broad protein bands of RSF at approximately 100 kDa might be related to the intermolecular interaction between the SF molecules, and similar results were reported in previous reports [2, 31]. After enzymatic treatment using FoodPro in the 1st step, the broad protein bands of RSF disappeared and distinct protein bands at 350–420 kDa and 60–70 kDa MW were observed. In the EHs obtained from FoodPro-treated RSF, a novel protein band at 27 kDa was detected and the intensities of several bands at approximately 10–12 and 15 kDa were enhanced. In enzymatic treatment using FoodPro at the 1st step, the RSF aggregates were dissociated and gradually degraded into low MW proteins at

Table 1: The specific enzyme activities of food-grade enzymes and the results of enzymatic hydrolysis of regenerated silk fibroin during 3 h reaction.

Food-grade enzyme	Specific activity (U/mg)	Conditions		Enzymatic hydrolysis	
		pH	Temperature (°C)	Residual protein (%)	Amino acid (mg/L)
Alcalase® AF 2.4 L	14.0 ± 0.66	8.0	60	71.8 ± 1.07^{b}	2,209 ± 37.7^{ab}
Alphalase® NP	4.86 ± 0.18	7.0	60	84.4 ± 0.53^{d}	2,074 ± 25.8^{c}
Bromelain BR1200	0.10 ± 0.00	7.0	50	98.2 ± 2.39^{h}	580 ± 87.4^{f}
Collupulin™ MG	2.09 ± 0.02	6.0	60	92.4 ± 0.71^{f}	1,228 ± 40.8^{e}
Flavourzyme® 500 MG	2.38 ± 0.02	7.0	50	$^{(1)}$54.0 ± 1.67^{a}	2,011 ± 90.7^{c}
FoodPro® alkaline protease	15.0 ± 0.80	8.0	60	78.0 ± 0.19^{c}	2,271 ± 51.8^{a}
Neutrase™ 0.8 L	1.72 ± 0.02	7.0	50	97.1 ± 0.16^{g}	489 ± 69.6^{f}
Promod™ 192P	$^{(2)}$0.59 ± 0.01	5.0	50	NA	NA
Promod™ 278MDP	0.88 ± 0.01	7.0	60	90.8 ± 0.40^{f}	1,461 ± 12.4^{d}
Promod™ 279MDP	$^{(2)}$2.62 ± 0.05	5.0	60	NA	NA
Protamex®	3.11 ± 0.03	7.0	50	81.8 ± 2.51^{e}	2,118 ± 89.6^{bc}

$^{(1)}$The silk fibroin started to precipitate during the enzymatic reaction with Flavourzyme. $^{(2)}$Enzymatic reaction was performed at pH 7 instead of pH 5 as the substrate precipitated at acidic pH 5. NA: enzymatic reaction was not observed as these enzymes are classified as exotype proteases. a–g: means in the same column followed by different letters differ significantly ($p < 0.05$).

Table 2: Effects of temperature on the enzymatic hydrolysis of regenerated silk fibroin using FoodPro and Alcalase at pH 8.0.

Enzyme		FoodPro		Alcalase	
Temperature (°C)	Time (h)	Residual protein (%)	Amino acid (mg/L)	Residual protein (%)	Amino acid (mg/L)
50	0	100.0 ± 1.16^{d}	62 ± 1.5^{h}	100.0 ± 1.14^{f}	62 ± 1.5^{h}
	3	86.1 ± 3.65^{c}	2,456 ± 4.5^{e}	86.9 ± 1.67^{e}	2,417 ± 15.7^{e}
	5	86.3 ± 0.60^{c}	2,671 ± 19.5^{a}	87.3 ± 2.97^{e}	2,662 ± 26.2^{c}
55	0	100.0 ± 1.16^{d}	64 ± 1.6^{h}	100.0 ± 1.14^{f}	64 ± 1.6^{h}
	3	80.5 ± 1.29^{b}	2,441 ± 13.1^{e}	84.5 ± 3.92^{d}	2,426 ± 19.3^{e}
	5	80.9 ± 1.09^{b}	2,602 ± 30.6^{c}	83.1 ± 3.40^{c}	2,536 ± 38.7^{d}
60	0	100.0 ± 1.13^{d}	62 ± 1.5^{h}	100.0 ± 1.10^{f}	62 ± 1.5^{h}
	3	77.2 ± 2.17^{a}	2,537 ± 18.9^{d}	75.8 ± 0.72^{b}	2,769 ± 17.4^{b}
	5	75.9 ± 2.41^{a}	2,645 ± 4.5^{b}	74.2 ± 0.37^{a}	2,891 ± 23.4^{a}
65	0	100.0 ± 1.14^{d}	67 ± 1.6^{h}	100.0 ± 1.13^{f}	67 ± 1.6^{h}
	3	98.0 ± 1.50^{d}	1,843 ± 10.7^{g}	100.5 ± 3.24^{f}	1,787 ± 23.0^{f}
	5	98.2 ± 1.12^{d}	1,876 ± 5.4^{f}	99.2 ± 2.93^{f}	1,750 ± 4.7^{g}

a–h: means in the same column followed by different letters differ significantly ($p < 0.05$).

Table 3: Effects of pH on the enzymatic hydrolysis of regenerated silk fibroin using FoodPro and Alcalase at 60 °C.

Enzyme		FoodPro		Alcalase	
pH	Time (h)	Residual protein (%)	Amino acids (mg/L)	Residual protein (%)	Amino acids (mg/L)
6.5	0	100.0 ± 0.92^{c}	27 ± 0.7^{i}	100.0 ± 2.55^{c}	27 ± 0.7^{f}
	3	84.9 ± 0.88^{b}	1,857 ± 10.0^{h}	86.4 ± 2.38^{b}	1,826 ± 42.8^{e}
	5	83.4 ± 4.87^{b}	2,058 ± 13.2^{g}	87.2 ± 2.53^{b}	1,895 ± 2.4^{d}
7.0	0	100.0 ± 0.49^{c}	27 ± 0.7^{i}	100.0 ± 1.62^{c}	27 ± 0.7^{f}
	3	80.6 ± 5.74^{ab}	2,223 ± 2.4^{f}	81.3 ± 0.69^{a}	2,072 ± 16.4^{c}
	5	80.7 ± 2.30^{ab}	2,254 ± 19.0^{e}	82.0 ± 2.45^{a}	2,156 ± 55.7^{c}
8.0	0	100.0 ± 1.92^{c}	27 ± 0.7^{i}	100.0 ± 1.83^{c}	27 ± 0.7^{f}
	3	79.7 ± 1.55^{ab}	2,355 ± 10.0^{d}	79.2 ± 2.59^{a}	2,300 ± 50.8^{b}
	5	77.4 ± 0.20^{a}	2,515 ± 25.5^{a}	79.0 ± 1.83^{a}	2,435 ± 6.4^{a}
9.0	0	100.0 ± 1.51^{c}	27 ± 0.7^{i}	100.0 ± 3.18^{c}	27 ± 0.7^{f}
	3	79.4 ± 4.45^{ab}	2,372 ± 14.0^{c}	79.5 ± 0.85^{a}	2,291 ± 148^{b}
	5	76.2 ± 1.50^{a}	2,442 ± 32.7^{b}	80.2 ± 1.24^{a}	2,397 ± 29.1^{a}

a–i: means in the same column followed by different letters differ significantly ($p < 0.05$).

10–27 kDa range. After Flavourzyme treatment (2nd step), the protein bands at 420 kDa of EHs obtained from FoodPro-treated RSF (1st step) gradually disappeared and a novel band at 315 kDa was detected. The intensities of bands at 10–12, 15, and 27 kDa were enhanced after Flavourzyme treatment (2nd step). Therefore, the SDS-

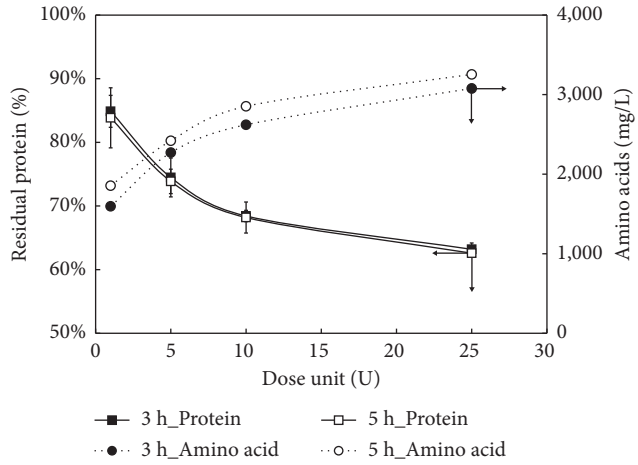

Figure 2: Effect of substrate (fibroin) : enzyme ratio on the proteolytic activity of FoodPro in 0.25 M citrate-phosphate buffer.

Table 4: Selection of the second proteolytic enzyme to enhance the efficiency of enzymatic hydrolysis of FoodPro-treated silk fibroin.

Enzyme treatment		Stage	Reaction condition			Residual protein (%)	Amino acids (mg/L)
			Time (h)	Temperature (°C)	pH		
Silk fibroin		—	0	60	—	100.0 ± 1.54^{c}	17 ± 0.7^{j}
1st step: FoodPro (FP)		1	3	60	8.0	70.6 ± 3.81^{b}	2,040 ± 23.7^{i}
2nd step	FP ⟶ Alcalase	2	+3	60	8.0	65.5 ± 5.67^{b}	2,611 ± 22.0^{d}
	FP ⟶ Alphalase	2	+3	60	7.0	65.6 ± 6.83^{b}	2,505 ± 28.7^{e}
	FP ⟶ Bromelain	2	+3	50	7.0	68.7 ± 9.73^{b}	2,455 ± 16.2^{fg}
	FP ⟶ Collupulin	2	+3	60	6.0	68.5 ± 8.32^{b}	2,227 ± 4.7^{h}
	FP ⟶ Flavourzyme	2	+3	50	7.0	55.1 ± 2.91^{a}	4,519 ± 42.1^{a}
	FP ⟶ Neutrase	2	+3	50	7.0	65.4 ± 8.68^{b}	2,453 ± 16.2^{fg}
	FP ⟶ Pomod 192	2	+3	50	5.0	67.1 ± 7.39^{b}	2,689 ± 54.7^{c}
	FP ⟶ Promod 278	2	+3	60	7.0	67.7 ± 7.61^{b}	2,438 ± 35.7^{g}
	FP ⟶ Promod 279	2	+3	60	5.0	65.0 ± 7.38^{b}	2,746 ± 18.7^{b}
	FP ⟶ Protamex	2	+3	50	7.0	66.6 ± 6.11^{b}	2,453 ± 25.7^{f}

+3: additional reaction time. a–j: means in the same column followed by different letters differ significantly ($p < 0.05$).

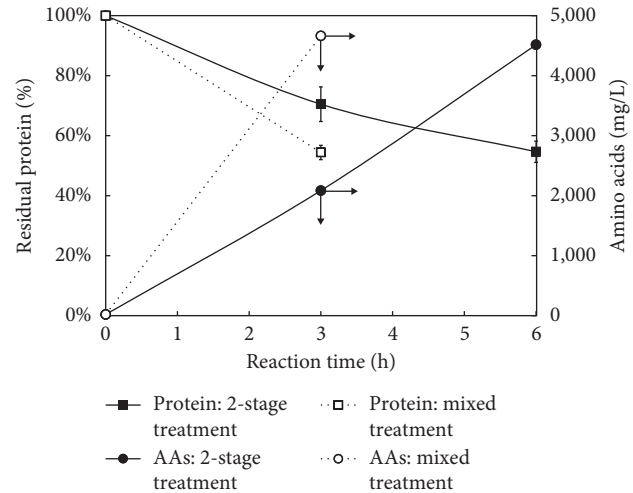

Figure 3: Comparison between the 2-stage and mixed treatments using FoodPro and Flavourzyme during the enzymatic hydrolysis of silk fibroin.

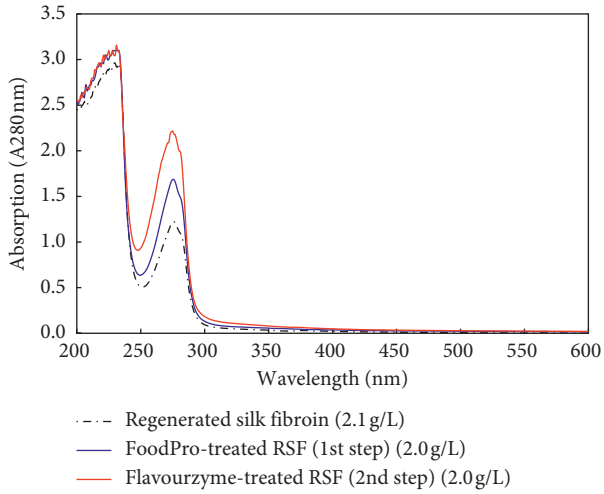

Figure 4: UV-visible spectra of regenerated fibroin and its enzymatic hydrolysates obtained using FoodPro in the 1st step and Flavourzyme in the 2nd step.

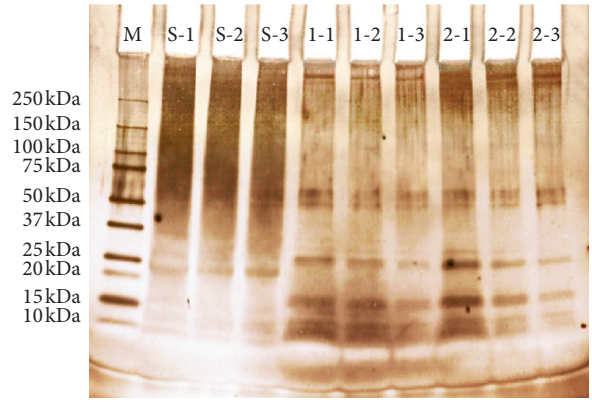

Figure 5: SDS-PAGE of the regenerated silk fibroin and its enzymatic hydrolysates obtained using FoodPro in the 1st step and Flavourzyme in the 2nd step. M: molecular weight marker. S-1: regenerated silk fibroin, 84 μg/well. S-2: regenerated silk fibroin, 42 μg/well. S-3: regenerated silk fibroin, 28 μg/well. 1-1: enzymatic hydrolysate obtained using FoodPro at the 1st step, 57 μg/well. 1-2: enzymatic hydrolysate obtained using FoodPro at the 1st step, 29 μg/well. 1-3: enzymatic hydrolysate obtained using FoodPro at the 1st step, 19 μg/well. 2-1: enzymatic hydrolysate obtained using Flavourzyme at the 2nd step, 45 μg/well. 2-2: enzymatic hydrolysate obtained using Flavourzyme at the 2nd step, 23 μg/well. 2-2: enzymatic hydrolysate obtained using Flavourzyme at the 2nd step, 15 μg/well.

PAGE results indicated that the aggregates and high MW proteins of RSF were dissociated and hydrolyzed in the 2-stage enzymatic treatment using FoodPro initially and then Flavourzyme.

3.7. MW Characteristics of RSF and Its EHs Using SEC. RSF samples (700 μg) and EHs (200–250 μg) were effectively separated using a 5Diol-300-II size-exclusion column with a good resolution (Figure 6). The untreated RSF exhibited

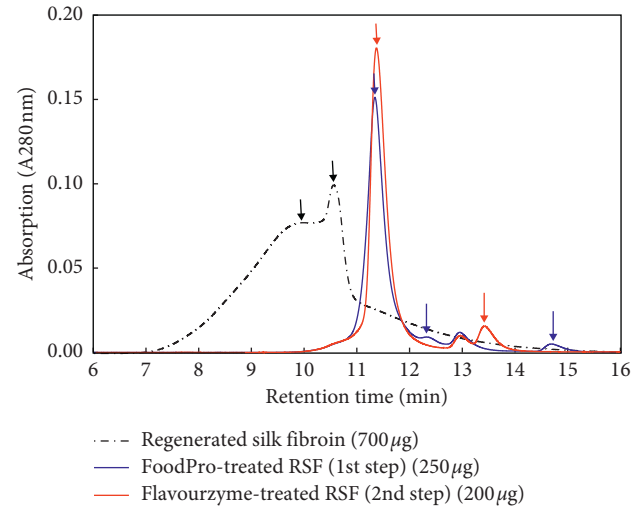

Figure 6: Size-exclusion chromatography of the regenerated silk fibroin and its enzymatic hydrolysates obtained using FoodPro in the 1st step and Flavourzyme in the 2nd step.

two peaks in the chromatogram. The first peak might be strongly associated to the intermolecular interaction, whereas the second peak represented the SF molecules. A previous report indicated that the elution profile of silk obtained after SEC exhibits an early-eluted peak that might represent the silk aggregates and the late-eluted peak represents the nonaggregated silk molecules [41]. This previous report suggested that Ajisawa's reagent produces more number of β-sheet structures and aggregates during dialysis owing to the high exposure of hydrophobic residues compared to the LiBr dissolution [41] and caused higher degradation of the SF heavy chains than other solvents [42]. In the SEC profile of EHs obtained from FoodPro-treated RSF, the peaks that represented untreated RSF disappeared and novel peaks were generated at low MW with enhanced intensities. In this study, the variations in absorption intensities during SEC were similar to those in UV-visible spectra analysis. These results were well matched to those of actinase-treated SF as the absorption intensity of the early peak of aggregated SF decreased with an increase in the later peak of nonaggregated SF molecules [22]. In the SEC profile of EHs, several peaks at 12.5, 13.0, and 14.8 min retention time points were observed after FoodPro treatment (1st step). After Flavourzyme treatment (2nd step), the peaks at 12.5 and 14.8 min retention time points were decreased and a novel peak at 13.5 min retention time was generated. The variations in the elution profiles of soluble SF were similar to those during the biodegradation of silk films using protease from *Streptomyces griseus* [13].

4. Conclusion

B. mori SF and its hydrolysates were investigated as functional materials in foods and alternative sources of food additives. To prepare the SF hydrolysates, enzymatic hydrolysis using commercial food-grade enzymes can replace the acid hydrolysis. The RSF solubility was relatively stable at

a narrow range of pH (5.0–6.5). FoodPro and Alcalase were selected as two of the best candidate enzymes to hydrolyze SF at pH range 6.5–9.0 and temperature between 50°C and 65°C. In a single enzyme treatment using either FoodPro or Alcalase, approximately 20–25% of SF was hydrolyzed and 2 g/L AAs were released from SF. In the 2-stage enzymatic treatment using the combination of FoodPro and Flavourzyme in a sequence, approximately 45% of SF was degraded and 4.5 g/L AAs were released within 6 h of reaction time. The RSF and its EHs were characterized by performing UV-visible spectra, SDS-PAGE, and SEC analyses. In the 2-stage enzymatic treatment using FoodPro initially and then Flavourzyme, the aggregates and high MW proteins of SF were dissociated and biodegraded into the low MW proteins/peptides (10–15 kDa and 27 kDa). SF hydrolysates that are used as functional food can be produced through environment-friendly enzymatic hydrolysis using commercial food-grade proteolytic enzymes.

Data Availability

The data used to support the findings of this study are available from the corresponding author upon request.

Conflicts of Interest

The authors declare that there are no conflicts of interest regarding the publication of this study.

Acknowledgments

This work was supported by Wonkwang University in 2017.

References

[1] K. M. Babu, *Silk: Processing, Properties and Applications*, Woodhead Publishing Ltd., Cambridge, UK, 2013.

[2] L. S. Wray, X. Hu, J. Gallego et al., "Effect of processing on silk-based biomaterials: reproducibility and biocompatibility," *Journal of Biomedical Materials Research Part B Applied Biomaterials*, vol. 99, no. 1, pp. 89–101, 2011.

[3] D. N. Rockwood, R. C. Preda, T. Yücel, X. Wang, M. L. Lovett, and D. L. Kaplan, "Materials fabrication from *Bombyx mori* silk fibroin," *Nature Protocols*, vol. 6, no. 10, pp. 1612–1631, 2011.

[4] B. Kundu, R. Rajkhowa, S. C. Kundu, and X. Wang, "Silk fibroin biomaterials for tissue regeneration," *Advanced Drug Delivery Reviews*, vol. 65, no. 4, pp. 457–470, 2013.

[5] B. Kundu, N. E. Kurland, S. Bano et al., "Silk proteins for biomedical applications: bioengineering perspectives," *Progress in Polymer Science*, vol. 39, no. 2, pp. 251–267, 2014.

[6] A. B. Li, J. A. Kluge, N. A. Guziewicz, F. G. Omenetto, and D. L. Kaplan, "Silk-based stabilization of biomacromolecules," *Journal of Controlled Release*, vol. 219, pp. 416–430, 2015.

[7] C. Vepari and D. L. Kaplan, "Silk as a biomaterial," *Progress in Polymer Science*, vol. 32, no. 8-9, pp. 991–1007, 2007.

[8] J. Melke, S. Midha, S. Ghosh, K. Ito, and S. Hofmann, "Silk fibroin as biomaterial for bone tissue engineering," *Acta Biomaterialia*, vol. 31, pp. 1–16, 2015.

[9] C. Z. Zhou, F. Confalonieri, M. Jacquet, R. Perasso, Z. G. Li, and J. Janin, "Silk fibroin: structural implications of a remarkable amino acid sequence," *Proteins: Structure, Function, and Genetics*, vol. 44, no. 2, pp. 119–122, 2001.

[10] B. Liu, Y. W. Song, L. Jin et al., "Silk structure and degradation," *Colloids and Surfaces B: Biointerfaces*, vol. 131, pp. 122–128, 2015.

[11] Y. Cao and B. Wang, "Biodegradation of silk biomaterials," *International Journal of Molecular Sciences*, vol. 10, no. 4, pp. 1514–1524, 2009.

[12] W. L. Stoppel, N. Raia, E. Kimmerling, S. Wang, C. E. Ghezzi, and D. L. Kaplan, "2.12 silk biomaterials," *Comprehensive Biomaterials II*, vol. 2, pp. 253–278, 2017.

[13] T. Arai, G. Freddi, R. Innocenti, and M. Tsukada, "Biodegradation of *Bombyx mori* silk fibroin fibers and film," *Journal of Applied Polymer Science*, vol. 91, no. 4, pp. 2383–2390, 2004.

[14] R. L. Horan, K. Antle, A. L. Collette et al., "*In vitro* degradation of silk fibroin," *Biomaterials*, vol. 26, no. 17, pp. 3385–3393, 2005.

[15] Q. Lu, B. Zhang, M. Li et al., "Degradation mechanism and control of silk fibroin," *Biomacromolecules*, vol. 12, pp. 1080–1086, 2011.

[16] C. Wongnarat and P. Srihanam, "Degradation behaviors of Thai *Bombyx mori* silk fibroins exposure to protease enzymes," *Engineering*, vol. 5, no. 1, pp. 61–66, 2013.

[17] R. You, Y. Xu, Y. Liu, X. Li, and M. Li, "Comparison of the *in vitro* and *in vivo* degradations of silk fibroin scaffolds from mulberry and nonmulberry silkworms," *Biomedical Materials*, vol. 10, no. 1, article 015003, 2015.

[18] R. You, Y. Zhang, Y. Liu, G. Liu, and M. Li, "The degradation behavior of silk fibroin derived from different ionic liquid solvents," *Natural Science*, vol. 5, no. 6, pp. 10–19, 2013.

[19] P. Srihanam and W. Simchuer, "Proteolytic degradation of silk fibroin scaffold by protease XXIII," *The Open Macromolecules Journal*, vol. 3, no. 1, pp. 1–5, 2009.

[20] Z. Luo, Q. Zhang, M. Shi, Y. Zhang, W. Tao, and M. Li, "Effect of pore size on the biodegradation rate of silk fibroin scaffolds," *Advances in Materials Science and Engineering*, vol. 2015, Article ID 315397, 7 pages, 2015.

[21] J. Brown, C. Lu, J. Coburn, and D. L. Kaplan, "Impact of silk biomaterial structure on proteolysis," *Acta Biomaterialia*, vol. 11, pp. 212–221, 2015.

[22] K. Chen, Y. Umeda, and K. Hirabayashi, "Enzymatic hydrolysis of silk fibroin," *Journal of Sericultural Science of Japan*, vol. 65, pp. 131–133, 1995.

[23] M. Sumida and V. Sutthikhum, "Fibroin and sericin-derived bioactive peptides and hydrolysates as alternative sources of food additive for promotion of human health: a review," *Research and Knowledge*, vol. 1, pp. 1–17, 2015.

[24] K. Hirao and K. Igarashi, "Teaching material study. Characteristics of silk fibroin preparations and its utilization for human food preparation," *Journal of Cookery Science of Japan*, vol. 46, pp. 54–58, 2013.

[25] K. Igarashi, K. Yoshioka, K. Mizutani, M. Miyakoshi, T. Murakami, and T. Akizawa, "Blood pressure-depressing activity of a peptide derived from silkworm fibroin in spontaneously hypertensive rats," *Bioscience, Biotechnology, and Biochemistry*, vol. 70, no. 2, pp. 517–520, 2006.

[26] K. J. Park, H. H. Jin, and C. K. Hyun, "Antigenotoxicity of peptides produced from silk fibroin," *Process Biochemistry*, vol. 38, no. 3, pp. 411–418, 2002.

[27] F. Z. Zhou, Z. Xue, and J. Wang, "Antihypertensive effects of silk fibroin hydrolysate by alcalase and purification of an ACE inhibitory dipeptide," *Journal of Agricultural and Food Chemistry*, vol. 58, no. 11, pp. 6735–6740, 2010.

[28] J. Kim, H. Hwang, J. Park, H. Y. Yun, H. Suh, and K. Lim, "Silk peptide treatment can improve the exercise performance of mice," *Journal of the International Society of Sports Nutrition*, vol. 11, no. 1, pp. 1–7, 2014.

[29] M. Watanabe, T. Kotera, A. Yura, and M. Sumida, "Enzymatic properties of fibroinase of silk gland from day one pupa of the silkworm, *Bombyx mori*," *Journal of Insect Biotechnology and Sericology*, vol. 75, pp. 39–46, 2006.

[30] M. Watanabe, K. Kamei, and M. Sumida, "Sericin digestion by fibroinase, a Cathepsin L-like cysteine proteinase, of *Bombyx mori* silk gland," *Journal of Insect Biotechnology and Sericology*, vol. 76, pp. 9–15, 2007.

[31] S. K. Kim, Y. Y. Jo, K. G. Lee et al., "Modification of the characteristics of silkworm powder by treatment with alkaline protease," *International Journal of Industrial Entomology*, vol. 31, no. 1, pp. 30–33, 2015.

[32] H. J. Chae, M. J. In, and E. Y. Kim, "Effect of solubilization conditions for molecular weight distribution of enzymatically-hydrolyzed silk peptides," *Korean Journal of Biotechnology and Bioengineering*, vol. 13, pp. 114–118, 1998.

[33] T. C. Mcilvaine, "A buffer solution for colorimetric comparison," *Journal of Biological Chemistry*, vol. 49, pp. 183–186, 1921.

[34] A. Ajisawa, "Dissolution of silk fibroin with calcium chloride-ethanol aqueous solution," *Journal of Sericultural Science of Japan*, vol. 67, pp. 91–94, 1998.

[35] O. H. Lowry, N. J. Rosebrough, A. L. Farr, and R. J. Randall, "Protein measurement with the Folin phenol reagent," *Journal of Biological Chemistry*, vol. 193, pp. 265–275, 1951.

[36] C. Cupp-Enyard, "Sigma's Non-specific protease activity assay - casein as a substrate," *Journal of Visualized Experiments*, vol. 19, p. e899, 2008.

[37] V. J. Harding and R. M. MzcLean, "The ninhydrin reaction with amines and amides," *Journal of Biological Chemistry*, vol. 25, pp. 337–350, 1916.

[38] C. Wong Po Foo, E. Bini, J. Hensman, D. P. Knight, R. V. Lewis, and D. L. Kaplan, "Role of pH and charge on silk protein assembly in insects and spiders," *Applied Physics A: Material Science and Processing*, vol. 82, no. 2, pp. 223–233, 2006.

[39] A. Matsumoto, A. Lindsay, B. Abedian, and D. L. Kaplan, "Silk fibroin solution properties related to assembly and structure," *Macromolecular Bioscience*, vol. 8, no. 11, pp. 1006–1018, 2008.

[40] M. Friedman, "Applications of the Ninhydrin reaction for analysis of amino acids, peptides, and proteins to agricultural and biomedical sciences," *Journal of Agricultural and Food Chemistry*, vol. 52, no. 3, pp. 385–406, 2004.

[41] Z. Zheng, S. Guo, Y. Liu et al., "Lithium-free processing of silk fibroin," *Journal of Biomaterials Applications*, vol. 31, no. 3, pp. 450–463, 2016.

[42] H. Yamada, H. Nakao, Y. Takasu, and K. Tsubouchi, "Preparation of undegraded native molecular fibroin solution from silkworm cocoons," *Materials Science and Engineering: C*, vol. 14, no. 1-2, pp. 41–46, 2001.